ISTANBUL TECHNICAL UNIVERSITY ★ GRADUATE SCHOOL OF SCIENCE ENGINEERING AND TECHNOLOGY

DIELECTRIC ELASTOMER ACTUATORS

M.Sc. THESIS

Azamet KARAOĞLAN

Department of Mechanical Engineering

Solid Mechanics Programme

JULY 2020

ISTANBUL TECHNICAL UNIVERSITY ★ GRADUATE SCHOOL OF SCIENCE ENGINEERING AND TECHNOLOGY

DIELECTRIC ELASTOMER ACTUATORS

M.Sc. THESIS

Azamet KARAOĞLAN
503171501

Department of Mechanical Engineering

Solid Mechanics Programme

Thesis Advisor: Assoc. Prof. Dr. Emin SÜNBÜLOĞLU

JULY 2020

ISTANBUL TEKNİK ÜNİVERSİTESİ ★ FEN BİLİMLERİ ENSTİTÜSÜ

DİELEKTRİK ELASTOMER AKTÜATÖRLER

YÜKSEK LİSANS TEZİ

Azamet KARAOĞLAN
503171501

Makina Mühendisliği Anabilim Dalı

Katı Cisimlerin Mekaniği Programı

Tez Danışmanı: Doç. Dr. Emin SÜNBÜLOĞLU

TEMMUZ 2020

Azamet Karaoğlan, a M.Sc student of İTU Graduate School of Science Engineering and Technology student ID 503171501, successfully defended the thesis/dissertation entitled "DIELECTRIC ELASTOMER ACTUATORS", which he prepared after fulfilling the requirements specified in the associated legislations, before the jury whose signatures are below.

Thesis Advisor :	**Assoc. Prof. Dr. Emin SÜNBÜLOĞLU** İstanbul Technical University	....
Jury Members :	**Assoc. Prof. Dr. Emin SÜNBÜLOĞLU** Istanbul Technical University	....
	Dr. Ergün BOZDAĞ Istanbul Technical University	....
	Prof. Dr. Melih PAPİLA Sabancı University	....

Date of Submission : 15 June 2020
Date of Defense : 16 July 2020

To my family and friends,

FOREWORD

This thesis would not be possible without some very important people. First of all I would like to thank my thesis advisor Assoc. Prof. Dr. Emin Sünbüloğlu for introducing me to the world of finite elements and non-linear solid mechanics and been always helpful in my academic life for over 6 years.

I would also like to thank my friends and colleagues Fatih Yamak and Yunus Emre Erginsoy for being second pair of eyes when I asked them in despair to find my errors.

I would also like to thank my closest friends for their mental supports and baring with me throughout this challenging period.

Finally, I would like to thank my parents who always showed their supports with the best of their ability during my whole life.

July 2020

Azamet KARAOĞLAN
MSc. in Mechanical Engineering

TABLE OF CONTENTS

Page

SYMBOLS

$\mathbf{p_{el}}$	**:** Electrostatic pressure
$\boldsymbol{\varepsilon_0}$	**:** Electric permittivity of free space
$\boldsymbol{\varepsilon_r}$	**:** Relative electric permittivity
V	**:** Potential Difference
d	**:** Elastomer film thickness
u(x,t)	: Displacement vector
e_i	: Orthogonal unit vectors
b(t)	: Rigid Body Translation
F	: Deformation gradient
I	: Identity matrix
δ_{ik}	: Kronecker-Delta function
C	: Right Cauchy-Green deformation tensor
I_1	: First invariant of deformation tensors
I_2	: Second invariant of deformation tensors
I_3	: Third invariant of deformation tensors
B	: Left Cauchy-Green deformation tensor
D_{int}	: Loacl entropy production
P	: First Piola-Kirchoff stress tensor
$\dot{e}$	: Internal energy rate
Θ	: Absolute temperature
ψ	: Strain-energy density function
σ	: Cauchy stress
J	: Jacobien of deformation gradient
λ_i	: Principal stretches
p	: Lagrangian multiplier for incompressibity assumption
C_1	: Material constant for Neo-Hooke material model
μ	: Shear modulus
ε	: Strain
γ	: Shear angle
C_{00}, C_{pq}	: Distortional material constants for Mooney-Rivlin material model

D_m	: Volumetric material constants for Mooney-Rivlin material model
J_m	: Extension limit for Gent material model
$\vec{a}_0$	: Initial orientation vector of 1st fibre family
$\vec{g}_0$	: Initial orientation vector of 2nd fibre family
$\vec{a}$	: Deformed orientation vector of 1st fibre family
$\vec{g}$	: Deformed orientation vector of 2nd fibre family
I_4	: Invariant concerning the strecth of fibre family 1
I_5	: Invariant concerning the relation between fibre family 1 and matrix
I_6	: Invariant concerning the strecth of fibre family 2
I_7	: Invariant concerning the relation between fibre family 2 and matrix
I_8	: Invariant concerning the relation between two fibre families
I_9	: Invariant concerning the relative orientation of two fibre families
q	: Stress found on inextensible fibres
₣	: Lorentz force
$\mathcal{q}$	: Electrical charge
$\mathbb{E}$	: Electric field vector
v	: Velocity vector
$\boldsymbol{\mathcal{B}}$	: Magnetic field vector
ρ	: Charge density
J_c	: Current density
μ_0	: Magnetic constant
σ_{Max}	: Maxwell stress
d	: Deformed electric field vector
D	: Undeformed electric field vector
N	: Shape function vector
w	: Weight function
$\bar{t}$	: Traction vector
K	: Global stiffness matrix
B_e	: Element strain matrix
K_e	: Element stiffness matrix
H	: Tangent modulus for hyperelasticity
S	: Second Piola-Kirchoff stress tensor
k	: Stiffness of end springs for FE models

LIST OF TABLES

Page

LIST OF FIGURES

Page

DIELECTRIC ELASTOMER ACTUATORS

SUMMARY

Dielectric elastomer actuators (DEA) are specific class of actuators transforming electrical energy to mechanical energy by deforming a dielectric rubber under electrical load. When a dielectric material is placed in a electric field, electrons do not flow through the material, however electric field polarizes the material creating an internal electric field within the material, causing reorientation of symmetry axes of molecules if the material is composed from weak bonded molecules like in elastomers. Manipulation of this phenomenon is the basis of dielectric elastomer actuators and they are the most promising candidate in the search for artificial muscles. Their lightweight properties combined with dielectricity grant this candidacy.

After an intensive literature review of past studies on the working principles of DEA and proposed designs summarized in the second chapter, necessary theoritical basis is explained for finite strain theory, transverse isotropy, electromagnetism theory and Maxwell stress and finite element method formulations for finitely elastic materials in the third chapter.

In the fourth chapter a mathematical model is derived for a hydraulically pressurized, reinforced with two symmetrical families of fibre, incompressible tubular Neo-Hookean DEA under axial and electrical load. Stress components and expressions for axial load and inner pressure as a function of stress components are given at the end of this chapter.

In the fifth chapter, a design of experiments is constructed in Isight with a finite element model of a hydraulically pressurized, reinforced with two symmetrical families of fibre of cotton thread, incompressible tubular DEA of VHB4910 created in ABAQUS, studying the effects of parameters such as fibre angle, inner pressure and electrical load on the actuation outputs. The obtained results are interpreted and presented in various graphs.

In the sixth chapter, an alternative design is proposed. A finite element model is created on ABAQUS for a incompressible tubular helix DEA of VHB4910 reinforced with two symmetrical families of fibre of cotton thread and pre-strecthed with a hydraulic pressure. The effects of fibre angle on actuation outputs were then analysed and presented.

In the seventh chapter, two alternative designs are proposed such as a hydraulically pressurized, reinforced with two symmetrical fibre families of cotton thread, accordion shaped cylindrical DEA of VHB4910 and its conical variant. Again, effects of fibre angle on actuation outputs are studied numerically with finite element models.

DİELEKTRİK ELASTOMER AKTÜATÖRLER

ÖZET

Dielektrik elastomer aktüatörler (DEA) elektrik enerjisini mekanik enerjiye çevirmeye yarayan araçlardır. Dielektrik malzemeler elektrik alana maruz bırakıldıklarında, elektronlar malzeme üzerinden akmak yerine malzemeyi polarize eder ve eğer malzeme elastomer gibi zayıf bağlı moleküllerden oluşuyorsa, moleküllerin simetri eksenleri bu polarizasyon sonucunda elektrik alan yönünde dönerek malzemede elastik bir deformasyona sebep olur. Dielektrik elastomer aktüatörler de bahsedilen bu deformasyonu kullanarak elektrik enerji ve mekanik eneji arasındaki dönüşümü sağlar.

Elastomerlerin düşük ağırlık özellikleri ve elektrik ile aktive edilebilmeleri DEA'ları yapay kas çalışmalarındaki en önemli adaylardan biri yapıyor. Ancak yüksek deformasyon altında bile verdikleri düşük kuvvet çıktıları aşılması gereken bir engel. Bunun için de çeşitli tasarımlar, lifler ile güçlendirme ve ön yükleme gibi metodlar denenmektedir. Ayrıca elektrik alanının malzeme için fazla gelmesi ile oluşabilecek elektrik atlamaları ve malzemede oluşacak elektrik dengesizlik de DEA'ler için çözülmesi gereken bir sorun.

Bu çalışmada öncelikli olarak DEA'lar ve yapay kas çalışmasında kullanılan diğer mekanizmalar hakkında yapılan bilimsel bulgular özetlendi. Şekil hafızalı alaşımlar, eletrik moturu kullanan sistemler, hidrolik ya da pnömatik aktüasyon kullanılan sistemler ve DEA'lerin bu sistemlere karşı sahip olduğu avantajlardan bahsedildi. Bunun yanı sıra DEA'ların çalışma mantığını, yüksek potansiyel fark sonucunda oluşan elektrik dengesizliği konu alan çalışmalar ve kuvvet-deplasman çıktılarını daha yüksek seviyeye çekmek amacıyla oluşturulan diğer tasarımlar hakkında da bilgi verildi.

Literatürde yer alan çalışmalar anlatıldıktan sonra, tezde yapılan çalışmanın kullandığı sonlu birim şekil değiştirme, lifli yapılar ve deformasyona etkileri, elektromanyetizma ve dielektrik malzemelerde görülen Maxwell Gerilme tensörü, sonlu elemanlar metodu ve hiperelastik malzemelerde uygulanması hakkında teorik bilgiler özetlendi.

Öncelikle sonlu birim şekil değiştirme teorisi için şekil değişiminin tanımı, gerilme ve birim şekil değiştirme ifadeleri için temel denklemler, farklı hiperelastik malzeme modelleri ve basit şekil değiştirme durumları için oluşacak gerilme ifadeleri verildi. Daha sonra lifler ile güçlendirilmiş bir modelde gerilme ifadelerinin nasıl değiştiği açıklandı. Akabinde elektromanyetizma teorisi ve dielektrik malzemelerde elektrik alana maruz bırakılma sonucunda oluşan gerilme (Maxwell gerilmesi) Lorentz kuvveti ve Maxwell yasaları kullanırak çıkarıldı. En son bölümde de sonlu elemanlar metodunun temel işleyişi anlatıldı ve basit bir çekme çubuğu modeli için güçlü form, zayıf form, direngenlik matrisi ve çekme çubuğunun hiperelastik olması durumunda Neo-Hooke malzeme modeli kullanıldığında direngenlik matrisinin nasıl değiştiği gösterildi.

Teorik bilgileri takip eden bölümde, iç yüzeyinde hidrolik basınç olan ve iki simetrik lif ailesi ile güçlendirilmiş silindir bir silindir DEA için eksenel yük ve kalınlık

doğrultusunda verilen elektrik alan altında oluşacak şekil değişimini açıklayan bir matematik model üretildi. Şekil değişimi açıklayan deformasyon gradyanı silindrik koordinat sisteminde malzemenin ilk ve son hallerini veren koordinatlara bağlı ifadeler cinsinden çıkarıldı. Daha sonra deformasyon gradyanı kullanılarak Sol Cauchy-Green deformasyon tensörü hesaplandı. Lifler ile güçlendirilmiş malzemeler için düzenlenmiş Neo-Hooke hiperelastik malzeme modeli, Cauchy gerilme tensrörü tanımı ve Maxwell gerilme tensörü kullanılarak tüm yüklemeler sonucunda oluşan toplam gerilme bulundu. Bölüm sonunda eksenel yükü ve iç basıncı gösteren ifadeler gerilme tensörünün bileşenleri cinsinden elde edildi.

İlk tasarım önerisi olarak, matematik modeli de çıkarılan hidrolik iç basınçlı, simetrik pamuk ipliğinden yapılmış iki lif ailesi ile güçlendirilmiş, VHB4910 isimli malzemeden yapılmış, silindirik bir DEA modeli çalışıldı. Model, öncelikle ABAQUS isimli program kullanılarak sonlu elemanlar yönetimi ile nümerik olarak oluşturuldu. Bu işlem sırasında dielektrik davranışı doğru bir şekilde aktarmak için hem Neo-Hooke hiperelastik malzeme modelini kullanan hem de elektrik alan vektörlerini kullanarak Maxwell gerilmesini hesaplayan bir UMAT (user material: kullanıcı malzemesi) altyordamı yazıldı. Daha sonra Isight isimli programda deney tasarımı yapılarak, liflerin eksenel doğrultu ile yaptığı açı, iç basınç ve elektrik alan büyüklüğü gibi parametrelerin eksenel doğrultuda oluşturduğu kuvvet, deplasman ve iş çıktılarına etkileri hakkında veri toplandı. Bu aşamada sadece parametlerinin çıktıları nasıl etkilediği değil ayrıca parametrelerin diğer parametrelerin çıktılar üzerindeki etkisini nasıl değiştirdiği de incelendi (Örnek: Lif açısının, iç basınç ile aktüasyon arasındaki ilişkiye etkisi). Ayrıca toplam eksenel uzama oranı ve eleman uzama oranı arasındaki ilişki yani eleman uzama oranlarının ne kadar verimli kullanıldığını görmek için bununla ilgili grafikler de bu bölümde sunuldu.

İkinci tasarım önerisi olarak hidrolik iç basınçlı, pamuk ipliğinden oluşuturlmuş simetrik iki lif ailesi ile güçlendirilmiş, VHB4910 malzemesinden üretilmiş, silindirik DEA, helisel bir profil çizer halde sonlu elemanlar yöntemi ile modellendi. Önceki bölümde kullanılan UMAT altyordamı ile liflerin helis tanjant vektörü ile açı yapmasını sağlayacak ve eleman yön vektörlerini helix normal ve tanjant vektörleri doğrultusunda çeviren bir ORIENT (yönelim) altyordamı yazıldı. Bu ikinci altyordam ayrıca elektrik alanının, helisin kesit alanında kalınlık boyunca radyal yönde verilmesini sağlamak için de kullanıldı. Oluşturulan sonlu elemanlar modeli kullanılarak lif açısının, helisin eksenel yönü doğrultusunda, elektrik alan sonucunda oluşan kuvvet, deplasman ve işteki değişimi üzerindeki etkileri araştırıldı ve grafikler aracılığıyla sunuldu.

Üçüncü ve son tasarım önerisi olarak, verilen ilk tasarım önerisi akordiyona benzeyecek şekilde yani tüp çeperleri eksenel doğrultuda zikzak profilinde olacak şekilde değiştirildi. Burada yine hidrolik iç basınç kullanıldı ve elastomer, pamuk ipliğinden yapılmış, simetrik iki lif ailesi ile güçlendirildi. Elastomer malzemesi olarak yine VHB4910 kullanıldı. Dielectrik ve hiperelastik davranışı vermek için önceki sonlu elemanlar modellerinde kullanılan UMAT ve lif açılarını eksenel doğrultu ile açı yapmasını sağlayacak ORIENT altyordamları kullanıldı. Bunun yanı sıra aynı modelin, aynı uzunlukta ve bir uçtaki çapı diğerinin iki katı olacak şekilde kesik konik versiyonu da üretildi. Bu iki tasarım için oluşturulan sonlu elemanlar modeli kullanılarak lif açılarının, elektrik alan sonunda eksenel doğrultuda oluşacak kuvvet, deplasman ve iş çıktılarındaki değişime etkisi incelendi.

Oluşturulan üç tasarım ve bunların sonlu elemanlar modeli üzerinde yapılan çalışmalar sonucunda çeşitli tasarım değişkenlerinin elektrik alan üzerindeki etkileri sonuç bölümünde karşılaştırılarak, yapay kas için aday arayışındaki en büyük engel olan düşük kuvvet çıktıları konusunda, çalışılan tasarımların ulaştığı sonuçlar değerlendirildi. Ayrıca çıkan sonuçları iyileştirme amacıyla önerilen tasarılarda yapılacabilecek muhtemel değişikler için öneriler sunuldu.

1. INTRODUCTION

Dielectric Elastomer Actuators (DEA) are the leading designs for artificial muscles. Their ability of converting electrical energy to mechanical work via relatively large strains (at on order of 10% to 30%) is the best candidate for biomimetic equivalent of real muscle fibres.

Dielectric elastomers (DE) are simply a capacitor composed of a thin layer film between two electrodes, however they are rather deformable. According to Pelrine et al. [1] the electrostatic pressure p_{el} can be calculated from applied voltage V and film thickness h as

$$p_{el} = \varepsilon_0 \varepsilon_r \left(\frac{V}{d}\right)^2 \tag{1.1}$$

where ε_0 is the permittivity of free space (8.85 E-12 F/m) and ε_r is the relative permittivity of elastomer. The attraction between the electrodes squeeze the elastomer film which results a contraction in the thickness and expansion in the planar direction due to conservation of volume (due to almost incompressible behaviour). This behaviour of planar expansion can be used to create force or displacement. Often these structures are pre-strained in order to increase the performance and decrease the electrical instability.

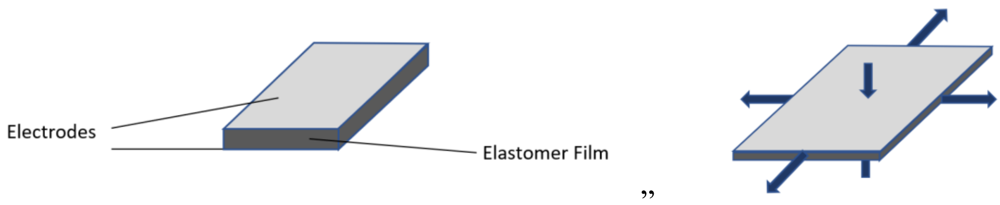

Figure 1.1 : Dielectric Behaviour of a Thin Elastomer Film

The most challenging aspect of DE materials is the small load bearing capacity (in the order of mN’s). Overcoming the small force output problem has been a research topic over for 30 years. Different designs such as cylindrical DEAs, stacked DEAs and folded DEAs are studied and analysed for an optimum outcome. To find a feasible solution and design a DEA, various studies should be conducted:

- Mathematical Model: A mathematical model of DEA design via constitutive equations and their coupling with electromechanical response should be generated. Elastomers are non-linear materials, thus finite strain theory for the hyperelasticity (visco-elasticity as well to capture the transients, however visco-elasticity has not been inspected in this study) should be taken into consideration.
- Numerical Model: A numerical model is crucial to observe actual working mechanism of real-life DEA designs. In this study Finite Element Method is preferred for numerical models.
- Experimental Validation: To verify that the material constants, electromechanical response comply with reality, and to discover possible problems, which has been overlooked or not expected during mathematical and/or numerical modelling, experiments should be conducted.

This study mainly aims at evaluating various designs of DEA candidates, and evaluate them against different criteria such as feasible work output (i.e. force vs displacement curve), design options, pre-stretch conditions, etc. To achieve this aim, several different DEA designs of VHB4910 material are examined for an optimum force outcome. These can be summarised as:

1. Hydraulically coupled fibre reinforced cylindrical DEA: Mathematical model of hyperelastic-dielectric behaviour for a hydraulically coupled fibre reinforced cylindrical DEA is generated and a finite element study (FE Model and Design of Experiments from FE Model) has been conducted to determine the effects of pressure, fibre orientation, denseness of fibre web and pre-strain on the uniaxial force output of electrical load. Numerical model verification with theoretical calculations has also been conducted at this level.
2. Hydraulically coupled fibre reinforced tubular DEA helix: Finite element study of a hydraulically coupled fibre reinforced tubular DEA helix is conducted and possible improvements (in contrast to cylindrical design) that can be obtained from the unidirectional attitude of helical shapes has been investigated.
3. Hydraulically coupled fibre reinforced accordion shaped DEA: Finite element study of a hydraulically coupled fibre reinforced accordion shaped DEA is conducted and possible improvements (in contrast to cylindrical design) that

can be obtained from the stacked structure of accordion like shapes has been investigated. This study also includes a conical variant of proposed design.

2. A REVIEW OF PREVIOUS RESEARCH ON TOPIC

Mimicking the motion of natural muscles fibres has been a long search for several years considering helping people with disabilities and making humanoid robots. Several candidates for artificial muscles have been studied, such as electro-magnetic motors, pneumatic systems, smart materials and dielectric elastomer actuators (DEAs) [1].

While electro-magnetic motors can easily match the energy density of muscles [2] which is the order of 150 J.kg-1 [3], their need to use heavy battery pack and gearing systems, excess heat, etc. limit their efficiency and usability.

Some pneumatics systems like McKibben actuators has also been considered for artificial muscles [4] which benefit from high actuation forces using pressure, however their need of heavy air pump systems and slow reaction time also limits their usability. Shape Memory Alloys (SMAs), Magneto Strictive Alloys (MSAs) and piezoelectrics also candidates for artificial muscles [5, 6]. However, while SMAs are capable of necessary displacements, they suffer from slow unloading process which makes them not suitable. MSAs and piezoelectrics also not suitable for artificial muscles due to their small strain capabilities.

Researching the possibility of this behaviour of Dielectric Elastomer Actuators (DEAs) as artificial muscles is a topic of mechanical engineering community over for 30 years. Large strain capabilities of up to 300% and fast response time make them a better candidate than all the other possibilities [7-12]. Dielectric elastomer powered arm prosthetics, ankle-foot orthosis and ventricular assist device are some of the application concepts which have promising results, yet they need development [13].

The concept of Dielectric Behaviour was first documented by Roentgen in 1880 [14], detecting physical change of a natural rubber film under large electric fields. Since this paper, a wide variability of DEAs and designs have been studied. Focus of these studies was mostly increasing the actuation force.

Cylindrical DEAs are most common since the actuation can be directed to one direction and grant a higher planar stiffness [15]. Various research on mathematical modelling and experimental tests of cylindrical DEAs has been previously done by Son and Goulbourne [16]. Rahn and Liu, and Goulbourne introduced fibre reinforcements to the cylindrical McKibben actuators using pressure to expand in radial direction and because of fibres causing axial deformation [17, 18] which in return causing higher actuation forces with same electric fields.

Other design such as Zhao and Suo studied, forming a gripping structure from a layer of dielectric elastomer by actuation by electric field [19]. Also, bending elastomer layer rolls were analysed for biomimicking knee and leg joints by Pei et al. [20]

Kovacs et al. considered stacking cylindrical dielectric elastomers by placing electrodes between each layer which overcomes the low force output by actuating more thickness stacked on a smaller volume [21].

Wang et al. inquired the effects of coupling two membranes of dielectric elastomer clamped on the outer radius with a non-compressible fluid in which they find that required electric field for actuation decrease significantly for the same deformation and actuation force orders [22].

Instability under electrical load is a major limit for the practical use of dielectric elastomers, Plante and Duboswsky found that DEAs should operate with high strain and on brief cycles [23]. Suo observed that the performance of DEAs improves greatly with prestretch [24] which cleared the path to more reliable designs.

Computational and mathematical modelling of dielectric behaviour in aspect of hyperelasticity and viscoelasticity is also considered heavily, since to find the right design and material, and optimize them a working model is necessary. Various researchers have found techniques to model dielectric behaviour and their coupled behaviours using commercial FEA programs [15, 24-25].

A combination of several positive findings of these studies such as a fibre reinforced hydrostatically coupled cylindrical DEA seems to be an area in which nearly no research has been done, yet alone finding an analytical solution and an optimized model. Moreover, behaviour of tubular helix and accordion shaped DEAs are also not studied and understanding behaviour of this shapes under electrical activation could bring some advance to this area.

3. THEORETICAL BACKGROUND

3.1 Finite Strain Theory of Hyperelasticity

Classical theory of elasticity (infinitesimal strain theory) deals with the mechanics of materials (industrial steel, aluminium, concrete, etc.) which exhibit small deformations under loading conditions. However, materials like rubber and soft biological tissues (muscles, arterial tissues and so on) shows exceptionally large deformations which causes substantial difference between initial and final geometrical configurations so that the assumption of infinitesimal strain theory becomes invalid. This situation requires a different theoretical approach for handling the kinematics of such deformations.

3.1.1 Geometrical definitions for finite strain theory

3.1.1.1 Displacement

Total displacement of a point on a solid body is a coupled result of rigid-body motions and relative motions among its neighbourhood. Rigid-body motion is the physical translation of the body in space and relative motions among neighbouring points is called deformation. Deformation, thus, is the reason for change in form/shape from reference configuration to final configuration under physical load (Fig. 1).

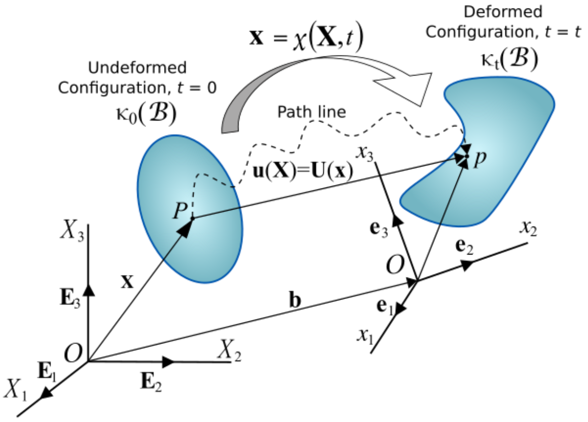

Figure 3.1 : Displacement of a body [27].

The transformation of the configuration of a body is described as the displacement field which is a vector field consisting of displacement vectors of all particles of the body. The change in the distance between any two particles implies a change in shape i.e. deformation.

3.1.1.2 Lagrangian description of material coordinates

The reference coordinates of a particle in the body is noted as **X** and the deformed coordinates is noted as **x**. The displacement vector is defined as the vector joining **x** and **X** coordinates. The Lagrangian description of displacement vector is given as;

$$\mathbf{u}(\mathbf{X},\mathrm{t}) = \mathrm{u_i}\mathbf{e_i} \tag{3.1}$$

where $\mathbf{e_i}$ are the orthonormal unit vectors which defines global coordinates system and i is the index defining 1st, 2nd and 3rd orthonormal directions. This field when expressed in terms of material coordinates becomes;

$$\mathbf{u}(\mathbf{X},\mathrm{t}) + \mathbf{b}(\mathrm{t}) = \mathbf{x}(\mathbf{X},\mathrm{t}) - \mathbf{X} \ \text{ or } \mathrm{u_i} + \mathrm{a_{ij}b_j} = \mathrm{x_i} - \mathrm{a_{ij}X_j} \tag{3.2}$$

where **b**(t) is the rigid-body translation.

3.1.1.3 Deformation gradient tensor

Taking the partial derivatives of displacement with respect to material coordinates gives displacement gradient tensor;

$$\nabla_{\mathbf{X}}\mathbf{u} = \nabla_{\mathbf{X}}\mathbf{x} - \mathbf{I} = \mathbf{F} - \mathbf{I} \text{ or } \frac{\partial \mathrm{u_i}}{\partial \mathrm{X_k}} = \frac{\partial \mathrm{x_i}}{\partial \mathrm{X_k}} - \delta_{\mathrm{ik}} = \mathrm{F_{ik}} - \delta_{\mathrm{ik}} \tag{3.3}$$

where **F** is the deformation gradient tensor, **I** is the 3x3 identity matrix and δ_{ik} is the Kronecker-Delta function.

Deformation gradient tensor is a two-point tensor (also known as double vectors, tensor like quantities used in continuum mechanics which defines transformation between reference and current configuration), and is the partial derivative of current coordinates with respect to reference coordinates.

$$\mathbf{F} = \begin{bmatrix} \frac{\partial x_1}{\partial X_1} & \frac{\partial x_2}{\partial X_1} & \frac{\partial x_3}{\partial X_1} \\ \frac{\partial x_1}{\partial X_2} & \frac{\partial x_2}{\partial X_2} & \frac{\partial x_3}{\partial X_2} \\ \frac{\partial x_1}{\partial X_3} & \frac{\partial x_2}{\partial X_3} & \frac{\partial x_3}{\partial X_3} \end{bmatrix} \tag{3.4}$$

The most used deformation tensor is the right Cauchy-Green deformation tensor which was defined in 1839 by George Green as;

$$\mathbf{C} = \mathbf{F}^{\mathrm{T}}\mathbf{F} \tag{3.5}$$

The right Cauchy-Green deformation tensor represents local change in distance due to deformation squared and used when the current configuration is inspected with respect to reference configuration. The invariants of this tensor are the variables of strain energy density function.

$$\mathrm{I}_1 = \mathrm{tr}(\mathbf{C}) = \mathrm{C}_{\mathrm{II}} = \lambda_1^2 + \lambda_2^2 + \lambda_3^2 \tag{3.6}$$

$$\mathrm{I}_2 = \frac{1}{2}[\left(\mathrm{tr}(\mathbf{C})\right)^2 - \mathrm{tr}(\mathbf{C}^2)] = \frac{1}{2}[\mathrm{C}_{\mathrm{JJ}}^2 - \mathrm{C}_{\mathrm{IK}}\mathrm{C}_{\mathrm{KI}}] \tag{3.7}$$

$$= \lambda_1^2\lambda_2^2 + \lambda_2^2\lambda_3^2 + \lambda_3^2\lambda_1^2$$

$$\mathrm{I}_3 = \det(\mathbf{C}) = \mathrm{C}_{\mathrm{II}} = \lambda_1^2\lambda_2^2\lambda_3^2 \tag{3.8}$$

where λ_1, λ_2 and λ_3 are the principal stretch ratios of deformation.
Another approach, the left Cauchy-Green deformations tensor is defined as;

$$\mathbf{B} = \mathbf{F}\mathbf{F}^{\mathrm{T}} \tag{3.9}$$

and has the same invariants as right Cauchy-Green deformation tensors.

3.1.2 Hyperelasticity

Hyperelasticity is a term that defines time independent large deformation behaviour of rubber-like materials and is a subset of finite strain theory. The stress strain relations of hyperelastic materials are derived from strain energy density function [28] which depends on different material models, and material itself and derived from the second law of thermodynamics.

The second law of thermodynamics states that entropy, that is energy dissipated and lost as heat during any process, of a system always increases which means, in mechanical engineering terms, mechanical energy may be converted to heat by internal or external conditions such as friction and can never be reverted back to mechanical energy [28]. There are mathematical definitions for this law. However, Clausius-Planck Inequality form is the most suitable in terms of this thesis' scope and defined as;

$$\mathrm{D}_{\mathrm{int}} = \mathbf{P}:\dot{\mathbf{F}} - \dot{\mathrm{e}} + \Theta\dot{\eta} \geq 0 \tag{3.10}$$

where $\mathrm{D}_{\mathrm{int}}$ is the local production of entropy, $\mathbf{P}$ is the 1st Piola-Kirchoff Stress, $\dot{\mathrm{e}}$ is the internal energy rate and Θ is the absolute temperature and $\dot{\eta}$ is the entropy rate. This inequality physically means that entropy production, that is the internal mechanical work rate ($\mathbf{P}:\dot{\mathbf{F}}$) minus internal energy rate plus entropy rate, cannot be negative. Introducing the strain density energy function ψ (also referred as Helmholtz free-energy function in thermodynamics) as [28];

$$\psi = \mathrm{e} - \Theta\eta \tag{3.11}$$

And by taking time derivative and substituting into equation (3.10);

$$\mathrm{D_{int}} = \mathbf{P}:\dot{\mathbf{F}} - \dot{\psi} - \eta\dot{\Theta} \geq 0 \tag{3.12}$$

Rewriting $\dot{\psi}$ and assuming perfectly elastic material (no local entropy production [27]) with constant temperature;

$$\mathrm{D_{int}} = \left(\mathbf{P} - \frac{\partial\psi(\mathbf{F})}{\partial\mathbf{F}}\right) : \dot{\mathbf{F}} = 0 \tag{3.13}$$

As said above, the stress strain relations of hyperelastic materials are defined from a strain energy density function, which is the stored energy per unit volume[28] and in a general way can be defined as;

$$\psi = \mathrm{f}(I_1, I_2, I_3) \tag{3.14}$$

and the 1st Piola-Kirchoff stress, stress stating the relation between forces in current configuration and geometry in reference configuration, from equation (3.13) is defined as;

$$\mathbf{P} = \frac{\partial\psi}{\partial\mathbf{F}} \tag{3.15}$$

and 1st Piola-Kirchoff stress can be transformed to Cauchy Stress tensor, true stress that is the relation between the forces on current configuration and geometry in current configuration, and for an incompressible isotropic material can be defined as;

$$\boldsymbol{\sigma} = \frac{1}{\mathrm{J}}\mathbf{P}\mathbf{F}^{\mathrm{T}} = \frac{2}{\mathrm{J}}\mathbf{F}\frac{\partial\psi}{\partial\mathbf{C}}\mathbf{F}^{\mathrm{T}} \tag{3.16}$$

$$\boldsymbol{\sigma} = \frac{2}{\mathrm{J}}\left[\left(\frac{\partial\psi}{\partial\mathrm{I}_1} + \mathrm{I}_1\frac{\partial\psi}{\partial\mathrm{I}_2}\right)\mathbf{B} - \frac{\partial\psi}{\partial\mathrm{I}_2}\mathbf{B}.\mathbf{B} + \mathrm{I}_3\frac{\partial\psi}{\partial\mathrm{I}_3}\mathbf{I}\right] \tag{3.17}$$

where J is Jacobian of **F** and basically the volume ratio and can be defined as;

$$\mathrm{J} = \det(\mathbf{F}) \tag{3.18}$$

If a material is assumed to be incompressible the volume must remain the same which means;

$$\mathrm{J} = 1 \ \rightarrow \lambda_1\lambda_2\lambda_3 = 1 \tag{3.19}$$

Multiplication of three principal stretches equals one means that only two of them are independent variables. For this situation, strain energy density function takes the form;

$$\psi = \psi[I_1(C), I_2(C)] - \frac{1}{2}p(I_3 - 1) \tag{3.20}$$

where p is a pressure like Lagrangian Multiplier and p(J-1) term does not contribute to ψ since it cancels out.

This change in the form of the strain energy density function yields the following forms as definitions of stress tensors for isotropic incompressible hyperelastic materials;

$$\mathbf{P} = -p\mathbf{F}^{-T} + \frac{\partial \psi}{\partial \mathbf{F}} \tag{3.21}$$

$$\boldsymbol{\sigma} = -p\mathbf{I} + \mathbf{F}\left(\frac{\partial \psi}{\partial \mathbf{F}}\right)^{T} \tag{3.22}$$

$$\boldsymbol{\sigma} = -p\mathbf{I} + 2\frac{\partial \psi}{\partial I_1}\mathbf{B} - 2\frac{\partial \psi}{\partial I_2}\mathbf{B}^2 \tag{3.23}$$

They can also be written in terms of principal stretches;

$$P_i = -\frac{1}{\lambda_i}p + \frac{\partial \psi}{\partial \lambda_i} \tag{3.24}$$

$$\sigma_i = -p + \lambda_i\frac{\partial \psi}{\partial \lambda_i} \tag{3.25}$$

As can be seen clearly from the definition of Cauchy stress tensor, the strain energy density function plays the main part for the calculation of stresses. However, there is no one universal strain energy density function to simplify this equation. This function is different for every hyperelastic material model that describes the behaviour with different assumptions and works better in different conditions (smaller stretch ratios, loading condition, etc).

3.1.2.1 Neo-Hookean solid

This material model is a non-linear version of Hooke's law to consider largely deformed materials' stress-strain relations [29] and was proposed by Ronald Rivlin in 1948. For this material model, the strain energy density function for an isotropic incompressible hyperelastic material is defined as;

$$\psi = C_1(I_1 - 3) \tag{3.26}$$

where I_1 is the first invariant of Left Cauchy Green deformation tensor, C_1 is the material constant. These material constants can be defined with respect to linear elasticity terms as;

$$C_1 = \frac{\mu}{2} \tag{3.27}$$

where μ is the shear modulus.

Substituting equation (3.26) into equation (3.23), Cauchy stress tensor for an incompressible material (J=1) becomes;

$$\boldsymbol{\sigma} = -\mathrm{p}\mathbf{I} + 2\mathrm{C}_1\mathbf{B} \tag{3.28}$$

Cauchy stress differences are given with respect to principal stretches, and can be calculated as;

$$\sigma_{11} - \sigma_{33} = \lambda_1.\frac{\partial\psi}{\partial\lambda_1} - \lambda_3.\frac{\partial\psi}{\partial\lambda_3}, \tag{3.29}$$

$$\sigma_{22} - \sigma_{33} = \lambda_{22}.\frac{\partial\psi}{\partial\lambda_{22}} - \lambda_{33}.\frac{\partial\psi}{\partial\lambda_{33}}$$

and strain energy density function can be rewritten in terms of principal stretches as;

$$\psi = \mathrm{C}_1(\lambda_1^2 + \lambda_2^2 + \lambda_3^2 - 3) \text{ and } \mathrm{J} = \det(\mathbf{F}) = \lambda_1\lambda_2\lambda_3 = 1 \tag{3.30}$$

therefore;

$$\frac{\partial\psi}{\partial\lambda_1} = 2\mathrm{C}_1\lambda_1 \qquad \frac{\partial\psi}{\partial\lambda_2} = 2\mathrm{C}_1\lambda_2 \qquad \frac{\partial\psi}{\partial\lambda_3} = 2\mathrm{C}_1\lambda_3 \tag{3.31}$$

and substituting equation (3.31) into (3.29), stress differences becomes;

$$\sigma_{11} - \sigma_{33} = 2\mathrm{C}_1(\lambda_1^2 - \lambda_3^2) \qquad \sigma_{22} - \sigma_{33} = 2\mathrm{C}_1(\lambda_2^2 - \lambda_3^2) \tag{3.32}$$

For uniaxial extension, the principal stretches are;

$$\lambda_1 = \lambda, \qquad \lambda_2 = \lambda_3 = \sqrt{\frac{1}{\lambda}} \tag{3.33}$$

substituting equation (3.33) to (3.29), stress differences becomes;

$$\sigma_{11} - \sigma_{33} = 2\mathrm{C}_1\left(\lambda^2 - \frac{1}{\lambda}\right), \qquad \sigma_{22} - \sigma_{33} = 0 \tag{3.34}$$

for small deformations ε << 1;

$$\sigma_{11} \approx 6\mathrm{C}_1\varepsilon = 3\mu\varepsilon = 3\frac{\mathrm{E}}{2(1+\nu)}\varepsilon \tag{3.35}$$

where ν is the Poisson's ratio and it is 0.5 for hyperelastic materials (this value is mathematically impossible for linear elastic materials). From this equation it is clear that, for small strains Neo-Hookean model gives Hooke's Law and this proves that it is a broadened version of Hooke's Law for large deformations.

For equibiaxial extension;

$$\lambda_1 = \lambda_2 = \lambda, \qquad \lambda_3 = \frac{1}{\lambda^2} \tag{3.36}$$

and for stress differences, when the same substitutions are made, they become

$$\sigma_{11}-\sigma_{22}=0, \qquad \sigma_{11}-\sigma_{33}=2C_1\left(\lambda^2-\frac{1}{\lambda^4}\right) \tag{3.37}$$

and under plane stress conditions;

$$\sigma_{11}=2C_1\left(\lambda^2-\frac{1}{\lambda^4}\right) \tag{3.38}$$

For simple shear;

$$\mathbf{F}=\begin{bmatrix}1 & \gamma & 0\\ 0 & 1 & 0\\ 0 & 0 & 1\end{bmatrix} \tag{3.39}$$

$$\mathbf{B}=\mathbf{F}\mathbf{F}^{\mathbf{T}}=\begin{bmatrix}1+\gamma^2 & \gamma & 0\\ \gamma & 1 & 0\\ 0 & 0 & 1\end{bmatrix} \tag{3.40}$$

where γ is the shear angle on the xy plane, thus Cauchy stress becomes;

$$\boldsymbol{\sigma}=\begin{bmatrix}-p+2C_1(1+\gamma^2) & 2C_1\gamma & 0\\ 2C_1\gamma & -p+2C_1 & 0\\ 0 & 0 & -p+2C_1\end{bmatrix} \tag{3.41}$$

3.1.2.2 Mooney-Rivlin solid

Mooney-Rivlin Model is a hyperelastic model in which strain energy density function is a polynomial of two invariants of left Cauchy-Green deformation tensor B [30]. It is a special case of generalized Rivlin model (also known as polynomial hyperelastic model [31]) and has the form;

$$\psi=\sum_{p,q=0}^{N} C_{pq}(\bar{I}_1-3)^p(\bar{I}_2-3)^q+\sum_{m=1}^{M} D_m(J-1)^{2m} \tag{3.42}$$

$$\bar{I}_1=J^{-\frac{2}{3}}\,I_1, \qquad \bar{I}_2=J^{-\frac{4}{3}}\,I_2 \tag{3.43}$$

C_{00} and C_{pq} are the distortional material constants, D_m are the volumetric material constants. N=M=1 gives the special form of isotropic incompressible Mooney-Rivlin material model;

$$\psi=C_{01}(I_1-3)+C_{10}(I_2-3) \tag{3.44}$$

For consistency with linear elasticity;

$$C_{01}+C_{10}=\frac{\mu}{2} \tag{3.45}$$

For an incompressible Mooney-Rivlin solid, Cauchy stress becomes;

$$\boldsymbol{\sigma}=-p\,\mathbf{I}+2[(C_{01}+I_1C_{10})\mathbf{B}-C_{10}\mathbf{B}.\mathbf{B}] \tag{3.46}$$

For uniaxial extension, the principal stretches are;

$$\lambda_1 = \lambda, \qquad \lambda_2 = \lambda_3 = \sqrt{\frac{1}{\lambda}} \tag{3.47}$$

$$\sigma_{11} - \sigma_{33} = 2C_{01}\left(\lambda^2 - \frac{1}{\lambda^2}\right) - 2C_{10}\left(\lambda^2 - \frac{1}{\lambda^2}\right) \tag{3.48}$$

In case of simple extension;

$$\sigma_{22} = \sigma_{33} = 0 \tag{3.49}$$

$$\sigma_{11} = 2C_{01}\left(\lambda^2 - \frac{1}{\lambda^2}\right) - 2C_{10}\left(\lambda^2 - \frac{1}{\lambda^2}\right) \tag{3.50}$$

For equibiaxial extension;

$$\sigma_{11} - \sigma_{33} = \sigma_{22} - \sigma_{33} = 2C_{01}\left(\lambda^2 - \frac{1}{\lambda^4}\right) - 2C_{10}\left(\lambda^2 - \frac{1}{\lambda^4}\right) \tag{3.51}$$

For simple shear using equation (3.40) and equation (3.46);

$$\sigma_{11} = -p + 2\{[C_{01} + (1+\gamma^2)\,C_{10}][1+\gamma^2] - C_{10}[(1+\gamma^2)^2 + \gamma^2]\} \tag{3.52}$$

$$\sigma_{22} = -p + 2\{[C_{01} + (1+\gamma^2)\,C_{10}] - C_{10}(1+\gamma^2)\} \tag{3.53}$$

$$\sigma_{33} = -p + 2\{C_{01} + \gamma^2\,C_{10}\} \tag{3.54}$$

$$\sigma_{12} = \sigma_{21} = 2\{[C_{01} + (1+\gamma^2)\,C_{10}]\gamma - C_{10}[\gamma(1+\gamma^2) + \gamma]\} \tag{3.55}$$

3.1.2.3 Yeoh solid

Yeoh material model is another special case of generalized Mooney-Rivlin model with M=3, N=0, and a phenomenological model works best for nearly incompressible materials (that is why N=0).

$$\Psi = C_1(I_1 - 3) + C_2(I_1 - 3)^2 + C_3(I_1 - 3)^3 \tag{3.56}$$

For an incompressible Yeoh solid, Cauchy stress becomes;

$$\boldsymbol{\sigma} = -p\mathbf{I} + 2[(C_1 I_1 + 2C_2 I_1(I_1 - 3) + 3C_3 I_1(I_1 - 3)^2)]\mathbf{B} \tag{3.57}$$

$$\boldsymbol{\sigma} = -p\mathbf{I} + 2[(C_1 - 6C_2 + 18C_3)I_1 + (2C_2 - 9C_3)I_1^2 + 3C_3 I_1^3]\mathbf{B} \tag{3.58}$$

For consistency with linear elasticity;

$$\mu = 2C_1 + 4C_2(I_1 - 3) + 6C_3(I_1 - 3)^2 \tag{3.59}$$

For uniaxial extension;

$$I_1 = \lambda^2 + \frac{2}{\lambda} \tag{3.60}$$

In case of simple extension;

$$\sigma_{22} = \sigma_{33} = -p + \frac{2}{\lambda}\frac{\partial\psi}{\partial I_1} = 0 \tag{3.61}$$

therefore;

$$p = \frac{2}{\lambda}\frac{\partial\psi}{\partial I_1} \tag{3.62}$$

$$\sigma_{11} = -p + 2\lambda^2\frac{\partial\psi}{\partial I_1} = 2\left(\lambda^2 - \frac{1}{\lambda}\right)\frac{\partial\psi}{\partial I_1} \tag{3.63}$$

For equibiaxial extension;

$$I_1 = 2\lambda^2 + \frac{1}{\lambda^2} \tag{3.64}$$

$$\sigma_{33} = -p + \frac{2}{\lambda^4}\frac{\partial\psi}{\partial I_1} = 0 \tag{3.65}$$

which gives;

$$p = \frac{2}{\lambda^4}\frac{\partial\psi}{\partial I_1} \tag{3.66}$$

therefore;

$$\sigma_{11} = \sigma_{22} = -p + 2\lambda^2\frac{\partial\psi}{\partial I_1} = 2\left(\lambda^2 - \frac{1}{\lambda^4}\right)\frac{\partial\psi}{\partial I_1} \tag{3.67}$$

For simple shear, using equation (3.40) and (3.58);

$$\begin{aligned}\sigma_{11} = -p + 2\{[C_1 - 6C_2 + 18C_3](1+\gamma^2)^2 + [2C_2 \\ - 9C_3](1+\gamma^2)^3 + 3C_3(1+\gamma^2)^4\}\end{aligned} \tag{3.68}$$

$$\begin{aligned}\sigma_{22} = \sigma_{33} = -p \\ + 2\{[C_1 - 6C_2 + 18C_3](1+\gamma^2) + [2C_2 \\ - 9C_3](1+\gamma^2)^2 + 3C_3(1+\gamma^2)^3\}\end{aligned} \tag{3.69}$$

$$\begin{aligned}\sigma_{12} = \sigma_{21} = 2\{[C_1 - 6C_2 + 18C_3](1+\gamma^2) + [2C_2 \\ - 9C_3](1+\gamma^2)^2 + 3C_3(1+\gamma^2)^3\}\gamma\end{aligned} \tag{3.70}$$

3.1.2.4 Gent solid

Gent hyperelastic material model assumes limited extension of elastomer chains. In Gent model when the limiting value I_m reaches to first invariant of left Cauchy-Green deformation tensor, strain energy density function becomes indefinite (since ln(0) is mathematically indefinite). This can be seen on;

$$\psi = -\frac{\mu J_m}{2}\ln\left(1 - \frac{I_1 - 3}{J_m}\right) \tag{3.71}$$

where

$$J_m = I_m - 3 \tag{3.72}$$

for incompressible Gent solid, Cauchy stress becomes;

$$\boldsymbol{\sigma} = -p\mathbf{I} + \frac{\mu J_m}{J_m - I_1 + 3}\mathbf{B} \tag{3.73}$$

For uniaxial extension;

$$\sigma_{11} = -p + \frac{\lambda^2 \mu J_m}{J_m - I_1 + 3}, \qquad \sigma_{22} = \sigma_{33} = -p + \frac{\mu J_m}{\lambda(J_m - I_1 + 3)} \tag{3.74}$$

In case of simple extension;

$$\sigma_{22} = \sigma_{33} = 0 \tag{3.75}$$

which gives;

$$p = \frac{\mu J_m}{\lambda(J_m - I_1 + 3)} \tag{3.76}$$

therefore;

$$\sigma_{11} = \left(\lambda^2 - \frac{1}{\lambda}\right)\frac{\mu J_m}{J_m - I_1 + 3} \tag{3.77}$$

For equibiaxial extension;

$$I_1 = 2\lambda^2 - \frac{1}{\lambda^4} \tag{3.78}$$

$$\sigma_{33} = -p + \frac{\mu J_m}{\lambda^4(J_m - I_1 + 3)} = 0 \tag{3.79}$$

$$p = \frac{\mu J_m}{\lambda^4(J_m - I_1 + 3)} \tag{3.80}$$

$$\sigma_{11} = \sigma_{22} = \left(\lambda^2 - \frac{1}{\lambda^4}\right)\frac{\mu J_m}{J_m - I_1 + 3} \tag{3.81}$$

For simple shear, using equation (3.40) and (3.73);

$$\sigma_{11} = -p + \frac{\mu J_m}{J_m - 2 - \gamma^2}(1 + \gamma^2) \tag{3.82}$$

$$\sigma_{22} = \sigma_{33} = -p + \frac{\mu J_m}{J_m - 2 - \gamma^2} \tag{3.83}$$

$$\sigma_{12} = \sigma_{21} = \frac{\mu J_m \gamma}{J_m - 2 - \gamma^2} \tag{3.84}$$

3.2 Reinforced Hyperelastic Materials

3.2.1 Transversely isotropic materials

Transversely isotropic materials consist of a matrix of main material and a family (or families) of fibres oriented in a specific direction. The term transversely isotropic means that the strength of material under load is not the same in every direction and it is related directly to the orientations of fibre families. The strength of fibres (orientation, material properties, etc.) affects the overall strength differently in every direction, and evidently, the resulting deformation. This change can be seen in Fig. 2 where $\overrightarrow{a_0}$ is initial fibre orientation, $\vec{a}$ is the deformed fibre orientation, λ is the stretch of fibre and **F** is the deformation gradient tensor.

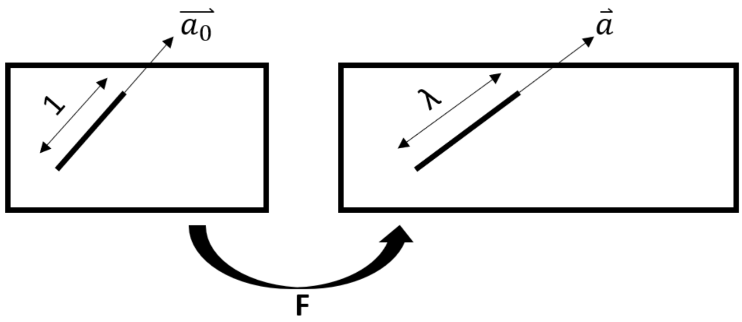

Figure 3.2 : The change in fibre orientation with deformation.

For this deformation;

$$|\mathbf{a_0}| = |\mathbf{a}| = 1 \tag{3.85}$$

$$\lambda\mathbf{a}(\mathbf{x},t) = \mathbf{F}(\mathbf{X},t)\mathbf{a_0}(\mathbf{X}) \tag{3.86}$$

$$\lambda^2 = \mathbf{a_0}\mathbf{F}^{T}\mathbf{F}\mathbf{a_0} \tag{3.87}$$

$$\lambda^2 = \mathbf{a_0}\mathbf{C}\mathbf{a_0} \tag{3.88}$$

The stretch of fibres also contributes to the stored energy, therefore, strain energy density function. ψ should be defined as an objective and frame indifferent function fibre structures [32].

$$\psi = f(\mathbf{C}; \mathbf{a_0} \otimes \mathbf{a_0}) \tag{3.89}$$

3.2.2 Hyperleastic materials with 2 families of reinforcements

Adding fibre families results the definition of new pseudo invariants[32] over basic three invariants;

$$I_4 = \lambda^2 = \mathbf{a_0}\mathbf{C}\mathbf{a_0} \tag{3.90}$$

$$I_5 = \mathbf{a_0}\mathbf{C}^2\mathbf{a_0} \tag{3.91}$$

$$I_6 = \mathbf{g_0}\mathbf{C}\mathbf{g_0} \tag{3.92}$$

$$I_7 = \mathbf{g_0}\mathbf{C}^2\mathbf{g_0} \tag{3.93}$$

$$I_8 = \mathbf{a_0}\mathbf{C}\mathbf{g_0} \tag{3.94}$$

$$I_9 = (\mathbf{a_0}\mathbf{g_0})^2 \tag{3.95}$$

where $\mathbf{g_0}$ is the initial direction of fibre family 2 and

I_4 is stretch of fibre family 1,

I_5 is fibre family 1 – matrix interaction,

I_6 is the stretch of fibre family 2,

I_7 is fibre family 2 – matrix interaction,

I_8 is cross interaction between fibre families,

I_9 is not related to deformation, it is just a measure of invariants [32].

For an isotropic incompressible fibre reinforced hyperelastic material (with one fibre family), the strain energy density function and Cauchy stress becomes;

$$\psi = \psi(I_1; I_2; I_4; I_5) - \frac{1}{2}p(I_3 - 1) \tag{3.96}$$

$$\boldsymbol{\sigma} = -p\mathbf{I} + 2\left[\frac{\partial\psi}{\partial I_1}\mathbf{B} - 2\frac{\partial\psi}{\partial I_2}\mathbf{B}^2 + I_4\frac{\partial\psi}{\partial I_4}(\mathbf{a}\otimes\mathbf{a}) + I_5\frac{\partial\psi}{\partial I_5}(\mathbf{aB}\otimes\mathbf{a} + \mathbf{a}\otimes\mathbf{Ba})\right] \tag{3.97}$$

As it can be seen, strain energy density function and Cauchy stress are the broadened versions of isotropic equation. If we add inextensibility of fibre, meaning λ=1, (3.96) and (3.97) becomes;

$$\psi = \psi(I_1; I_2; I_5) - \frac{1}{2}p(I_3 - 1) - \frac{1}{2}q(I_4 - 1) \tag{3.98}$$

$$\boldsymbol{\sigma} = -p\mathbf{I} + 2\left[\frac{\partial\psi}{\partial I_1}\mathbf{B} - 2\frac{\partial\psi}{\partial I_2}\mathbf{B}^2 + \frac{q}{2}(\mathbf{a}\otimes\mathbf{a}) + I_5\frac{\partial\psi}{\partial I_5}(\mathbf{aB}\otimes\mathbf{a} + \mathbf{a}\otimes\mathbf{Ba})\right] \tag{3.99}$$

where q is the stress found for constrained fibre extensions.

With two different fibre families, for incompressible hyperelastic materials, the relations become;

$$\psi = \psi(I_1; I_2; I_4; I_5; I_6; I_7; I_8) - \frac{1}{2}p(I_3 - 1) \tag{3.100}$$

$$\begin{aligned}\boldsymbol{\sigma} = -p\mathbf{I} + 2\Big[&\frac{\partial\psi}{\partial I_1}\mathbf{B} - 2\frac{\partial\psi}{\partial I_2}\mathbf{B}^2 + I_4\frac{\partial\psi}{\partial I_4}(\mathbf{a}\otimes\mathbf{a}) \\ &+ I_5\frac{\partial\psi}{\partial I_5}(\mathbf{aB}\otimes\mathbf{a} + \mathbf{a}\otimes\mathbf{Ba}) + I_6\frac{\partial\psi}{\partial I_6}(\mathbf{g}\otimes\mathbf{g}) \\ &+ I_7\frac{\partial\psi}{\partial I_7}(\mathbf{gB}\otimes\mathbf{g} + \mathbf{g}\otimes\mathbf{Bg}) + \frac{1}{2}I_8\frac{\partial\psi}{\partial I_8}(\mathbf{a}.\mathbf{g})(\mathbf{a} \\ &\otimes\mathbf{g} + \mathbf{g}\otimes\mathbf{a}\Big]\end{aligned} \tag{3.101}$$

And for inextensible two families of fibre ($I_4 = I_6 = 1$);

$$\psi = \psi(I_1; I_2; I_5; I_7) - \frac{1}{2}p(I_3 - 1) - \frac{1}{2}q_1(I_4 - 1) - \frac{1}{2}q_2(I_6 - 1) \tag{3.102}$$

$$\boldsymbol{\sigma} = -p\mathbf{I} + 2\left[\frac{\partial\psi}{\partial I_1}\mathbf{B} - 2\frac{\partial\psi}{\partial I_2}\mathbf{B}^2 - \frac{1}{2}q_1(\mathbf{a}\otimes\mathbf{a}) - \frac{1}{2}q_2(\mathbf{g}\otimes\mathbf{g}) + I_5\frac{\partial\psi}{\partial I_5}(\mathbf{aB}\otimes\mathbf{a} + \mathbf{a}\otimes\mathbf{Ba}) + I_7\frac{\partial\psi}{\partial I_7}(\mathbf{gB}\otimes\mathbf{g} + \mathbf{g}\otimes\mathbf{Bg})\right] \tag{3.103}$$

In case of two family of fibres, if the fibres are orthogonal to each other, then $I_9=0$. However, different materials may result in orthogonal material behaviour even tough fibres are not orthogonal. Also, the symmetry of fibres families results in same stress for inextensible fibres ($q_1=q_2$).

3.3 Electromagnetism and Maxwell Stress

3.3.1 Electromagnetic theory

Electromagnetism studies the physics of electromagnetic particles and their interaction between them. The force between charged particles, known as electromagnetic force, is a vector field, which is a combination of electricity and magnetism. It is one of the four fundamental forces that explains the nature of the universe together with the weak force, strong force and gravitation. At first, electricity and magnetism thought to be separate concepts, however in 1873 A Treatise on Electricity and Magnetism by James Clerk Maxwell postulated that they are combined and works in tandem.

In electricity, particles with opposite charges attract and particles with same charges repel each other. The influence of a charged particle to its surrounding charged particles can be quantified and described as;

$$₣ = q\mathbb{E} \tag{3.104}$$

where ₣ is force, q is the charge of the particle and $\mathbb{E}$ is the electric field.

Magnetism differs from electricity on some working principles. Charged particles are monopoles but magnetic particles are dipoles (north and south) meaning the interaction happens between two poles of a particles and/or opposite poles of different particles.

The magnetic field is a field from the north pole to the south pole. Similar to electricity, opposite poles attract, and same poles repel.

A change in electric field can create magnetic field and vice versa. An electric charge moving in a electro-magnetic field has a force exerted on it and it is defined as Lorentz force;

$$\mathbf{F} = q(\mathbb{E} + \mathbf{v} \times \boldsymbol{\mathcal{B}}) \tag{3.105}$$

where v is the velocity vector of particle and $\boldsymbol{\mathcal{B}}$ is the magnetic field. Electric and magnetic field are orthogonal vectors.

Maxwell’s theory of electromagnetism consists of 4 fundamental laws,

1. Gauss’s Law states that a charged particle creates an electric field around it.

$$\oiint \mathbb{E} d\mathbf{A} = \frac{1}{\varepsilon_0} \iiint \rho dV \tag{3.106}$$

$$\nabla . \mathbb{E} = \frac{\rho}{\varepsilon_0} \tag{3.107}$$

where d**A** is the infinitesimal area, ε_0 is the electric permittivity, ρ is charge density and dV is the infinitesimal volume.

2. Gauss’s Law for magnetism states that divergence of magnetic field is zero, meaning magnetic field is a solenoidal vector i.e. magnetic monopoles does not exist.

$$\oiint \boldsymbol{\mathcal{B}} d\mathbf{A} = 0 \tag{3.108}$$

$$\nabla . \boldsymbol{\mathcal{B}} = 0 \tag{3.109}$$

3. Faraday’s Law states that a change in electric field creates magnetic field.

$$\oint \mathbb{E} dl = \int \frac{\partial \boldsymbol{\mathcal{B}}}{\partial t} dA \tag{3.110}$$

$$\nabla x \mathbb{E} = -\frac{\partial \boldsymbol{\mathcal{B}}}{\partial t} \tag{3.111}$$

4. Ampere-Maxwell Law states that electric currents and electric field change create magnetic field.

$$\oint \boldsymbol{\mathcal{B}} dl = \mu_{\mathbf{0}} \iint \mathbf{J_c} dA + \mu_{\mathbf{0}} \varepsilon_{\mathbf{0}} \frac{d}{dt} \iint \mathbb{E} dA \tag{3.112}$$

$$\nabla x \boldsymbol{\mathcal{B}} = \mu_{\mathbf{0}} \left(\mathbf{J_c} + \varepsilon_0 \frac{\partial \mathbb{E}}{\partial t} \right) \tag{3.113}$$

where $\mathbf{J_c}$ is current density and $\mu_{\mathbf{0}}$ is magnetic constant.

3.3.2 Maxwell Stress

Maxwell stress is the stress on a dielectric material created by an electromagnetic field exerted on it. The tensor is derived from the fundamental laws of electromagnetism. If equation (3.84) is rewritten as a per volume version;

$$\mathbf{f} = \rho\mathbb{E} + \mathbf{J_c} x \boldsymbol{\mathcal{B}} \tag{3.114}$$

Substituting ρ using equation (3.107) and **J** using equation (3.113);

$$\mathbf{f} = \varepsilon_0(\nabla.\mathbb{E})\mathbb{E} + \frac{1}{\mu_0}(\nabla \text{ x } \boldsymbol{\mathcal{B}})\text{x } \boldsymbol{\mathcal{B}} - \varepsilon_0\frac{\partial\mathbb{E}}{\partial t} \text{ x } \boldsymbol{\mathcal{B}} \tag{3.115}$$

rewriting time derivative of $\mathbb{E}$**;**

$$\mathbf{f} = \varepsilon_0(\nabla.\mathbb{E})\mathbb{E} + \frac{1}{\mu_0}(\nabla \text{ x } \boldsymbol{\mathcal{B}})\text{x } \boldsymbol{\mathcal{B}} - \varepsilon_0\frac{\partial}{\partial t}(\mathbb{E} \text{ x } \boldsymbol{\mathcal{B}}) \tag{3.116}$$

$$- \varepsilon_0 \, \mathbb{E} \text{ x } (\nabla \text{ x } \mathbb{E})$$

rearranging;

$$\mathbf{f} = \varepsilon_0[(\nabla.\mathbb{E})\mathbb{E} - \mathbb{E} \text{ x } (\nabla \text{ x } \mathbb{E})] + \frac{1}{\mu_0}[(\nabla \text{ x } \boldsymbol{\mathcal{B}})\text{x } \boldsymbol{\mathcal{B}}] \tag{3.117}$$

$$- \varepsilon_0\frac{\partial}{\partial t}(\mathbb{E} \text{ x } \boldsymbol{\mathcal{B}})$$

to reassure symmetry for $\mathbb{E}$ and **B**, adding Gauss's Law for magnetism;

$$\mathbf{f} = \varepsilon_0[(\nabla.\mathbb{E})\mathbb{E} - \mathbb{E} \text{ x } (\nabla \text{ x } \mathbb{E})] + \frac{1}{\mu_0}[(\nabla.\boldsymbol{\mathcal{B}})\boldsymbol{\mathcal{B}} - \boldsymbol{\mathcal{B}} \text{ x } (\nabla \text{ x } \boldsymbol{\mathcal{B}})] \tag{3.118}$$

$$- \varepsilon_0\frac{\partial}{\partial t}(\mathbb{E} \text{ x } \boldsymbol{\mathcal{B}})$$

using vector identities from tensor calculus;

$$\mathbb{E} \text{ x } (\nabla \text{ x } \mathbb{E}) = \frac{1}{2}\nabla(\mathbb{E}^2) - (\mathbb{E}.\nabla)\mathbb{E} \tag{3.119}$$

$$\boldsymbol{\mathcal{B}} \text{ x } (\nabla \text{ x } \mathbb{E}) = \frac{1}{2}\nabla(\boldsymbol{\mathcal{B}}^2) - (\boldsymbol{\mathcal{B}}.\nabla)\boldsymbol{\mathcal{B}} \tag{3.120}$$

substituting equation (3.119) and (3.120) into (3.118);

$$\mathbf{f} = \varepsilon_0[(\nabla.\mathbb{E})\mathbb{E} + (\mathbb{E}.\nabla)\mathbb{E}] + \frac{1}{\mu_0}[(\nabla.\boldsymbol{\mathcal{B}})\boldsymbol{\mathcal{B}} + (\boldsymbol{\mathcal{B}}.\nabla)\boldsymbol{\mathcal{B}}] \tag{3.121}$$

$$- \frac{1}{2}\nabla\left(\varepsilon_0\mathbb{E}^2 - \frac{1}{\mu_0}\boldsymbol{\mathcal{B}}^2\right) - \varepsilon_0\frac{\partial}{\partial t}(\mathbb{E} \text{ x } \boldsymbol{\mathcal{B}})$$

introducing the Maxwell stress tensor [33];

$$\sigma_{ij} = \varepsilon_0\left[E_iE_j - \frac{1}{2}\delta_{ij}E^2\right] + \frac{1}{\mu_0}\left[B_iB_j - \frac{1}{2}\delta_{ij}B^2\right] \tag{3.122}$$

omitting magnetism related part of equation (3.122) and rewriting to avoid confusion with standard continuum mechanics notation;

$$\sigma_{\max} = \varepsilon_0 \left[\mathbf{d} \otimes \mathbf{d} - \frac{1}{2} \mathbf{I}\mathbf{d}^2 \right] \tag{3.123}$$

where **d** is the electric field vector at the current configuration and **D** is the electric field vector at the initial configuration and have the relation $\mathbf{d}=\mathbf{F}^{-1}\mathbf{D}$.

Adding Maxwell stress tensor to Cauchy stress tensor for an incompressible isotropic hyperelastic material under an electric field gives the true stress as;

$$\boldsymbol{\sigma} = -\mathrm{p}\mathbf{I} + 2\left[\frac{\partial\psi}{\partial \mathrm{I}_1}\mathbf{B} - 2\frac{\partial\psi}{\partial \mathrm{I}_2}\mathbf{B}^2\right] + \varepsilon\left[\mathbf{d} \otimes \mathbf{d} - \frac{1}{2}\mathbf{I}\mathbf{d}^2\right] \tag{3.124}$$

In case of incompressible hyperelastic material reinforced with two fibre families;

$$\begin{aligned}\boldsymbol{\sigma} = -\mathrm{p}\mathbf{I} + 2\left[\frac{\partial\psi}{\partial \mathrm{I}_1}\mathbf{B} - 2\frac{\partial\psi}{\partial \mathrm{I}_2}\mathbf{B}^2\right] + \mathrm{I}_4\frac{\partial\psi}{\partial \mathrm{I}_4}(\mathbf{a} \otimes \mathbf{a}) \\ + \mathrm{I}_4\frac{\partial\psi}{\partial \mathrm{I}_5}(\mathbf{aB} \otimes \mathbf{a} + \mathbf{a} \otimes \mathbf{Ba}) + \mathrm{I}_6\frac{\partial\psi}{\partial \mathrm{I}_6}(\mathbf{g} \otimes \mathbf{g}) \\ + \mathrm{I}_6\frac{\partial\psi}{\partial \mathrm{I}_7}(\mathbf{gB} \otimes \mathbf{g} + \mathbf{g} \otimes \mathbf{Bg}) \\ + \varepsilon\left[\mathbf{d} \otimes \mathbf{d} - \frac{1}{2}\mathbf{I}\mathbf{d}^2\right]\end{aligned} \tag{3.125}$$

3.4 Finite Element Method

The Finite Element Method (FEM) is a numerical method developed to solve -mostly- engineering problems. FEM is used in a variety of engineering areas such as structural analysis, heat transfer, fluid dynamics and electromagnetic potential. The partial differential equations that explains these phenomena are analytically solvable for simple problems, however for complicated geometries and coupled problems, using a numerical method such as FEM is more optimal.

The main principle of FEM formulation is to divide the problem into smaller and simpler subs (elements) and combine the response of these subs as a system of algebraic equations using variational calculus to approximate the solution. It can be thought as an analogy of taking the integral to find the area under a curve with sum of infinitesimally narrow rectangular areas yet with finitely small elements. The approximation error approaches to zero when element number goes to infinity. However, since in engineering, the time consumed to solve a problem is also a limitation, to find a finite number fitting to the specific problem is wise hence the name Finite Element Method.

3.4.1 Shape function concept

Elements in FEM have basic and simple geometric shapes as line, triangle, quadrilateral, tetrahedron, hexahedron, etc. The combination of one or more type of these shapes approximate the problem geometry. The formulation of these shapes is defined as shape functions.

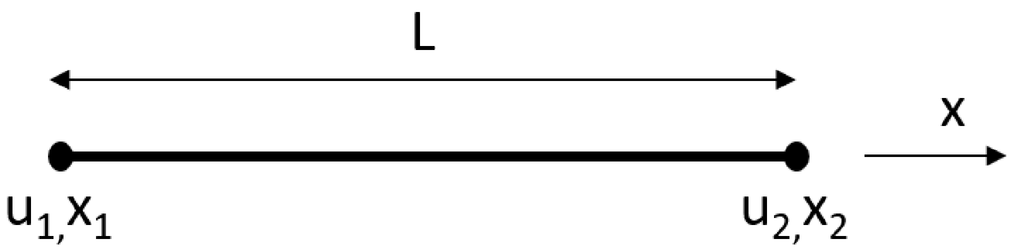

Figure 3.3 : FE representation of a 1D bar element.

Figure 3.3 shows a bar element that can only carry load in x direction, has a length of L, coordinates of left and right points (nodes 1 and 2 in FEM) are x_1 and x_2 and the displacements are u_1 and u_2, respectively. Let us assume the relation between the coordinate and displacement of any given point on the element is linear and can be described as;

$$u = a_1 + a_2 x \tag{3.126}$$

where a_1 and a_2 are coefficients to be found. Writing the equation in matrix form;

$$u = \begin{bmatrix} 1 & x \end{bmatrix} \begin{bmatrix} a_1 \\ a_2 \end{bmatrix} \tag{3.127}$$

If the equations for node 1 and 2 are written as a system of linear equations;

$$\begin{bmatrix} u_1 \\ u_2 \end{bmatrix} = \begin{bmatrix} 1 & x_1 \\ 1 & x_2 \end{bmatrix} \begin{bmatrix} a_1 \\ a_2 \end{bmatrix} \tag{3.128}$$

$$\begin{bmatrix} a_1 \\ a_2 \end{bmatrix} = \frac{1}{x_2 - x_1} \begin{bmatrix} x_2 & -x_1 \\ -1 & 1 \end{bmatrix} \begin{bmatrix} u_1 \\ u_2 \end{bmatrix} \tag{3.129}$$

Substituting equation (3.128) into (3.126);

$$u = \begin{bmatrix} 1 & x \end{bmatrix} \frac{1}{x_2 - x_1} \begin{bmatrix} x_2 & -x_1 \\ -1 & 1 \end{bmatrix} \begin{bmatrix} u_1 \\ u_2 \end{bmatrix} \tag{3.130}$$

Rearranging;

$$u = \frac{1}{L} \begin{bmatrix} 1 & x \end{bmatrix} \begin{bmatrix} x_2 & -x_1 \\ -1 & 1 \end{bmatrix} \begin{bmatrix} u_1 \\ u_2 \end{bmatrix} \tag{3.131}$$

$$u=\frac{1}{L}\begin{bmatrix}x_2-x & x-x_1\end{bmatrix}\begin{bmatrix}u_1\\u_2\end{bmatrix} \tag{3.132}$$

$$u=\begin{bmatrix}\frac{x_2-x}{L} & \frac{x-x_2}{L}\end{bmatrix}\begin{bmatrix}u_1\\u_2\end{bmatrix} \tag{3.133}$$

equation (3.132) defines the linear approximation of displacement of any given point on element. Rewriting this equation in generic form;

$$u=\begin{bmatrix}N_1 & N_2\end{bmatrix}\begin{bmatrix}u_1\\u_2\end{bmatrix} \tag{3.134}$$

$$\mathbf{N}=\begin{bmatrix}N_1 & N_2\end{bmatrix}=\begin{bmatrix}\frac{x_1-x}{L} & \frac{x-x_2}{L}\end{bmatrix} \tag{3.135}$$

where N_1 and N_2 are the shape functions of linear bar element.

3.4.2 Weak form and strong form

The differential equation for displacement in a linear elastic bar under axial load is;

$$\frac{d}{dx}\left(AE\frac{du}{dx}\right)+f=0 \text{ on } 0<x<l \tag{3.136}$$

where A is cross sectional area of bar, E is Young Modulus and f is axial load. This equation is called strong form of the problem. The integration of differential equation multiplied by the weight function, which is and arbitrary function, over the length and evanishing;

$$\int_0^l w\left[\frac{d}{dx}\left(AE\frac{du}{dx}\right)+f\right]dx=0 \text{ and } w(l)=0 \tag{3.137}$$

where w(x) is the weight function. If equation (3.136) is rearranged;

$$\int_0^l w\left[\frac{d}{dx}\left(AE\frac{du}{dx}\right)\right]dx+\int_0^l wfdx=0 \text{ and } w(l)=0 \tag{3.138}$$

$$\left(wAE\frac{du}{dx}\right)\Big|_0^l-\int_0^l\frac{dw}{dx}AE\frac{du}{dx}dx+\int_0^l wfdx=0 \text{ and } w(l)=0 \tag{3.139}$$

To simplify equation (3.138);

$$\frac{du}{dx}=\varepsilon(x) \tag{3.140}$$

$$\sigma(x)=E\varepsilon(x) \tag{3.141}$$

$$\sigma(0)=-\bar{t} \tag{3.142}$$

where $\bar{t}$ is traction (force per unit area).

Substituting equation (3.140) and (3.141) into (3.138);

$$(wA\sigma)_{x=l} - (wA\bar{t})_{x=0} - \int_0^l \frac{dw}{dx} AE \frac{du}{dx} dx + \int_0^l wfdx \tag{3.143}$$

$$= 0 \text{ and } w(l) = 0$$

It was assumed already that w(l)=0, therefore equation (3.142) becomes;

$$\int_0^l \frac{dw}{dx} AE \frac{du}{dx} dx + (wA\bar{t})_{x=0} - \int_0^l wfdx = 0 \text{ and } w(l) = 0 \tag{3.144}$$

Equation (3.121) is called the weak form of the problem. The first term of this equation is can be rewritten as energy operator and defined in matrix form as;

$$\int_0^l \mathbf{U}^T AE \mathbf{U} dx \tag{3.145}$$

3.4.3 Derivation of element stiffness matrix

Stiffness matrices are, as the name suggests, the mathematical formulation of mechanical properties for FEM. For a static problem, system of linear equations to be solved is given by [34];

$$\mathbf{Ku} = \mathbf{F} \tag{3.146}$$

where **K** is global stiffness matrix, **u** is displacement vector and **F** is applied force vector. Global stiffness matrix is the assembly of individual element stiffness matrices and combined with respect to element location and relations with neighbouring elements. Element stiffness matrix found by using energy operator as described below, for the previous example of bar element;

$$\mathbf{B_e} = \frac{d}{dx} \mathbf{N_e} = \begin{bmatrix} \frac{dN_{e_1}}{dx} & \frac{dN_{e_2}}{dx} \end{bmatrix} = \frac{1}{L_e} [-1 \quad 1] \tag{3.147}$$

where $\mathbf{B_e}$ is element strain matrix and $\mathbf{K_e}$ element stiffness matrix is;

$$\mathbf{K_e} = \int_0^l \frac{1}{L_e^2} \begin{bmatrix} -1 \\ 1 \end{bmatrix} AE [-1 \quad 1] dx \tag{3.148}$$

Rearranging equation (3.147);

$$\mathbf{K_e} = \frac{1}{L_e^2} \begin{bmatrix} -1 \\ 1 \end{bmatrix} [-1 \quad 1] \int_0^l AEdx \tag{3.149}$$

$$\mathbf{K_e} = \frac{1}{L_e^2} \begin{bmatrix} 1 & -1 \\ -1 & 1 \end{bmatrix} AEL_e \tag{3.150}$$

$$\mathbf{K_e} = \frac{AE}{L_e} \begin{bmatrix} 1 & -1 \\ -1 & 1 \end{bmatrix} \tag{3.151}$$

3.4.4 Derivation of stiffness matrix for a 1D incompressible Neo-Hookean bar element

Wriggers states the weak form for a hyperelastic bar element as [35];

$$\int_X \delta E_X S_X A dX - \int_X w_X b_X A dX - \sum_k w_{Xk} P_k = 0 \tag{3.152}$$

where δE_X is the variation of Green Strain Tensor, S is 2nd Piola-Kirchoff Stress Tensor, A is cross sectional area, w_X is the x component of weight function, b_X is body forces and P_k is nodal forces. Writing this equation with the symbols used before and for 1D;

$$\int_0^L \left(1 + \frac{\partial u}{\partial x}\right) \frac{\partial w}{\partial x} S_X A dX - \int_0^L wfAdX - \sum_k w_k P_k = 0 \tag{3.153}$$

Wriggers also gives the definition for the element stiffness matrix for 3D hyperelastic bar element as [35];

$$K_e^T = \begin{bmatrix} A_1 + A_2 & -(A_1 + A_2) \\ -(A_1 + A_2) & A_1 + A_2 \end{bmatrix} \tag{3.154}$$

and A_1 and A_2 are defined as;

$$\mathbf{A_1} = \frac{HA}{L_e} \begin{bmatrix} (1 + u_{e,x})^2 & (1 + u_{e,x}) v_{e,x} & (1 + u_{e,x}) w_{e,x} \\ (1 + u_{e,x}) v_{e,x} & v_{e,x}^2 & u_{e,x} w_{e,x} \\ (1 + u_{e,x}) w_{e,x} & u_{e,x} w_{e,x} & w_{e,x}^2 \end{bmatrix} \tag{3.155}$$

$$\mathbf{A_2} = \frac{S_x A}{L_e} \begin{bmatrix} 1 & 0 & 0 \\ 0 & 1 & 0 \\ 0 & 0 & 1 \end{bmatrix} \tag{3.156}$$

where H is tangent modulus and has the form $H = C_1 \lambda$ for the Neo-Hookean material [35]. Again, for 1D;

$$A_1 = \frac{HA}{L_e} (1 + u_{e,x})^2 \tag{3.157}$$

$$A_2 = \frac{S_x A}{L_e} \tag{3.158}$$

Taking the derivative of equation (3.132);

$$u_{e,x} = \frac{u_2 - u_1}{L} \tag{3.159}$$

Since the problem is in 1D, deformation gradient tensor becomes a zero-degree tensor (scalar) and

$$F = \lambda \tag{3.160}$$

and from equation (3.25) and (3.30);

$$\sigma_{11} = 2C_1\lambda^2 \tag{3.161}$$

and the transformation from Cauchy Stress to 2nd Piola-Kirchoff Stress;

$$\mathbf{S} = J\mathbf{F}^{-1}\boldsymbol{\sigma}\mathbf{F}^{-\mathbf{T}} \tag{3.162}$$

$$S_{11} = \frac{1}{\lambda^2}\sigma_{11} = 2C_1 \tag{3.163}$$

The stiffness matrix of 1D hyperelastic incompressible bar element becomes;

$$\mathbf{K_e} = \left[\frac{C_1\lambda A}{L_e}\left(1 + \frac{u_2 - u_1}{L_e}\right)^2 + \frac{2C_1A}{L_e}\right]\begin{bmatrix} 1 & -1 \\ -1 & 1 \end{bmatrix} \tag{3.164}$$

Finally, simplifying equation (3.164);

$$\mathbf{K_e} = (2 + \lambda^3)\frac{C_1A}{L_e}\begin{bmatrix} 1 & -1 \\ -1 & 1 \end{bmatrix} \tag{3.165}$$

For a linear elastic element, stiffness matrix is only dependent on material properties and element dimensions (see equation (3.151)). However, in case of finite strain, element stiffness matrix is a function of λ, which means element stiffness matrix depends on and changes with deformation for hyperelastic materials.

4. MATHEMATICAL MODEL FOR A CYLINDRICAL DEA UNDER INNER PRESSURE, AXIAL FORCE AND ELECTRIC LOAD

In this chapter, a mathematical model for an incompressible, reinforced with two inextensible fibre family cylindrical hollow DEA under inner pressure, axial tension and electrical load is generated. The DEA has the length L, thickness H and the mid surface radius of R, and is under axial load created by inner pressure and electric field exerted from the electrodes on the inner and outer surfaces (Fig. 4.1).

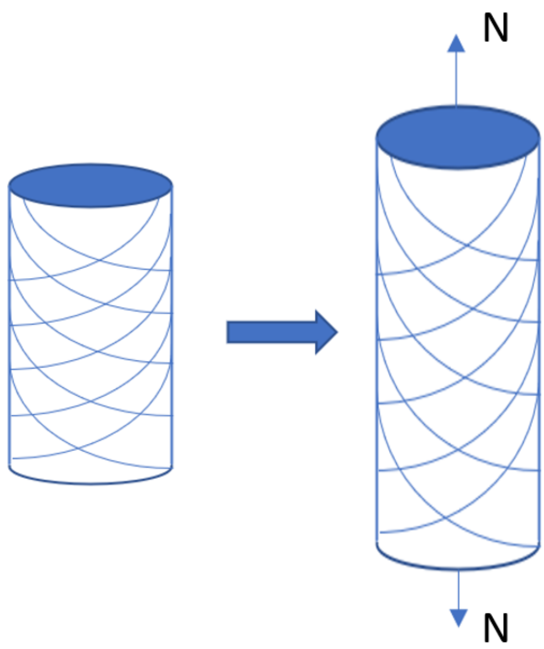

Figure 4.1 : Deformation of tubular DEA.

The geometry can be described in the initial configuration as;

$$A \leq R \leq B, \qquad 0 \leq \Theta \leq 2\pi, \qquad 0 \leq Z \leq L \tag{4.1}$$

where A is inner radius, B is outer radius, L is the length and R, Θ, Z are the initial coordinates. The deformation kinematics can be described as;

$$a \leq r \leq b, \qquad 0 \leq \theta \leq 2\pi, \qquad 0 \leq z \leq l \tag{4.2}$$

$$r = f(R), \qquad \theta = \Theta, \qquad z = \lambda_z Z \tag{4.3}$$

where small letter notations are deformed counterparts of initial configuration and λ_z is the axial stretch.

From incompressibility condition f(R), can be found as;

$$r = \left(\frac{R^2 - A^2}{\lambda} + a^2\right)^{\frac{1}{2}} \tag{4.4}$$

To find the solution, the polar decomposition of deformation gradient is considered since it will give a more general form for deformation gradient. For the right stretch tensor and rigid rotation tensor, instead of tube, a rectangular film of DEA is stretched, rotated to align with initial configuration coaxially and rolled up to a cylinder as seen in Fig. 4.2.

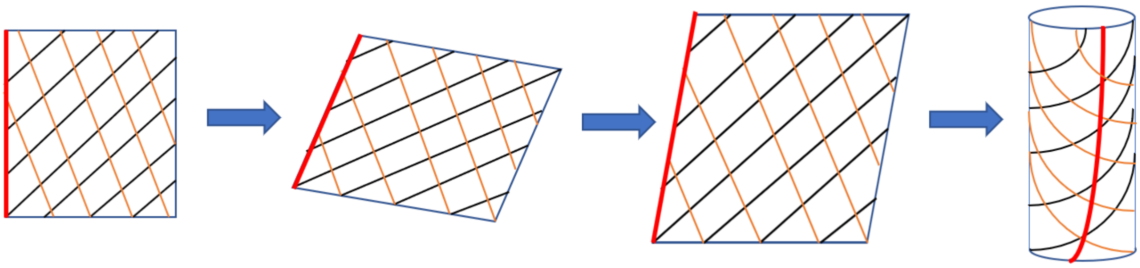

Figure 4.2 : Stretch-Rotation-Roll up for kinematic analysis.

Let us say the black family of fibres in Fig. 4.3 has the orientation vector of N_1 and has the angle with horizontal axis α_1, and orange family of fibres has the orientation vector N_2 and has the angle with horizontal axis α_2. As principal axis of deformation, vector N_f (has the equal angle between black and orange family) and vector M_f (orthogonal to N_f) are defined.

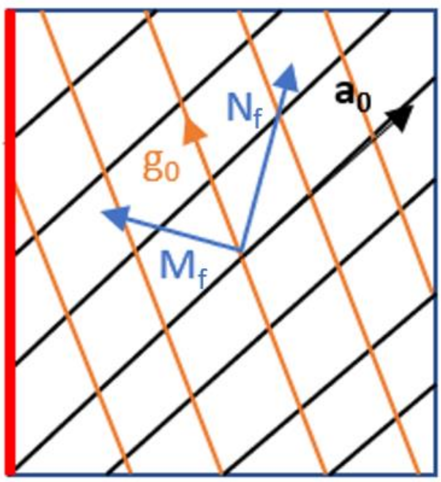

Figure 4.3 : Orientation vector of fibre families and deformation.

$$\mathbf{a_0} = \cos\alpha_1 \mathbf{e_1} + \sin\alpha_1 \mathbf{e_2}, \qquad \mathbf{g_0} = \cos\alpha_2 \mathbf{e_1} + \sin\alpha_2 \mathbf{e_2} \tag{4.5}$$

$$\mathbf{N_f} = \cos\alpha \mathbf{e_1} + \sin\alpha \mathbf{e_2}, \qquad \mathbf{M_f} = -\sin\alpha \mathbf{e_1} + \cos\alpha \mathbf{e_2} \tag{4.6}$$

where $\alpha = (\alpha_1 + \alpha_2)/2$.

The right stretch tensor is stated by He and Lau [38] as;

$$\mathbf{U} = \lambda_1 \mathbf{M_f} \otimes \mathbf{M_f} + \lambda_2 \mathbf{N_f} \otimes \mathbf{N_f} + \frac{1}{\lambda_1 \lambda_2} \mathbf{L} \otimes \mathbf{L} \tag{4.7}$$

where λ_1 and λ_2 are the principal stretches and $\mathbf{L}$ is the unit vector e_3.

The principal stretches can be calculated with respect to γ (the angle between fibre families after deformation) and $\gamma_0 = \alpha_2 - \alpha_1$ from geometry as;

$$\lambda_1 = \frac{\sin\left(\frac{\gamma}{2}\right)}{\sin\left(\frac{\gamma_0}{2}\right)}, \qquad \lambda_2 = \frac{\cos\left(\frac{\gamma}{2}\right)}{\cos\left(\frac{\gamma_0}{2}\right)} \tag{4.8}$$

The rotation angle β to rotate the stretched form to orient with undeformed form can be found from;

$$\mathbf{Ue_1} = (\lambda_1 \sin^2(\alpha) + \lambda_2 \cos^2(\alpha))\mathbf{e_1} + (\lambda_2 - \lambda_1)\cos\alpha \sin\alpha \mathbf{e_2} \tag{4.9}$$

$$\beta = \arctan\left(\frac{(\lambda_2 - \lambda_1)\cos\alpha \sin\alpha}{\lambda_1 \sin^2(\alpha) + \lambda_2 \cos^2(\alpha)}\right) \tag{4.10}$$

and $\mathbf{R}$ rotation tensor is;

$$\mathbf{R} = \mathbf{m_f} \otimes \mathbf{M_f} + \mathbf{n_f} \otimes \mathbf{N_f} + \mathbf{l} \otimes \mathbf{L} \tag{4.11}$$

where;

$$\mathbf{n_f} = \cos(\alpha + \beta)\mathbf{e_1} + \sin(\alpha + \beta)\mathbf{e_2}, \tag{4.12}$$

$$\mathbf{m_f} = -\sin(\alpha + \beta)\mathbf{e_1} + \cos(\alpha + \beta)\mathbf{e_2}$$

The deformation gradient tensor $\mathbf{F}$ is;

$$\mathbf{F} = \mathbf{RU} = \lambda_1 \mathbf{m_f} \otimes \mathbf{M_f} + \lambda_2 \mathbf{n_f} \otimes \mathbf{N_f} + \frac{1}{\lambda_1 \lambda_2} \mathbf{l} \otimes \mathbf{L} \tag{4.13}$$

And it can be written in cylindrical coordinates as;

$$\mathbf{F} = \mathbf{RU} = \lambda_1 \widetilde{\mathbf{m_f}} \otimes \widetilde{\mathbf{M_f}} + \lambda_2 \widetilde{\mathbf{n_f}} \otimes \widetilde{\mathbf{N_f}} + \frac{1}{\lambda_1 \boldsymbol{\lambda_2}} \tilde{\mathbf{l}} \otimes \tilde{\mathbf{L}} \tag{4.14}$$

where tilde forms of vectors are same as originals with unit vectors of $\mathbf{e_R}, \mathbf{e_\Theta}, \mathbf{e_Z}, \mathbf{e_r}, \mathbf{e_\theta}$ and $\mathbf{e_z}$

Therefore, the deformation gradient tensor $\mathbf{F}$ becomes;

$$\mathbf{F} = \begin{bmatrix} \frac{1}{\lambda_1 \lambda_2} & 0 & 0 \\ 0 & \begin{matrix} \lambda_1 \sin\alpha \sin(\alpha + \beta) \\ +\lambda_2 \cos\alpha \cos(\alpha + \beta) \end{matrix} & \begin{matrix} -\lambda_1 \cos\alpha \sin(\alpha + \beta) \\ \lambda_2 \sin\alpha \cos(\alpha + \beta) \end{matrix} \\ 0 & \begin{matrix} -\lambda_1 \sin\alpha \cos(\alpha + \beta) \\ \lambda_2 \cos\alpha \sin(\alpha + \beta) \end{matrix} & \begin{matrix} \lambda_1 \cos\alpha \cos(\alpha + \beta) \\ +\lambda_2 \sin\alpha \sin(\alpha + \beta) \end{matrix} \end{bmatrix} \tag{4.15}$$

and it can be deduced that;

$$\lambda_z = \lambda_1 \cos\alpha \cos(\alpha+\beta) + \lambda_2 \sin\alpha \sin(\alpha+\beta) \tag{4.16}$$

$$\lambda_\theta = \frac{r}{R} = \lambda_1 \sin\alpha \sin(\alpha+\beta) + \lambda_2 \cos\alpha \cos(\alpha+\beta) \tag{4.17}$$

From deformation gradient, Left Cauchy-Green deformation tensor can be calculated;

$$\mathbf{B} = \mathbf{F}\mathbf{F}^{\mathbf{T}} \tag{4.18}$$

$$= \begin{bmatrix} \frac{1}{\lambda_1^2\lambda_2^2} & 0 & 0 \\ 0 & \begin{matrix}\lambda_1^2 \sin^2(\alpha+\beta) \\ +\lambda_2^2 \cos^2(\alpha+\beta)\end{matrix} & \begin{matrix}\sin(\alpha+\beta)\cos(\alpha+\beta) \\ (\lambda_2^2-\lambda_1^2)\end{matrix} \\ 0 & \begin{matrix}\sin(\alpha+\beta)\cos(\alpha+\beta) \\ (\lambda_2^2-\lambda_1^2)\end{matrix} & \begin{matrix}\lambda_1^2 \cos^2(\alpha+\beta) \\ +\lambda_2^2 \sin^2(\alpha+\beta)\end{matrix} \end{bmatrix}$$

For this study, fibres are symmetrical in axial direction, therefore;

$$\alpha = \frac{\pi}{2}, \qquad \beta = 0 \tag{4.19}$$

$$\mathbf{F} = \begin{bmatrix} \frac{1}{\lambda_1\lambda_2} & 0 & 0 \\ 0 & \lambda_1 & 0 \\ 0 & 0 & \lambda_2 \end{bmatrix} \tag{4.20}$$

$$\mathbf{B} = \mathbf{F}\mathbf{F}^{\mathbf{T}} = \begin{bmatrix} \frac{1}{\lambda_1^2\lambda_2^2} & 0 & 0 \\ 0 & \lambda_1^2 & 0 \\ 0 & 0 & \lambda_2^2 \end{bmatrix} \tag{4.21}$$

$$\lambda_\theta = \frac{r}{R} = \lambda_1, \qquad \lambda_z = \lambda_2 \tag{4.22}$$

$$\mathbf{a} = \frac{\mathbf{F}\mathbf{a_0}}{norm(\mathbf{F}\mathbf{a_0})} = \frac{\mathbf{F}\mathbf{a_0}}{\sqrt{I_4}} = \frac{1}{\sqrt{I_4}} \left[\lambda_1 \sin\left(\frac{\gamma_0}{2}\right) + \lambda_2 \cos\left(\frac{\gamma_0}{2}\right)\right] \tag{4.23}$$

For the Neo-Hookean material, the strain energy density function with two fibre families is given as [37];

$$\psi = C_1(I_1 - 3) + \frac{E_1(I_4-1)^2}{4} + \frac{E_2(I_6-1)^2}{4} \tag{4.24}$$

where E_i is material modulus describing degree of anisotropy for fibres [37] and

$$I_4 = I_6 = \lambda_1^2 \sin^2\left(\frac{\gamma_0}{2}\right) + \lambda_2^2 \cos^2\left(\frac{\gamma_0}{2}\right) = I_f \tag{4.25}$$

combining equation (4.1), (4.16), (4.18) and (4.20), and substituting into (3.125);

$$\boldsymbol{\sigma} = -p\mathbf{I} + 2C_1\mathbf{B} + E_f I_f (I_f - 1)(\mathbf{a} \otimes \mathbf{a}) \tag{4.26}$$

$$+ E_f I_f (I_f - 1)(\mathbf{g} \otimes \mathbf{g}) + \varepsilon\left[\mathbf{d} \otimes \mathbf{d} - \frac{1}{2}\mathbf{I}\mathbf{d}^{\mathbf{2}}\right]$$

where **d** is the electrical field vector after deformation, and is calculated as shown in the equation (4.27).

$$\mathbf{d} = \mathbf{F}^{-1}\mathbf{D} = \begin{bmatrix} \mathrm{d_r} \\ 0 \\ 0 \end{bmatrix} \tag{4.27}$$

where d_r is the electrical field in the radial direction (through the thickness of the cylinder) and is defined as;

$$\mathrm{d_r} = \frac{\phi\lambda_1\lambda_2}{\mathrm{H}} \tag{4.28}$$

where ϕ is potential difference. In equation (4.25), there is only one term for fibres and the reason why is that the fibres families are made from same material, and thus invariants and metric tensors of orientation vectors at current configuration are equal due to symmetry.

From equation (4.21) and (4.24), and substituting current orientation vector of fibres as a function of N, M and γ, the components of Cauchy Stress tensor become;

$$\sigma_{\mathrm{rr}} = -\mathrm{p} + 2\mathrm{C}_1\frac{1}{\lambda_1^2\lambda_2^2} + \frac{\varepsilon}{2}\left(\frac{\phi}{\mathrm{H}}\right)^2\lambda_1^2\lambda_2^2 \tag{4.29}$$

$$\sigma_{\theta\theta} = -\mathrm{p} + 2\mathrm{C}_1\lambda_1^2 + \mathrm{E_f}(\mathrm{I_f} - 1)\lambda_1^2\sin^2\left(\frac{\gamma_0}{2}\right) - \frac{\varepsilon}{2}\left(\frac{\phi}{\mathrm{H}}\right)^2\lambda_1^2\lambda_2^2 \tag{4.30}$$

$$\sigma_{\mathrm{zz}} = -\mathrm{p} + 2\mathrm{C}_1\lambda_2^2 + \mathrm{E_f}(\mathrm{I_f} - 1)\lambda_2^2\cos^2\left(\frac{\gamma_0}{2}\right) - \frac{\varepsilon}{2}\left(\frac{\phi}{\mathrm{H}}\right)^2\lambda_1^2\lambda_2^2 \tag{4.31}$$

$$\sigma_{\theta\mathrm{z}} = \sigma_{\mathrm{z}\theta} = 0 \tag{4.32}$$

where $E_f = E_1 = E_2$. The inner pressure and axial force can be calculated without the lagrangian multiplier for incompressibility p as [39];

$$\mathrm{P} = \int_a^b (\sigma_{\theta\theta} - \sigma_{rr})\frac{dr}{r} \tag{4.33}$$

$$\mathrm{N} = \pi\int_a^b (2\sigma_{zz} - \sigma_{\theta\theta} - \sigma_{rr})rdr \tag{4.34}$$

These equations have two independent unknown variables λ_z and a. However, the results of above integrals are non-linear equations, therefore, a straightforward solution is not possible. This is why a numerical solution is generated by using equation (4.33) and (4.34) for two variables with the material parameters shown in Table 4.1 and 4.2. Figure 4.4 shows the fibre angle and some calculated values can be seen in Figure 4.5 through 4.9 for 0.025 MPa of inner pressure and 24 N of axial force for different fibre angles.

Table 4.1 : Neo-Hookean material constants for analytical solution.

C_1 [MPa]	D_1
0.2587	0.001583

Table 4.2 : Fibre properties for analytical solution.

Diameter [mm]	Fibre Number	Young Modulus [Mpa]
0.158	72	200

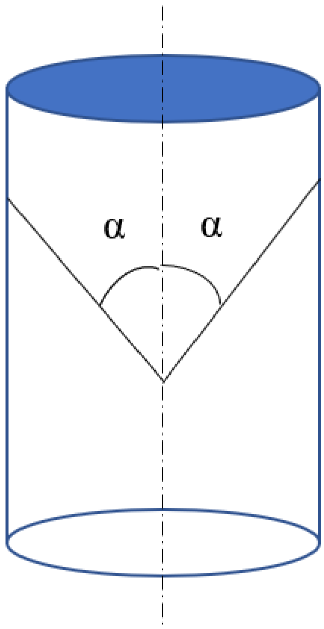

Figure 4.4 : Fibre orientations.

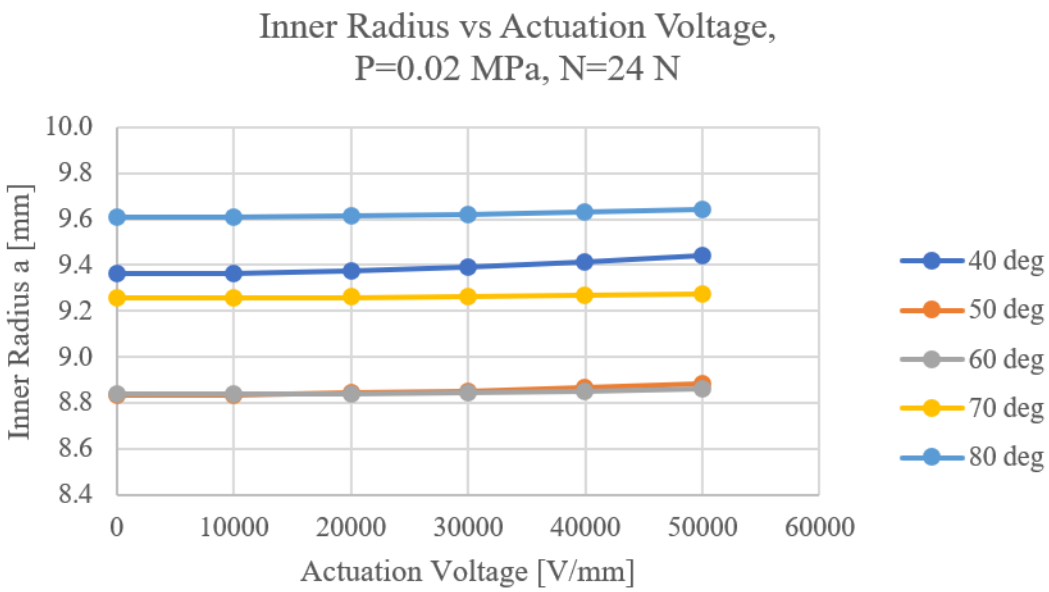

Figure 4.5 : Effect of actuation voltage on inner radius of the cylinder.

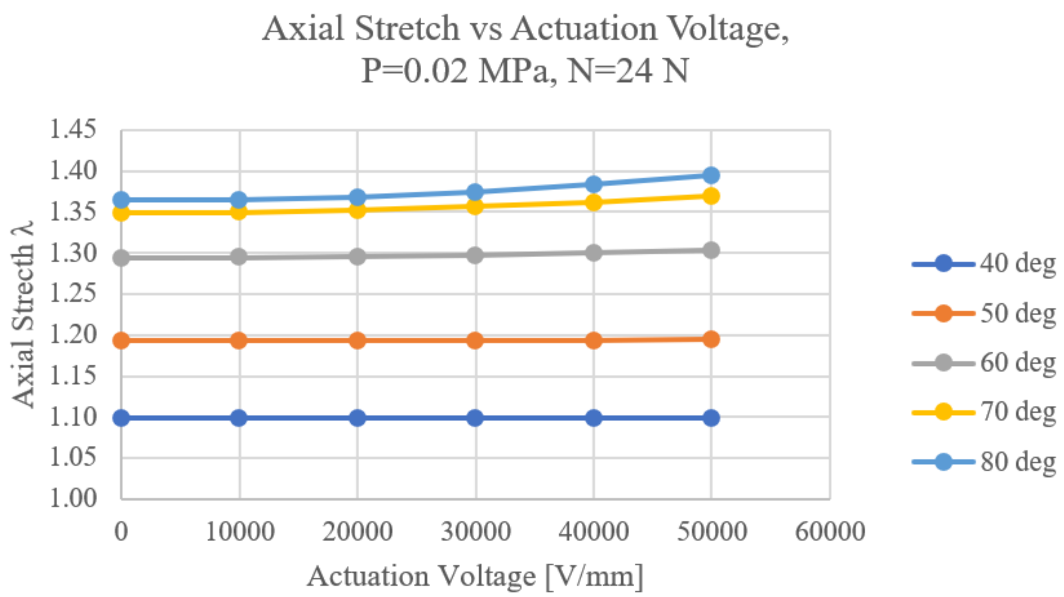

Figure 4.6 : Effect of actuation voltage on axial stretch.

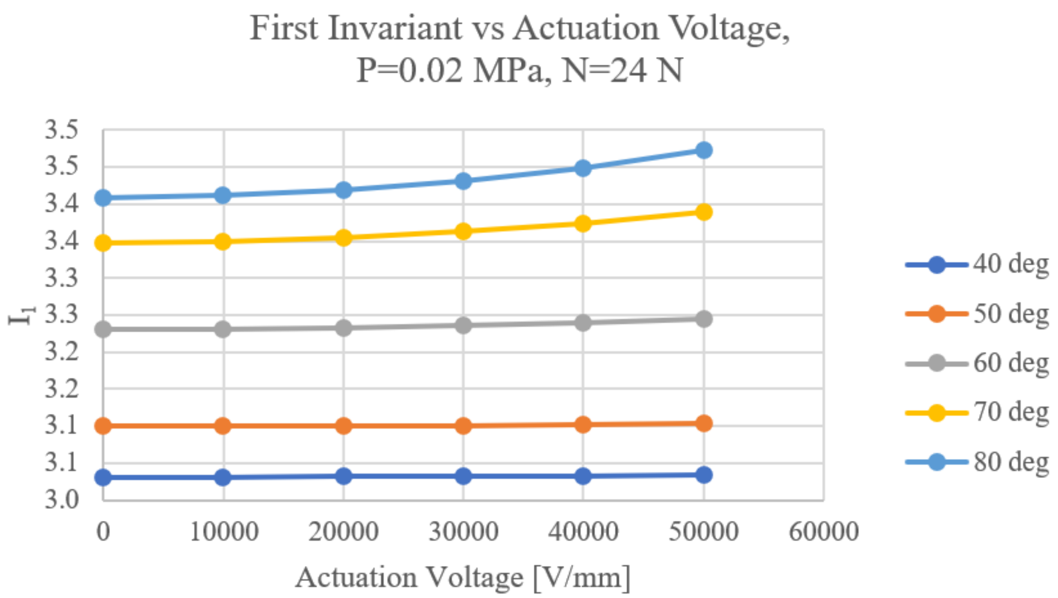

Figure 4.7 : Effect of actuation voltage on the first invariant of Left Cauchy-Green Deformation tensor.

Except inner radius, all the graphs shows similar behaviour, which an increase (or decrease for the stretch of fibres) as the fibres angles approaches 90 degrees i.e. parallel with axial direction. Only for the inner radius the model with 40 degrees fibre angle disprupts the pattern. The reason for this difference is that 40 degrees is very close to to 54°44' which is the fibre angle for axial expansion without radial expansion for cylindrical reinforced elastomers [16].

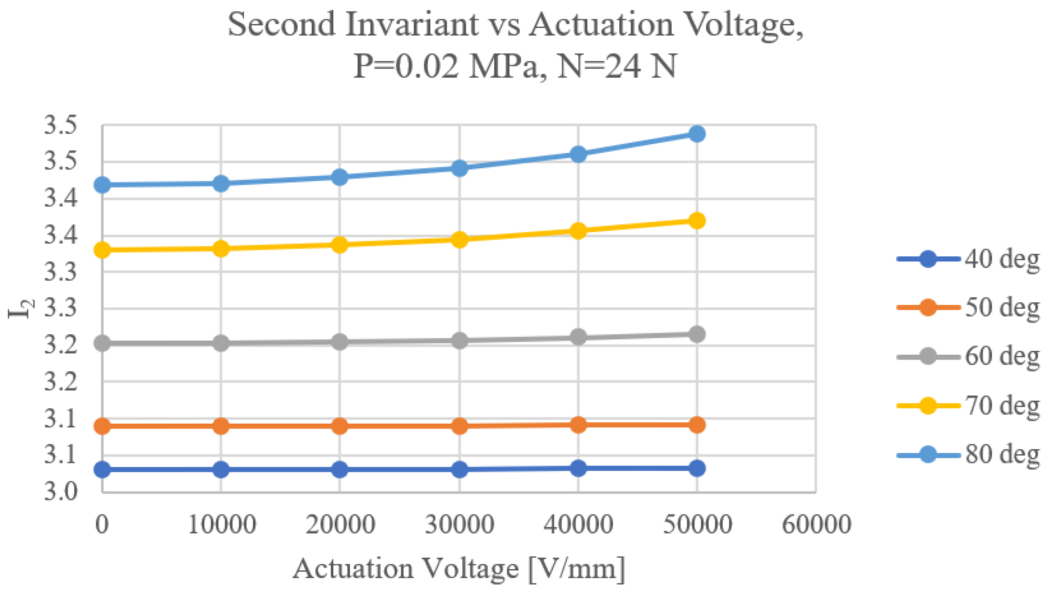

Figure 4.8 : Effect of actuation voltage on the second invariant of Left Cauchy-Green Deformation tensor.

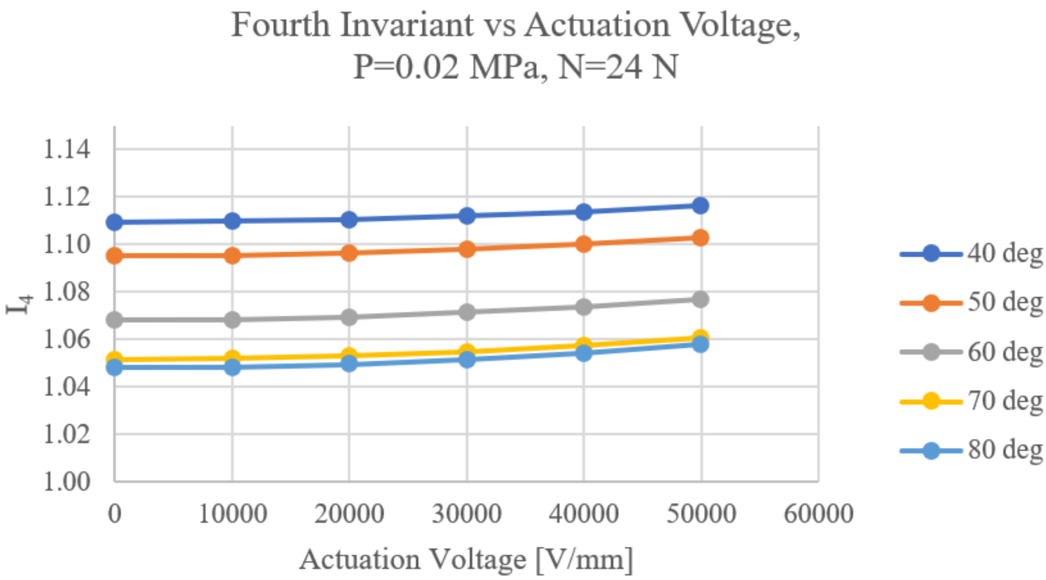

Figure 4.9 : Effect of actuation voltage on the fourt invariant (strecth of fibres).

5. CYLINDRICAL DEA MODEL

As stated in the Chapter 2, cylindrical DEAs are the most common designs for artificial muscle studies. The design studied in this chapter is a variation of the design suggested by Goulbourne and Rahn and Liu [15-16] with pre-stretching applied hydraulically instead of pneumatically.

The cylinder is reinforced with a web of fibres consisting two sets that makes positive and negative angle with axial direction, which in the end generates a double helix shape having the same axial direction as cylinder. Two sets are symmetric with respect to axial direction to cancel out shear effects.

The additional incompressibility of the fluid is expected to be beneficial for increasing the load bearing proportion of fibres without drastically constraining high strain property of elastomer, since the pressure will help to restrain the decrease in the radial direction and causing more strain in the axial direction. Moreover, the fibres will change their orientation without deforming massively (nearly inextensible), which will conceivably result in higher force and work output. The related study that found hydrostatic pressure decreases the necessary potential difference levels was explained in Chapter 2 [22].

Studies shows that electrostriction, that is the pre-stretch of elastomer before electrical load, improves the stability and the performance [23]. For this design, a FE Model is generated in ABAQUS and the model is pre-stretched first with an inflation step in which the tube is inflated with a hydraulic pressure, and tensioned axially in tension step. Finally, the electrical load is applied in the radial direction through the thickness of the tube causing a decrease in the thickness and increase in length. The work output considered is the deformational work by electrical load.

A design of experiment (DOE) is constructed with different initial rebar orientations, different rebar numbers, that is the fibre string number along the tangential direction, and different magnitude of inner pressure. The results are extracted in order to see the effects these parameters have on work output and as well as final fibre orientations, the fibres force ratio to axial force, the effect of total pre-stretch, etc. in search of a better understanding of the mechanism.

5.1 FE Model

5.1.1 Geometry and boundary conditions

The model consists of VHB 4910 [29] elastomer tube with an outer diameter of 10.5 mm, an inner diameter of 9.5 mm and a length of 50 mm. The tube is closed on two ends with hollow domes of HDPE (High Density PolyEthylene) to enclose the inner volume for fluid. However, deformation of these domes is neglected since they are not the major concerns. The tube and end domes are modelled with 3D elements.

Fibres are modelled as a rebar layer inside a shell cylinder with a dummy material (only accommodate rebar layers and not to affect overall strength) and arranged as two fibres families (one positive and one negative) at every 5 degrees along the tangential direction. Shell cylinder has a diameter of 10 mm and a length of 50 mm.

Since the model has radial symmetry, to reduce the computational cost, only 30° portion is modelled and meshed. One twelfth part is then multiplied by the cyclic symmetry function of ABAQUS. Since a great number of jobs will be run, cyclic symmetry will grant a tremendous shortening on run times.

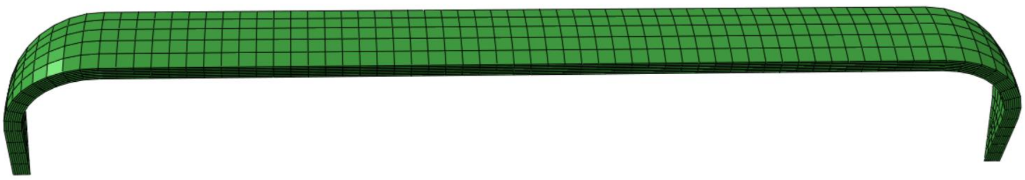

Figure 5.1 : One twelfth Model of Elastomer and HDPE Domes.

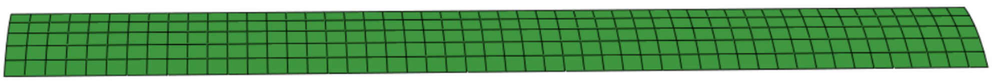

Figure 5.2 : One twelfth Model of Rebar Layer.

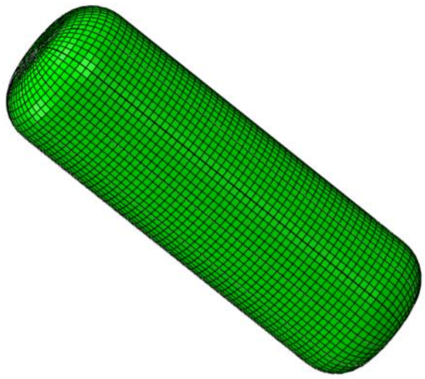

Figure 5.3 : Full Model of Elastomer and HDPE Domes.

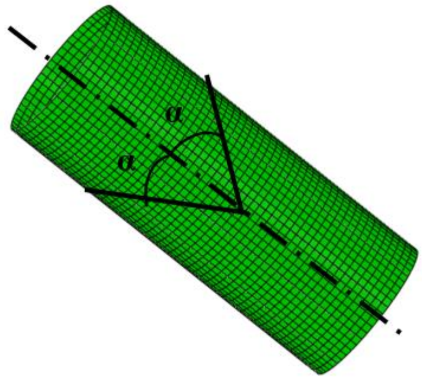

Figure 5.4 : Full Model of Rebar Layer and fibre orientations.

The fibres are modelled, as mentioned before, as a rebar layer on a dummy shell matrix. When this function is used, ABAQUS creates a layer on the section that it is created on with equivalent thickness, using its cross-sectional area and the distance between fibres with the anisotropy caused by the orientation [36].

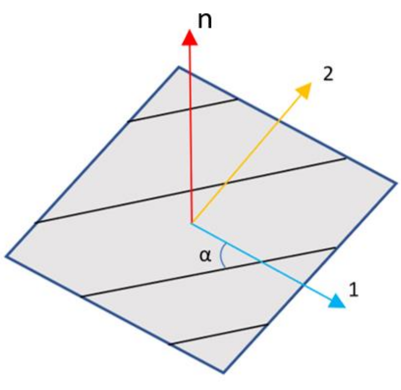

Figure 5.5 : Rebar Layer oriented with angle α with respect to 1st direction of shell element.

The relation between fibres and elastomer matrix are set by embedded geometry constraint in ABAQUS by eliminating translational nodal displacement of rebar layer elements, and setting up a geometric relation with solid elements nodal displacements [36].

Elastomer cylinder is constrained with springs on both ends and other ends of springs are fixed in all directions. Springs are used for displacement and force reading by using a high stiffness spring (1000 N/mm) for reading reaction forces and low stiffness spring (1 N/mm) for reading displacements. Work created by activation is calculated by the change of the elastic energy of the springs.

The hydraulic pressure is applied with the fluid cavity property of ABAQUS. ABAQUS automatically creates hydrostatic elements to fill the defined enclosed volume (cavity) and from a defined reference point a mass flux flows into or from this cavity to ensure constant pressure throughout whole procedure.

5.1.2 Material properties

Although ABAQUS has dielectricity properties, it does not have the electromechanical coupling embedded in its code. However, ABAQUS allows to analyse different material behaviours using User Material (UMAT) subroutines. For this model, an UMAT is written combining Neo-Hookean hyperelastic material strain-stress relations with Maxwell stress produced by applied electrical field. Subroutine takes material constants, electric permittivity constants and the potential difference of electric field as inputs. Then, for the elements with a node on which a temperature field is defined (almost tricking ABAQUS to use temperature as electric field), UMAT calculates Cauchy stress tensor from the strain energy density function with given constants, Maxwell stress using deformation gradient exported from ABAQUS and temperature value for electric field, sums up and returns total stress for each element. ABAQUS then uses stress from UMAT and updates the model for each increment.

For Neo-Hookean hyperelastic material constants, values given in Table 5.1 are used.

Table 5.1 : Neo-Hooke material constants for cylindrical DEA.

C_1 [MPa]	D_1
0.2587	0.001583

Table 5.2 shows the material properties for fibres. Since continuum theory approach is used, for a more homogenized reinforcements, small diameter and high fibre number (fibre number on circumference of the cylinder) was choosen. Also, when choosing fibre material, one of the main considerations should be the stiffness superiority to its matrix. For this case, Young's Modulus of fibre should be much higher than shear modulus of hyperelastic material [37]. It can be clearly seen that 200 MPa >> 0.5174 MPa (see equation (3.23)).

Table 5.2 : Fibre properties for cylindrical DEA.

Diameter [mm]	Fibre Number	Young Modulus [MPa]
0.158	72	200

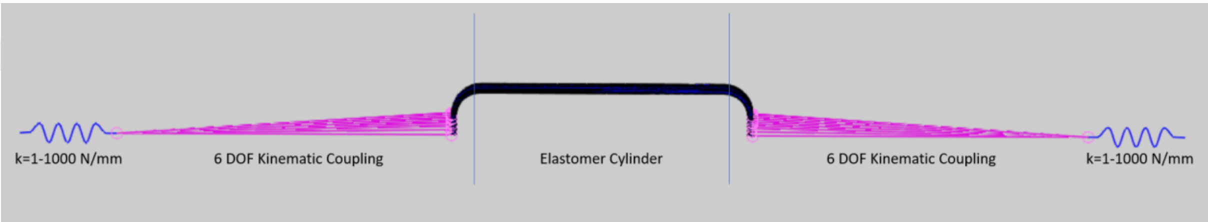

Figure 5.6 : Model structure for cylindrical DEA.

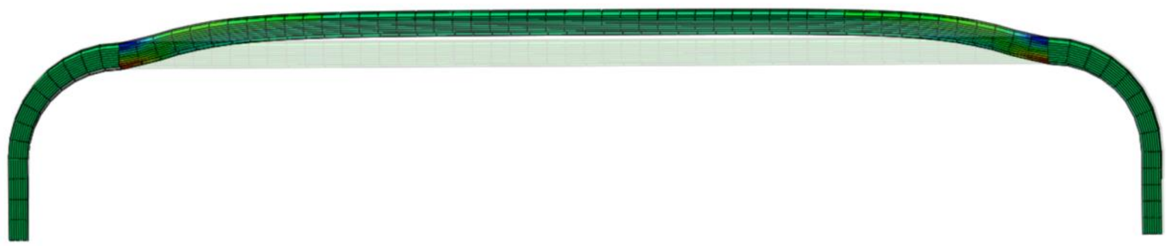

Figure 5.7 : Undeformed and deformed state of cylindrical DEA.

5.2 Model Validation

5.2.1 UMAT Validation

To make sure that UMAT subroutine is working properly a simple uniaxial extension of a beam with 100 mm length and 100 mm^2 cross-section under electrical load is both solved analytically (with the help of expressions derived on Chapter 3) and numerically on ABAQUS using same UMAT subroutine and same Neo-Hookean material constants. Table 5.3 shows the loading conditions and error for stretch calculations. The difference between analytical and numerical solutions are at very acceptable levels reaching a maximum of 1.68 %. Since this small study is a demonstration to show that UMAT results correlates with analytical solution, a coarse mesh was used which caused some level of error. The end effects, that is the different behaviour on the ends where the boundary conditions and loads are applied, being inevitable on FE studies, are also a contributor to obtained errors.

Table 5.3 : Comparison of inner radius and axial stretch values for FE and analytical solutions.

		λ		
Force [N]	Elec. Load [kV/mm]	Abaqus	Analytical	Error
10	10	1.1084	1.1100	0.14%
20	10	1.1767	1.1690	-0.65%
30	10	1.2444	1.2277	-1.34%
10	15	1.1673	1.1584	-0.76%
20	15	1.2242	1.2129	-0.92%
30	15	1.2861	1.2676	-1.44%
10	20	1.2284	1.2152	-1.07%
20	20	1.2843	1.2655	-1.46%
30	20	1.3387	1.3162	-1.68%

5.2.2 Cylindrical Model Validation

For validation of FE Model with the mathematical model, various loading configurations are calculated with both models. End springs are omitted to grant the same boundary conditions as the model described and solved in Chapter 4. Table 5.4 shows the calculated deformed inner radius a and axial stretch λ values, and differences between FE and analytical solution.

Table 5.4 : Comparison of inner radius and axial stretch values for FE and analytical solutions.

Loading Configuration				Analytical Solution		FE Solution		Difference [%]	
Pressure [Mpa]	Axial Force [N]	γ_0 [°]	Voltage	a [mm]	λ	a [mm]	λ	a [mm]	λ
0.025	24	80	0	9.3618	1.0985	9.4281	1.1116	-0.704%	-1.181%
0.025	24	100	0	8.8346	1.1926	8.9230	1.2010	-0.990%	-0.697%
0.025	24	120	0	8.8386	1.2944	8.8998	1.2968	-0.688%	-0.186%
0.025	24	140	0	9.2580	1.3490	9.2868	1.3497	-0.310%	-0.052%
0.025	24	160	0	9.6083	1.3640	9.6262	1.3652	-0.186%	-0.086%

Some level of errors are always expected when comparing analytical and numerical solutions. In mathematical model, DEA is assumed to maintain its cylindrical shape, however, in FE model, end effects occur because of end caps. Also, in mathematical model, DEA is assumed to be incompressible yet in ABAQUS, the model is nearly incompressible. Nonetheless, despite these differences, errors are in acceptable levels.

5.3 Desing of Experiments

To understand the effects of fibre orientation, pre-stretch, fibre denseness, etc. to the mechanism of model, a design of experiments is constructed on Isight software. Isight takes ABAQUS input file (.inp) and result file (.odb), changes defined parameters, and writes and runs a series of ABAQUS input files. After every job is run, Isight catalogues indicated result parameters for data analysis.

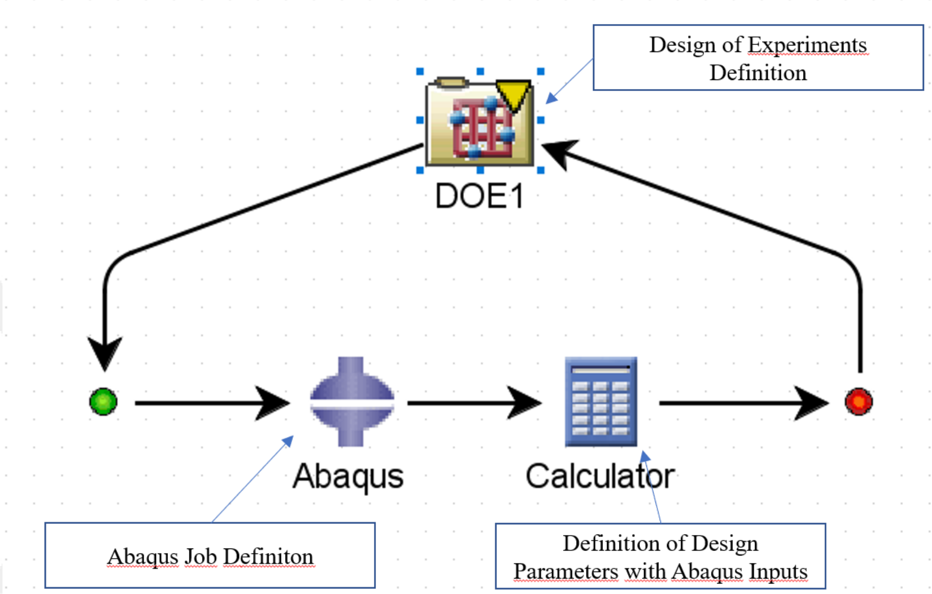

Figure 5.8 : Isight Design of Experiments Flowchart.

Before Isight job, some modifications on the Abaqus job must be made. Input file is parametrised with *PARAMETER keyword on ABAQUS for fibre orientation, electrical load, tension force and inner pressure.

In Calculator components, new parameters are defined to have a more meaningful data set. They are defined as,

$$\mathrm{Work} = \mathrm{Work}_{\mathrm{spring}} = \Delta \mathrm{L}_{\mathrm{spring}_{k=1}} * \mathrm{F}_{\mathrm{spring}_{k=1000}} \tag{5.1}$$

which is defined with the assumption of the energy stored in springs are a result of deformation from electrical load. In Design of Experiments, the lower and upper bounds for fibre angle, inner pressure and potential difference were set. With this information, Isight created a series of ABAQUS jobs with 8 different fibre angles, 6 different inner pressures and 4 different potential differences. With the addition of high and low stiffnesses for end springs this means a total of 384 ABAQUS jobs. DOE results used in graphs documented in this chapter can be found in Appendix chapter.

5.4 Results

For the extraction of data, models with springs having 1 N/mm stiffness were used for displacement assessment and models with springs having 1000 N/mm stiffness were used for force assessment.

Figure 5.9 shows the effects of inner pressure (i.e. pre-stretch) on the actuation force, that is the change in force at the fixed nodes of end springs due the activation from electric field, for different fibre orientation angles under constant electrical load. It can be seen that an increase in inner pressure also increases the actuation force for the same fibre angle, which is expected since higher pressure creates higher degree of axial loads, and the effect of electrical load would be higher under more pressure. Figure 5.9 also shows that as the fibre angle with the axial axis of the cylinder increases, actuation force also increases since inner pressure is counterbalanced more by the fibres and a as result, the forces generated by much stiffer fibres are greater and as stated above, higher forces means higher actuation forces. Moreover, as the fibre angles increases the growth rates of exponential curves decreases, meaning that fibre angle and inner pressure contribution is in inverse proportion. Furthermore, for 60 degrees of fibre angle, the relation between actuation force and inner pressure is almost linear.

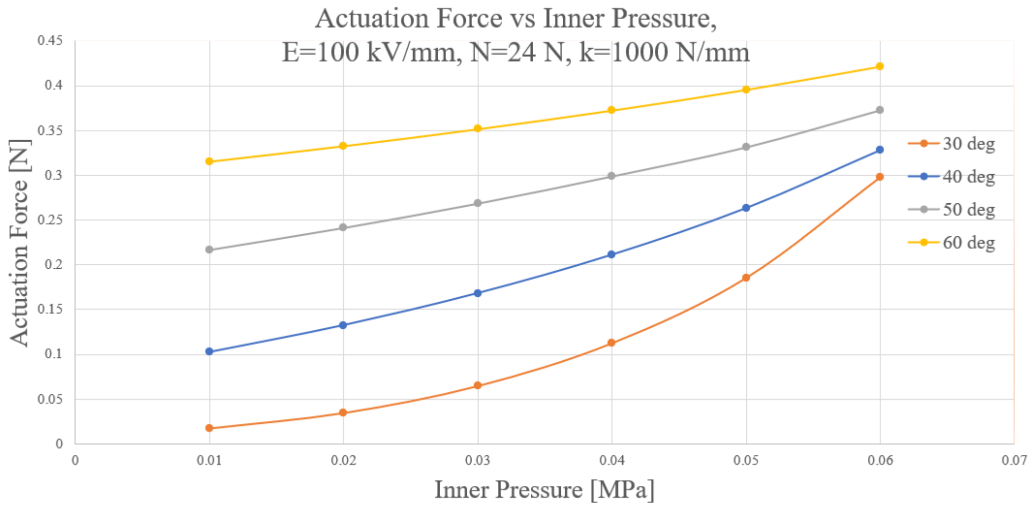

Figure 5.9 : The effect of inner pressure on actuation force for different fibre angles.

Figure 5.10 shows the effect of inner pressure on actuation displacement for different fibre angles. Figure 5.9 and 5.10 have nearly the same behaviour, increase in fibre angle increases the actuation displacement and have the same effect on contribution of inner pressure on actuation displacement.

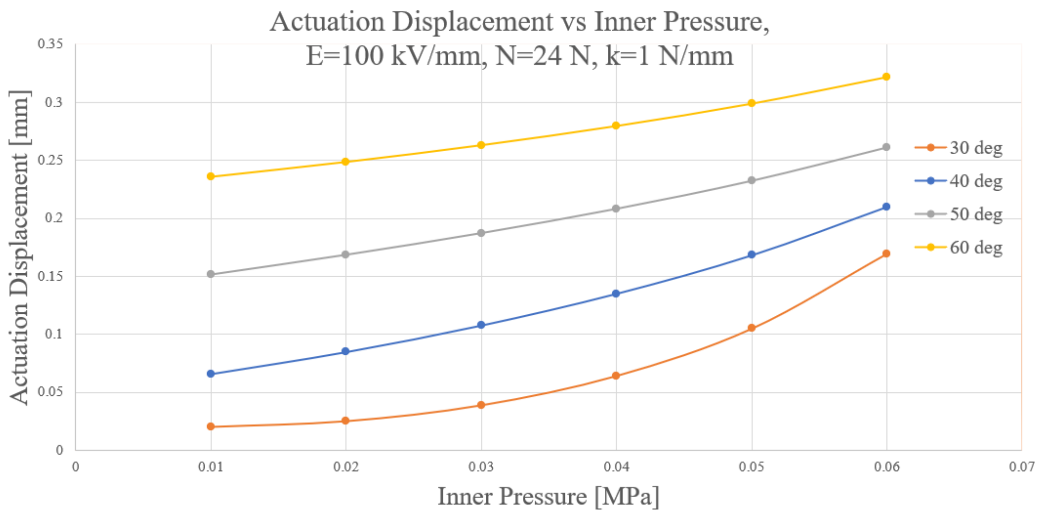

Figure 5.10 : The effect of inner pressure on actuation displacement for different fibre angles.

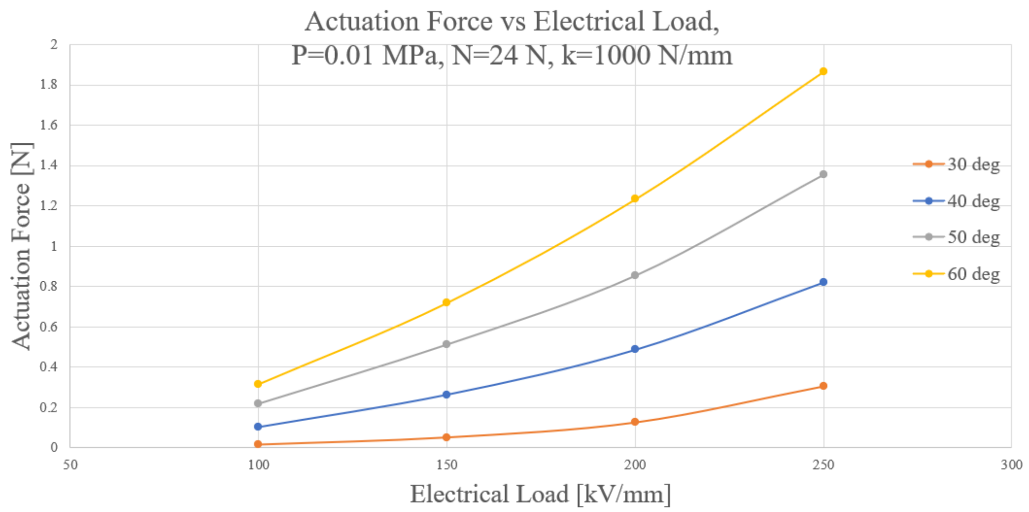

Figure 5.11 : Effect of electrical load on actuation force for different fibre angles.

The effect of electric field magnitude on actuation force with constant inner pressure for different fibre angles can be seen in Figure 5.11. Since the electric field vector for Maxwell stress is defined as potential difference/thickness ratio in the preferred direction, and as the actuation voltage increases, thickness of elastomer will decrease more, which means higher electric field magnitude and so on, thus, actuation force increases exponentially with increasing voltage. This phenomenon can be seen clearly for 50 and 60 degree curves. One could also deduce that as the angle of fibres increases, the growth rate also increases. This is why 30 degrees curves seems linear since the growth rates are much lower from the other curves.

On Figure 5.12, again, actuation displacement shows similar behaviour as actuation force graphs. Displacements increase exponentially as electrical load increases and higher fibre angle results in greater growth rate, which is expected since all the energy used to generate force on springs now generates displacement because of low stiffness.

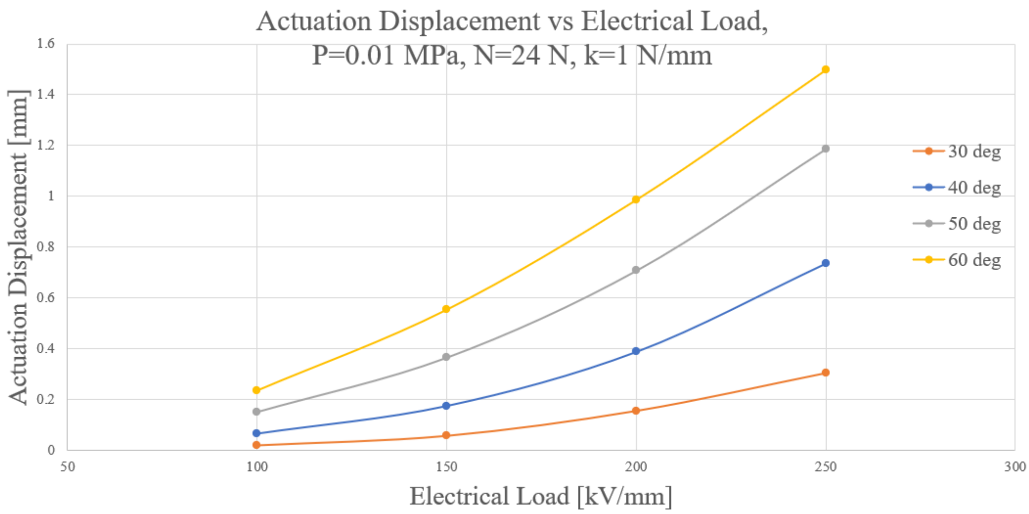

Figure 5.12 : Effect of electrical load on actuation displacement for different fibre angles.

Figure 5.13 and 5.14 can shed more light on the effect of fibre angle on actuation force and displacement. From these figures, the effect of fibre angle is clearly sinusoidal like having the minimum around 20 degrees and maximum around 80 degrees. The derivation of exponential like behaviour from Figure 5.11 and 5.12 is understandable since sinusoidal functions are exponential functions (Euler’s Identity). Liu and Rahn found that for fibre reinforced McKibben Actuators the angle for axial elongation without radial expansion with pressure is 54°44’ [16], and the behaviour of curves seems to change around this value. Since this value is a known design parameter for cylindrical composite structures, it is prefectly normal to observe such effect for this design. However, the exponential behaviour consideration is still valid since for the same angle (i.e. same horizontal coordinate), distances between curves increases with higher electrical load which implies exponential growth. Moreover, it can be also seen in Figure 5.13 and 5.14, higher electrical load results in higher magnitude of sinusoidal wave. Overall, it can be said that increasing fibre angle behaves like an amplifier on the effects of electrical load on cylindrical DEAs.

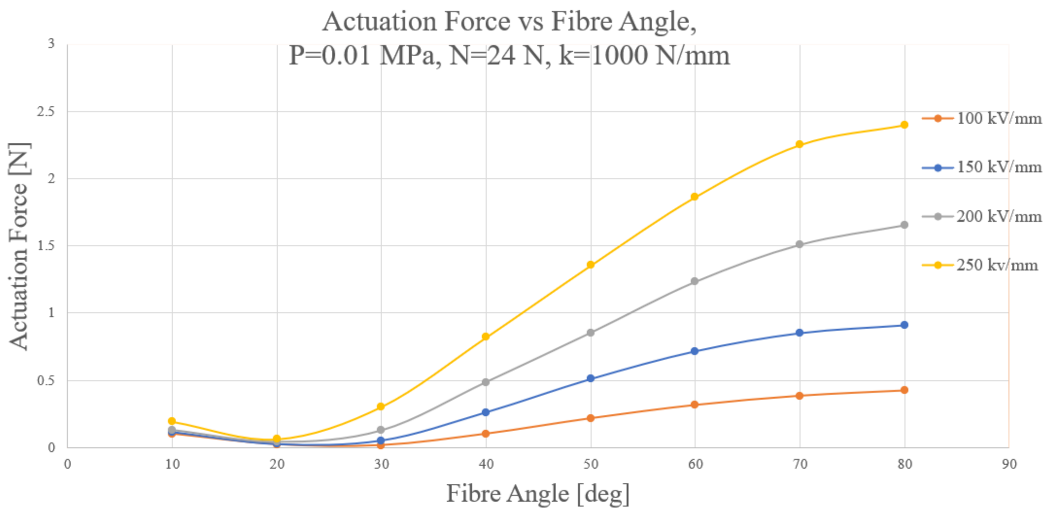

Figure 5.13 : Effects of fibre angle on actuation force for different electrical loads.

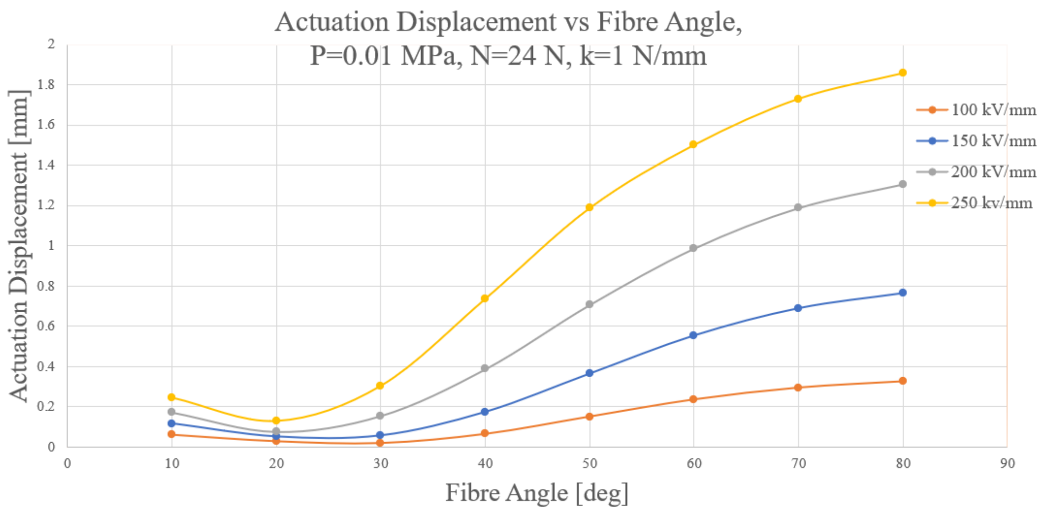

Figure 5.14 : Effects of fibre angle on actuation displacement for different electrical loads.

Figure 5.15 shows the relation between maximum element axial stretch and fibre angle for different electrical loads. As the fibre angle increases, tube elongates and inflates rather than just elongating, which means cylinder expands on every direction, as a result axial stretch decreases for higher fibre angle. Considering the fact that as the fibre angle approaches 90 degrees (parallel to axial direction of the cylinder), force and displacement outputs increases, the relation between maximum element axial stretch and fibre angle becomes highly crucial and it seems to be an exponential decay function. Again, the distance between curves at same horizontal coordinate increases exponentially with electrical load.

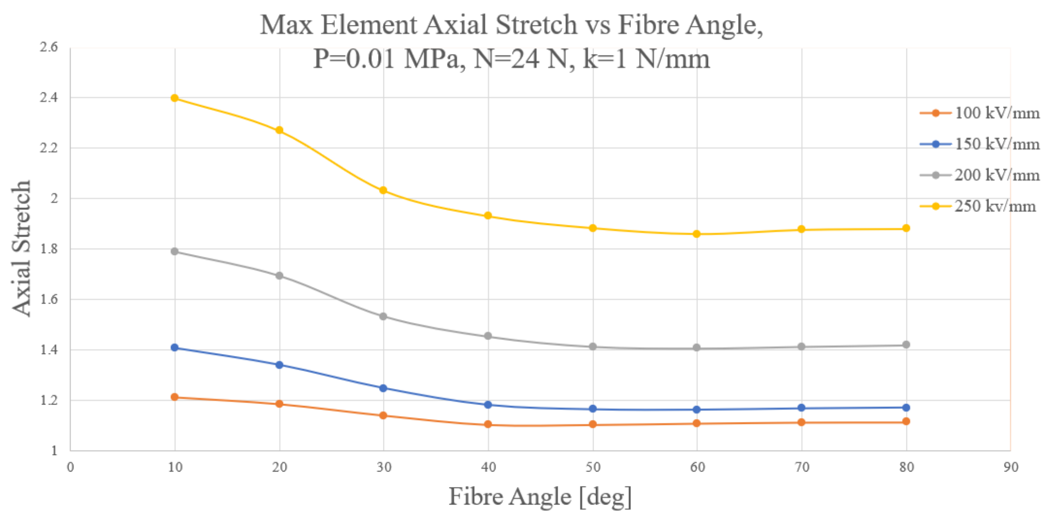

Figure 5.15 : Effects of fibre angle on maximum element axial stretch.

Figure 5.16, 5.17 and 5.18 display the variation of actuation work with the change in values of parameters, such as electrical load, inner pressure and fibre angle, respectively. For every figure, constant parameters are also stated for that particular set of analyses. For these figures, actuation work is calculated as the integral of the force displacement curve, created by outputs for different spring stiffness values, and both end springs are considered for this calculation. Therefore, it is logical to see same behaviour on the curves for same parameters. Again, as in the previously discussed displacement and force plots, the most effective parameter on work output is by far the fibre angle influencing not only total work yet also the effect of other parameters have on the work outputs.

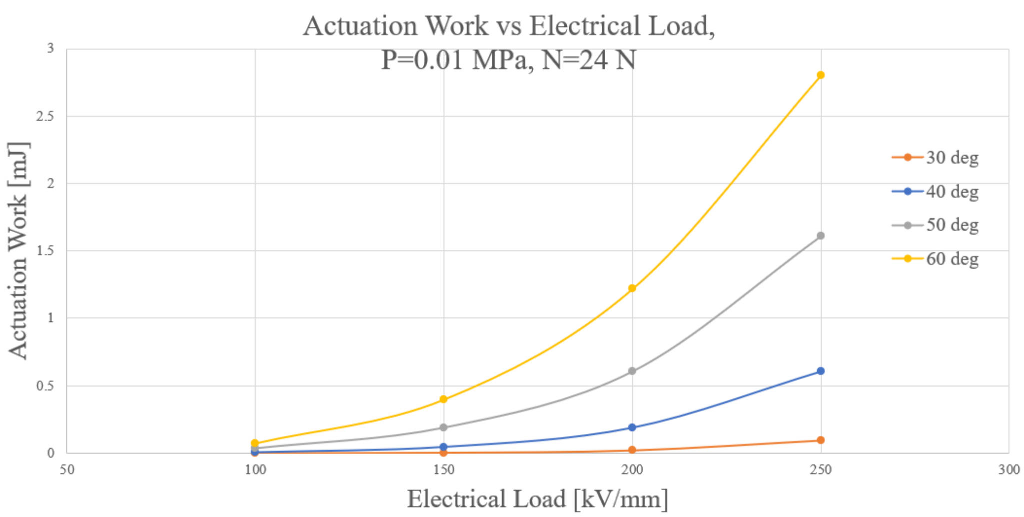

Figure 5.16 : The relation between actuation work and electrical load for different fibre angles.

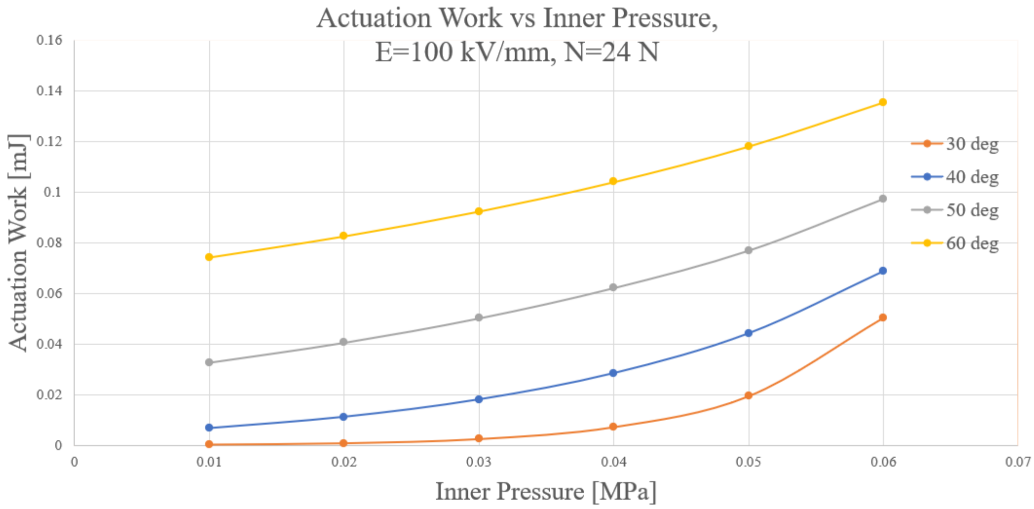

Figure 5.17 : The relation between actuation work and inner pressure for different fibre angles.

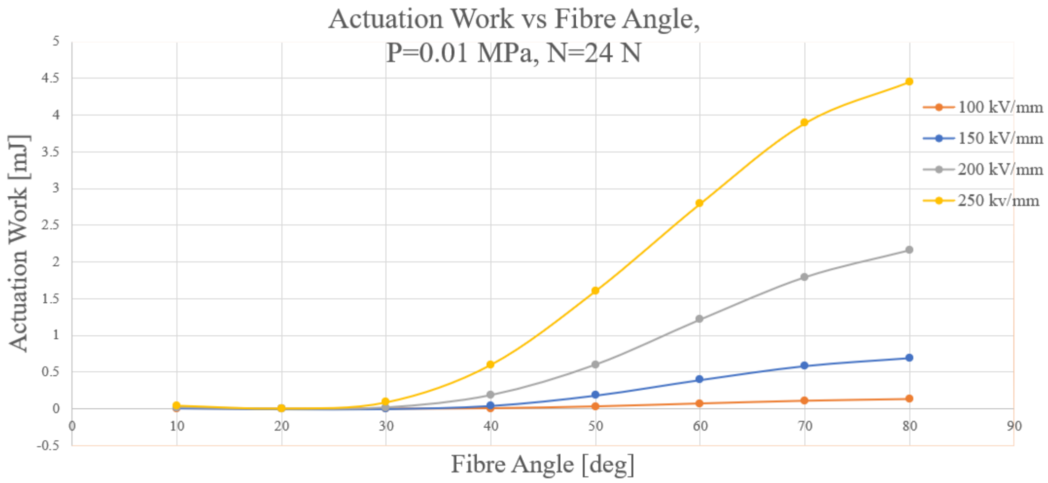

Figure 5.18 : The relation between actuation work and fibre angle for different electrical loads.

Table 5.5 shows the inner radius and axial stretch values for the cylindrical DEA at the end of every step for 20 degrees and 80 degrees. It can be clearly seen that for 20 degrees, cylinder inflates rather than elongate and most of the energy granted by activation is used for radial expansion. However, for 80 degrees, even though some inflation occurs, axial stretch is greater than radial stretch (i.e. change in radius), which means 3D expansion (radial, tangential and axial). Thus, including the results presented in previous figures, most axial (unidirectional) actuation occurs when the cylinder is expanded in every direction. Fibre angle is the most effective parameter for the actuation outputs since it is the main parameter affecting deformation shape of the tube in case of inner pressure and axial tension. Moreover, the foundings displayed in previous figures show that fibre angle changes the relation between outputs and other parameters backing the most effective parameter argument.

Table 5.5 : Inner radius and axial stretch for 20 and 80 degrees.

P=0.01 MPa N=24 N E=100 kV/mm k=1 N/mm	20°		80°	
	a [mm]	λ	a [mm]	λ
Initial	9.5	1	9.5	1
Inflation	10.70	0.99	9.7	1.01
Tension	10.63	1.01	9.69	1.04
Electric	11.39	1.01	9.79	1.05

6. TUBULAR HELIX DEA MODEL

Helixes are a common design shape to achieve uniaxial force and displacement output, and the most familiar example is steel springs. To use same advantages of this shape, a tubular helix DEA is proposed in this chapter.

The helix is reinforced with two family of fibres making a positive and negative angle with helix tangent vector. Again, the reason for symmetrical fibre families as in cylindrical DEAs, is to cancel out shear effects.

As it was explained in Chapter 5, benefits of hydraulic pressure are also used on this design. The incompressibility of fluid will help -expectedly- further actuation in axial direction. Moreover, fibres will again change orientation improving force and displacement output in the axial direction of helix.

A FE Model of tubular helix DEA is created in ABAQUS. The structure is first pre-stretched by a hydraulic pressure resulting in a movement in the axial direction of helix and radial expansion, next a tension load is applied in the axial direction of helix and then an electrical load for activation of DEA is applied through the thickness in the radial direction of cross section which is changing orientations with the helix tangent vector.

This design is proposed only to examine possible developments over cylindrical model and compare them hence DOE model is not generated for this design. Only the effects of fibre angles on the output is studied for this design.

6.1 FE Model

6.1.1 Geometry and boundary conditions

A VHB4910 tubular helix with inner diameter of 19.5 mm, outer diameter of 20.5 mm, helix radius of 50 mm and a helix step of $50/\pi$ solid model is generated with the help of a basic MATLAB code. Helix makes only one tour for the sake of not spending redundant computational power. The inner volume is closed with semi domes on the ends to meet fluid cavity requirements of ABAQUS.

A shell cylindrical helix with a diameter of 20 mm and same helical properties as the solid model is created again with the same MATLAB code to use as a dummy matrix for fibres. The shell elements are embedded in solid elements using same procedure explained in Chapter 5.

Fibres are then created as rebar layers on this dummy shell elements on ABAQUS, applying the same procedure mentioned in Chapter 5 (equivalent homogeneous layer), and arranged as two fibres families (one with positive angle and one with negative angle) at every 5 degrees along the tangential direction of the cross-section (72 fibres on cross-section, 36 positive and 36 negative). However, even though ABAQUS automatically calculates element normal for shell elements, the correct orientation of directions 1 and 2 represented in Figure 6.2 should be stated in a manner to coincide with helix tangent and normal vectors, respectively to have the intended fibre orientations.

ABAQUS does not have a direct way to accomplish the definition of helical coordinates, therefore an ORIENT subroutine calculating helical directions for every point on the tubular helix shape had to be generated and implemented on the model. The subroutine code is generated using node coordinates and the relation between local nodes to orient directions 1 and 2 with normal and tangent helix directions, respectively for every single element. Although this code is generated for shell elements, it is also working for solid elements which is necessary to correctly apply electrical load in radial direction through the thickness.

As in cylindrical DEA, a fluid cavity is defined using enclosed volume inside the solid elements and ends of tubular helix is closed with HDPE caps. A reference point is also defined inside this volume for fluid cavity and a constant hydraulic pressure is applied on inner surface. A flux of fluid into or out from this volume is regulated by ABAQUS to guarantee constant pressure throughout loading.

The helix is connected to uni-directional springs (oriented at axial direction of helix) on both ends again for force and displacement extractions. For force value extraction spring stiffness is set to 1000 N/mm and for displacement extraction is set to 1 N/mm. The work done by electrical actuation is calculated as the total elastic energy change on springs, as calculated in the cylindrical DEA design.

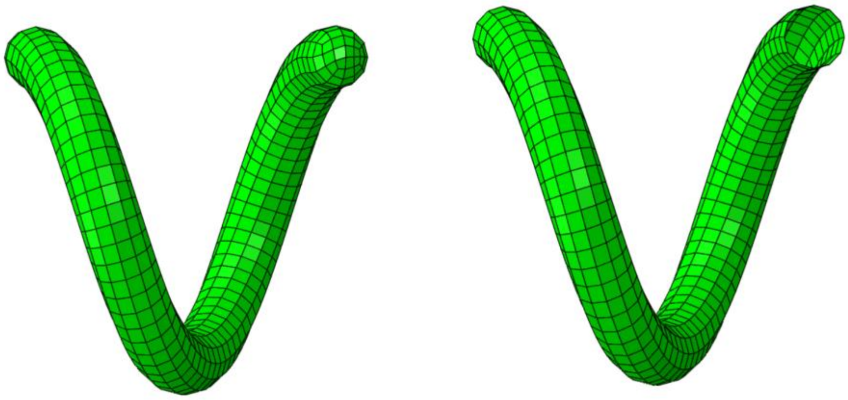

Figure 6.1 : Tubular Helix DEA Solid and Shell Elements.

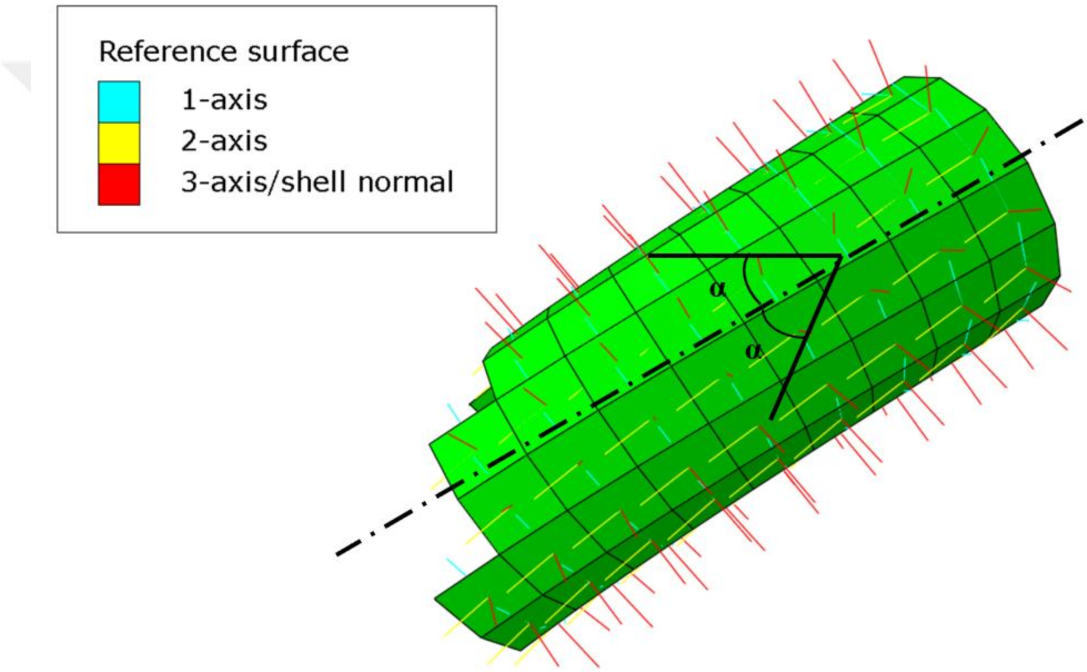

Figure 6.2 : Element Orientations on shell elements.

6.1.2 Material properties

The elastomer part (i.e. helical part) of the material is again defined using UMAT subroutine. Only difference is that UMAT works in conjunction with an ORIENT subroutine. ORIENT subroutine defines the directions of elements by the procedure explained before and UMAT calculates Cauchy stress and Maxwell stress according to this orientation definitions.

For Neo-Hookean hyperelastic material constants and fibre material properties, again same constants as cylindrical DEA model are used. For a more comfortable read, Tables 5.1 and 5.2 are restated here as Table 6.1 and Table 6.2.

Table 6.1 : Neo-Hooke material constants for tubular helix DEA.

C_1 [MPa]	D_1
0.2587	0.001583

Table 6.2 : Fibre properties for tubular helix DEA.

Diameter [mm]	Fibre Number	Young Modulus [Mpa]
0.158	72	200

6.2 Results

The deformation is, as expected, is different from cylindrical design, which can bring new possibilities of force outputs. For example, cylindrical DEA is deformed symmetrically in axial direction and minimum principal strains are zero. However, as seen in Figure 6.3, minimum principal strains are negative and in the orders that cannot be neglected, and the distribution is somehow resembles to principal strains on a bending beam. The reason for that is the helix is actually bending. The normal force on any cross-section created by pressure creates a bending moment on fixed end.

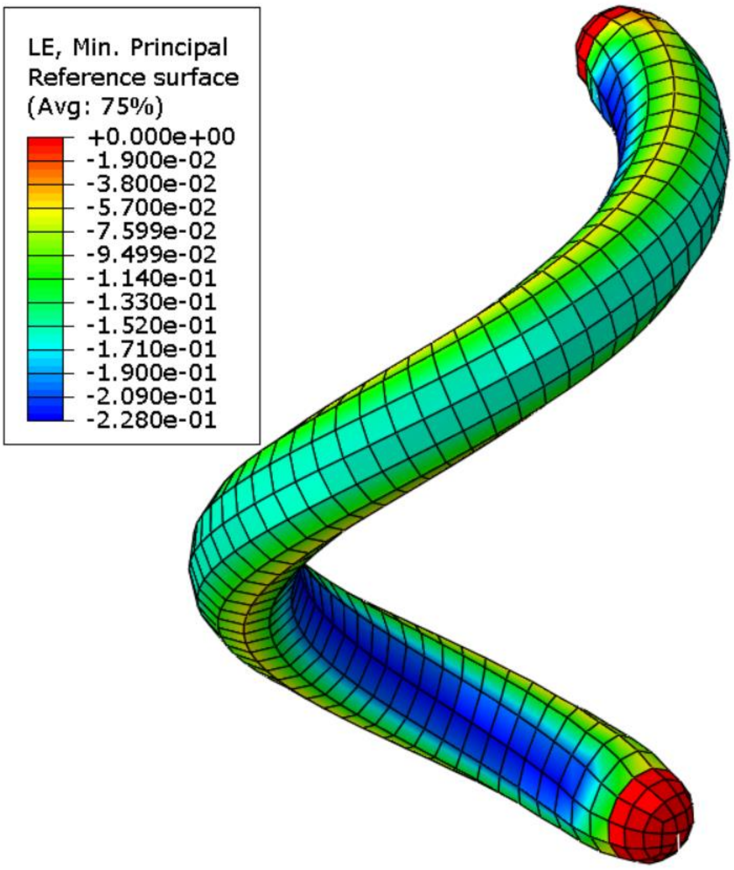

Figure 6.3 : Min. principal LE at the end of inflation step.

The bending like minimum principal strain distribution continues in the electric step since as seen on the cylindrical DEA, the deformation is same for inflation, axial stretch and electrical actuation. Therefore, it is logical to see same pattern in these steps (on Figure 6.3 and 6.4) too.

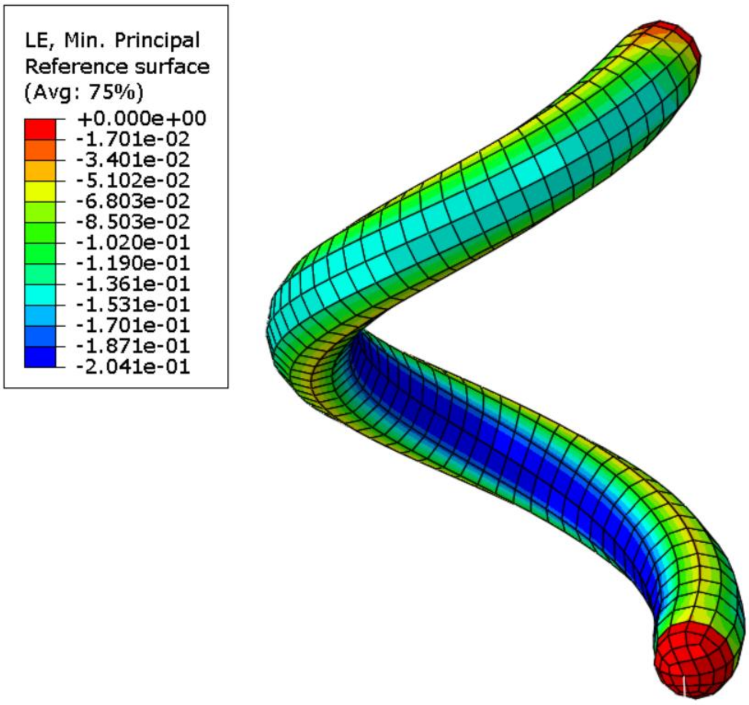

Figure 6.4 : Min. principal LE at the end of electric step.

Figure 6.5 shows the axial displacement of one of the ends for a model with fibres having a 20 degrees angle with the tangent vector of helix. Ends moves 23.53 mm after inflation and activation of DEA causes 2.47 mm retracements, which means an actuation stretch of 0.0247 on 1.235 total stretch.

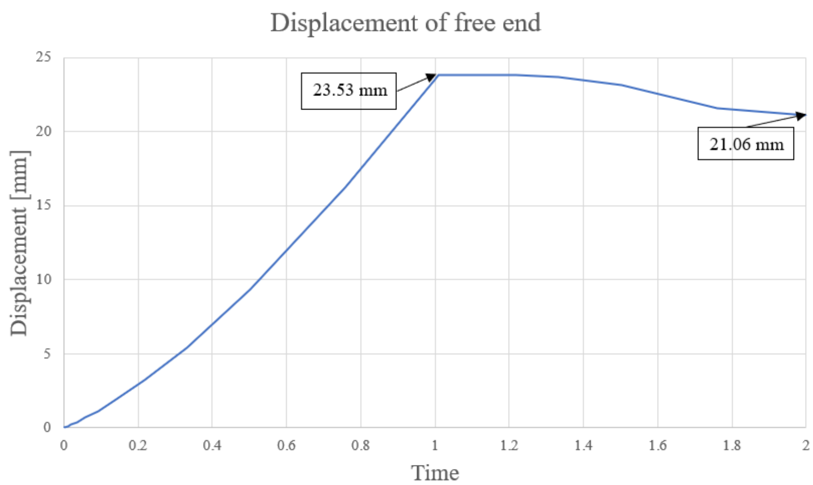

Figure 6.5 : Axial displacement of helix ends.

These preliminary results prove that, this design shows promise for an optimum use of design parameters for overcoming low force and displacement limitations. The helical stretch output is more or less the same as element stretches, which was not the case for cylindrical DEAs, as can be seen in Figure 6.6.

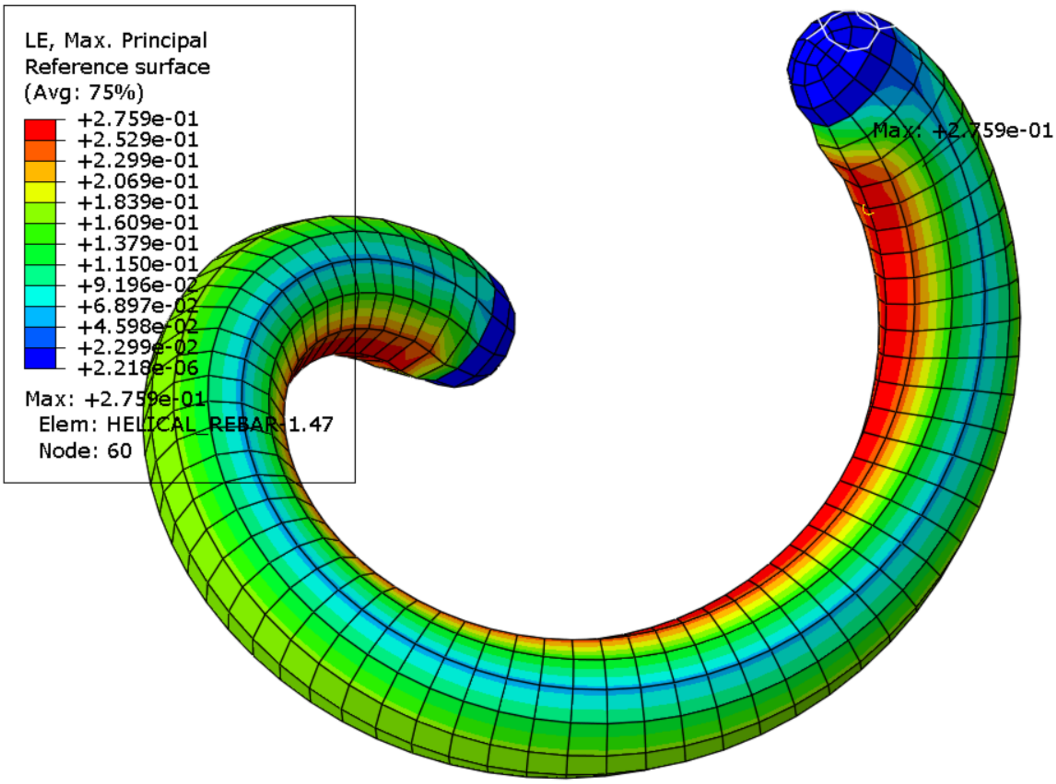

Figure 6.6 : Maximum principal strains on the model.

Figure 6.7 shows the actuation displacement as a function of fibre angles for 0.01 N/mm end spring stiffness. For fibres parallel to tangent vector of helix, actuation displacement is around -2 mm and increases from that point. Maximum actuation occurs around 15 degrees and has a value of 3.5 mm. 55 degrees model has the minimum actuation reaching nearly 0 mm, which does not mean that actuation does not happen. All the energy created by electrical load causes radial expansion on the cross section of tubular helix. However, since outputs on the axial direction of helix is the desired uniaxial output, it can be said that there is no “useful” outputs at 50 degrees. The actuation of the elastomer thus changes direction, it contracts the DEA instead of stretching.

Figure 6.8 represents the variation on actuation force with respect to fibre angles. Figure 6.8 and 6.9 shows similar behaviours except between 25 and 50 degrees.

Nonetheless, from 50 degrees to 80 degrees, there is practically no usefull force and the maximum actuation occurs with the model with 20 degrees fibres.

For the calculation of activation work, a curve is created between force and displacement values for every fibre with 0.01 N/mm and 1000 N/mm springs. The area under this curve is accepted as the actuation work. Figure 6.10 shows the work outputs for every fibre angle.

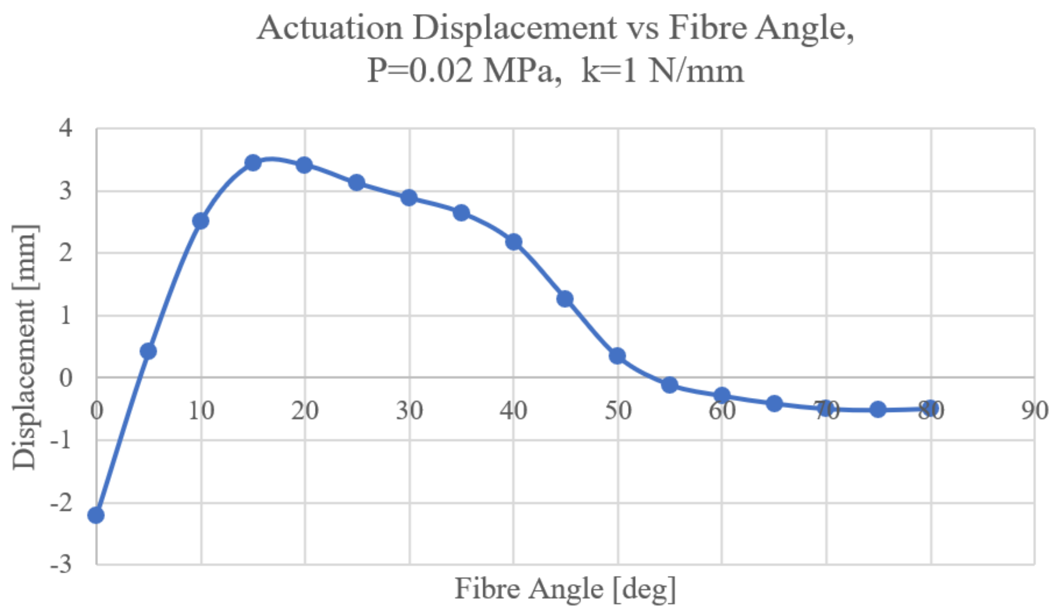

Figure 6.7 : The effect of fibre angles on actuation displacements for soft springs.

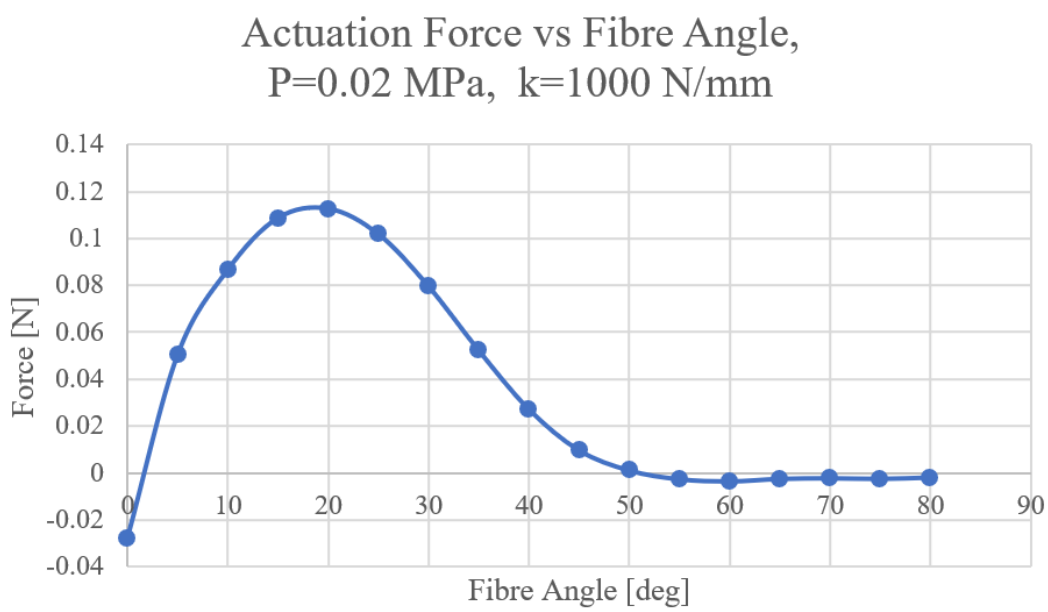

Figure 6.8 : The effect of fibre angles on actuation forces for stiff springs.

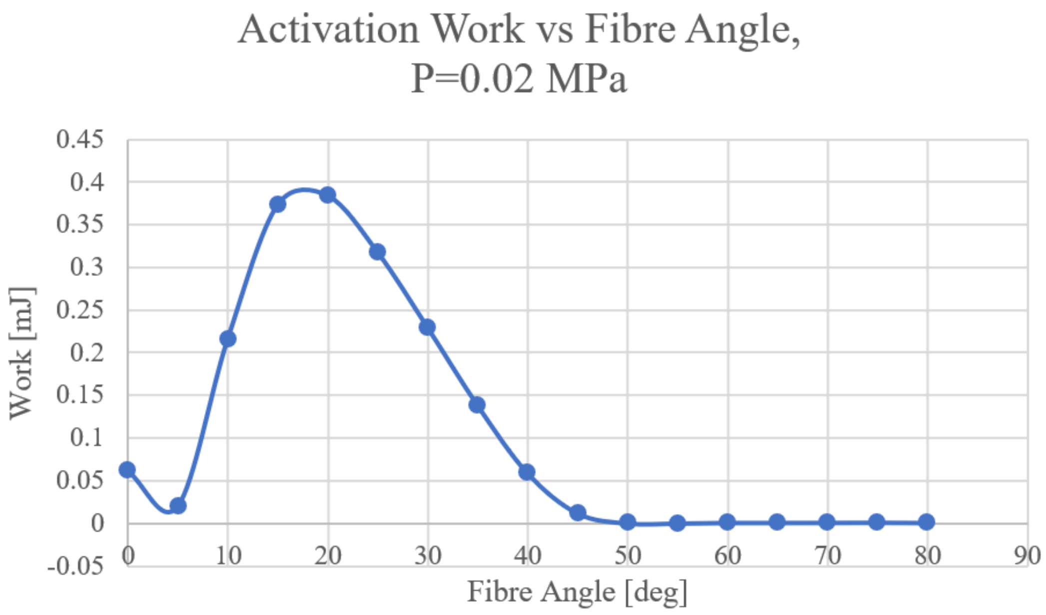

Figure 6.9 : The effect of fibre angles on actuation work.

Maximum useful work as can be deduced from force and displacement curves, occurs between 15 and 20 degrees and for the fibre angles higher than 50 degrees the energy created by actuation is used on radial expansion of helix (i.e. increase in helix radius).

Nearly 3.5 mm of actuation for an axial length of 100 mm is a good result for pre-stretched fibre reinforced elastomers. Even though DEAs are capable of more than this level of actuations on itself (i.e. without reinforcement), reinforcements limit the length change while increasing force outputs. However, this design slightly overcomes the actuation limitations without losing much force achievements granted by fibres and can be multiplied by using multiple tours of helix. This could be explained by a better use of element stretches. For same output levels, element stretches are much lower than results obtained for cylindrical DEA design. Since helix shape, as mentioned before, is a go to geometry for unidirectional output, this is expectable. It is suspected that outputs are highly related to helix dimensions (helix radius and helix step height) as well as thickness of tube and mid surface radius. By a geometrical parameter optimization, use of lower element stretches could be manipulated to enhance the results obtained on this chapter.

7. ACCORDION DEA MODEL

This proposition of DEA design consists of a tube with varying radius forming zigzags along the axial direction. The inner volume will increase with pressure more than cylindrical DEA as the walls will straighten and grant axial elongation without causing a great deal of additional strain.

A variation of accordion DEA is also studied in this chapter. A geometry is created with the same lentgh as accordion, however, the diameter of one end is half of the other end (i.e. conical accordion).

The accordions are reinforced with a web of fibres formed by two sets of fibre families with one having positive angle and one having negative angle with respect to axial direction. Again, two sets are symmetrical to cancel out shear effects and also, they follow the zigzag lines forming the axial cross section of accordion causing a helix shape with oscillating helix radius.

As said above, a hydraulic pressure is applied to inner surface of DEA causing inflation and axial elongation, straightening the wall and forming a near perfect tube (a truncated conic tube in case of conical accordion). Incompressibility of fluid will help to maintain pre-strecthed shape during electrical load. The fibres will change orientation less since most of the energy created by the pressure will be spent to straighten the zigzags.

Only 30° portion of these models are generated as in the cylindrical DEA using cyclic symmetry property of ABAQUS, in order to decrease the computational cost and also availability since these designs also have radial symmetry.

As the other design propositions, this design is also pre-stretched with inner pressure and tension in axial direction and afterwards is actuated by electrical load. This is a conceptual design to study the possibility of bringing stacking effects to cylindrical DEA designs that is why only the effects of fibre angle on actuation outputs and output levels are examined in this chapter.

7.1 Accordion DEA

7.1.1 FE model

7.1.1.1 Geometry and boundary conditions

A VHB4910 accordion like structure is modelled with dimensions specified in Figure 7.1. The wall thickness, where the electric load is applied, is 1 mm throughout the whole structure. Elastomer part and -again to enclose the inner volume- semi dome caps are modelled as solid elements.

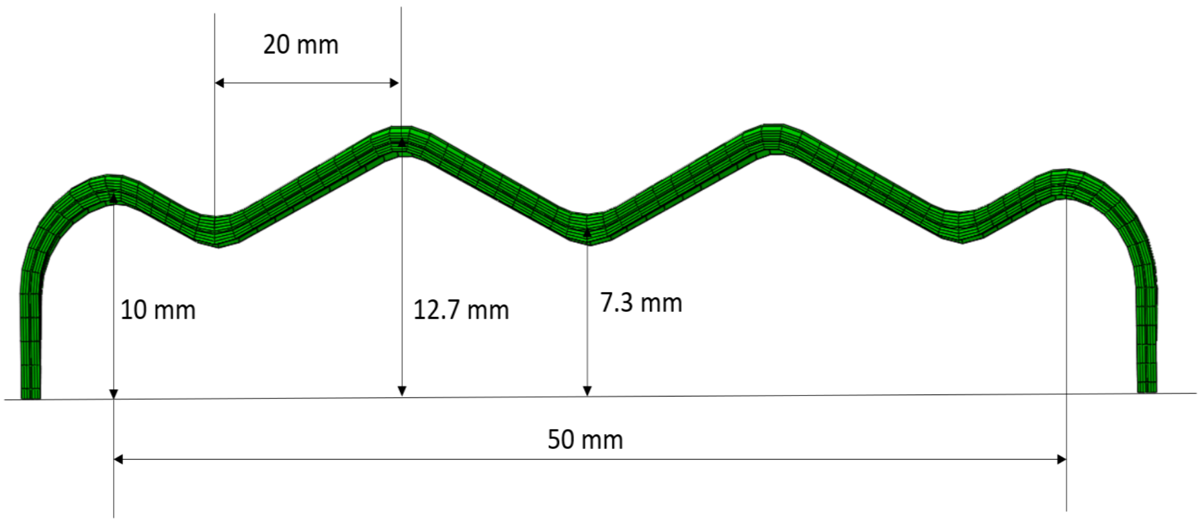

Figure 7.1 : Accordion model dimensions.

A shell dummy matrix to be fitted on the mid-surface of solid geometry is also created to accommodate fibres. This matrix have almost no strength on its own and specificially set this way in order to neglect its effects. Fibres are created as rebar layers and arranged as to place two fibres (one positive and one negative) at every 5 degrees along the tangential direction.

Fluid cavity is defined over enclosed volume inside the accordion and a reference point located in this volume. For inflation step, a hydraulic pressure is applied from cavity reference point to inner surface. An axial force is applied for further shape stabilisation (formation of cylindrical shape) and an electrical load is applied.

DEA is connected at both ends with uni-directional (oriented in axial direction) springs. For force extraction, springs with 1000 N/mm stiffness and for displacement extraction springs with 1 N/mm stiffness are used. Actuation work is calculated by the total elastic energy change on the springs.

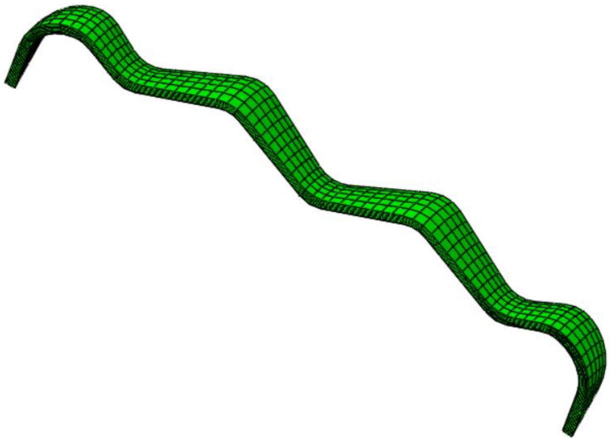

Figure 7.2 : 30° portion of solid elements.

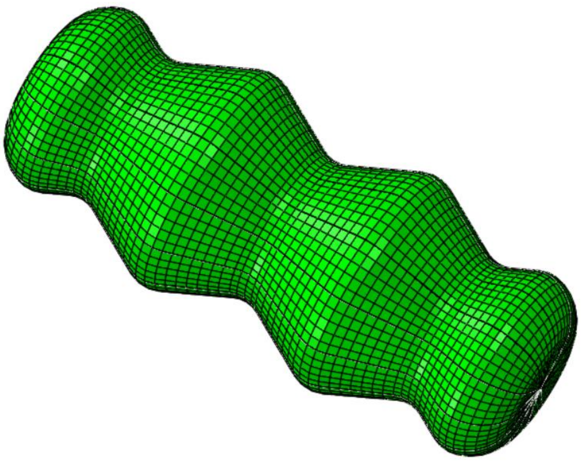

Figure 7.3 : Full representation of solid elements.

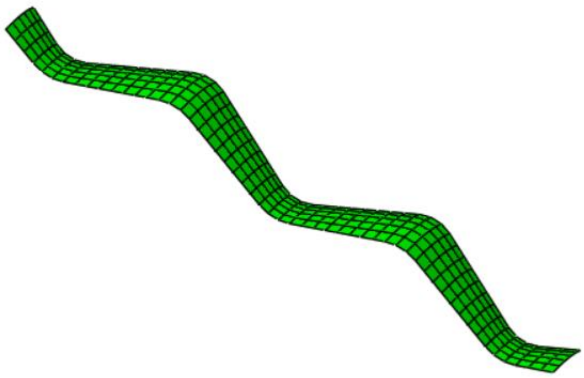

Figure 7.4 : 30° portion of shell elements.

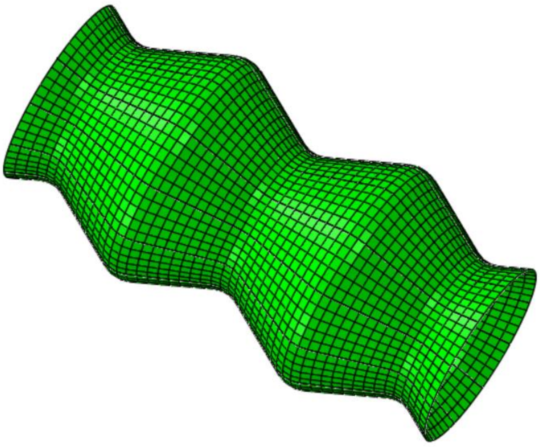

Figure 7.5 : Full representation of shell elements.

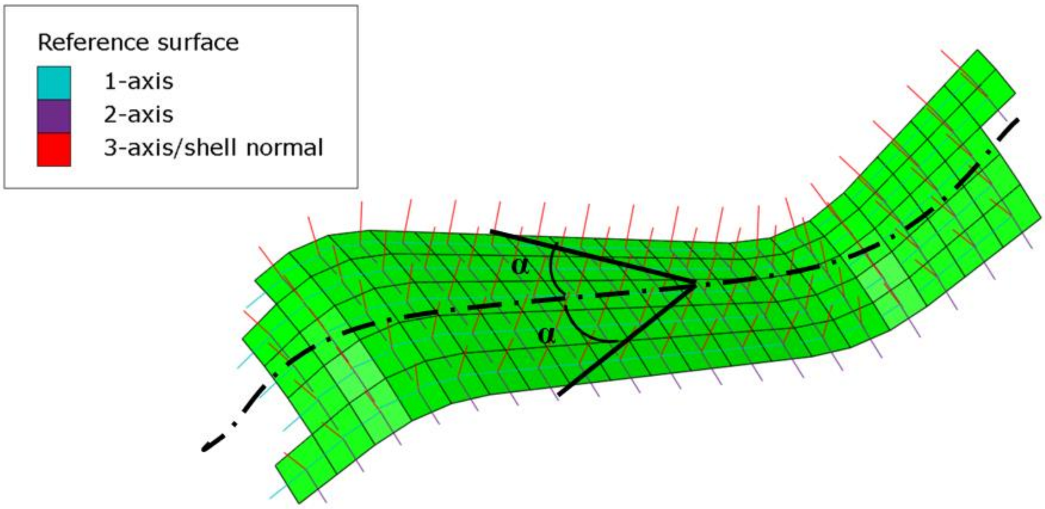

Figure 7.6 : Material orientations calculated by ORIENT subroutine.

7.1.1.2 Material properties

Same UMAT subroutine that calculates combined electromechanical response is used here. A shell dummy matrix for fibre layers are also created to fit the mid-surface of solid part.

Fibres are created as rebar layers on dummy shell matrix on ABAQUS. ORIENT subroutine is also used here to state proper element and consequently fibre directions (see Figure 6.6). 1st direction of elements is following the curvature of tube's wall and other directions are calculated from this direction.

For this design also, same Neo-Hookean material constants for elastomer part and generic cotton thread material for fibres as in the previous cylindrical and tubular helix are used.

7.1.2 Results

Figure 7.5, 7.6 and 7.7 shows inflation, tension and electric step, respectively for the specimen with 80 degree fibre angles and 1 N/mm stiffness for end springs. After the inflation, as previously discussed strain values are in the order of 1% on the lower bounds of “zigzag” line. As the structure inflates, the middle part enlarges with next to no change in length. However, with the axial tension, shape starts to ressemble a regular cylinder. Electical load establish the original shape with an increase in length and pre-stretch.

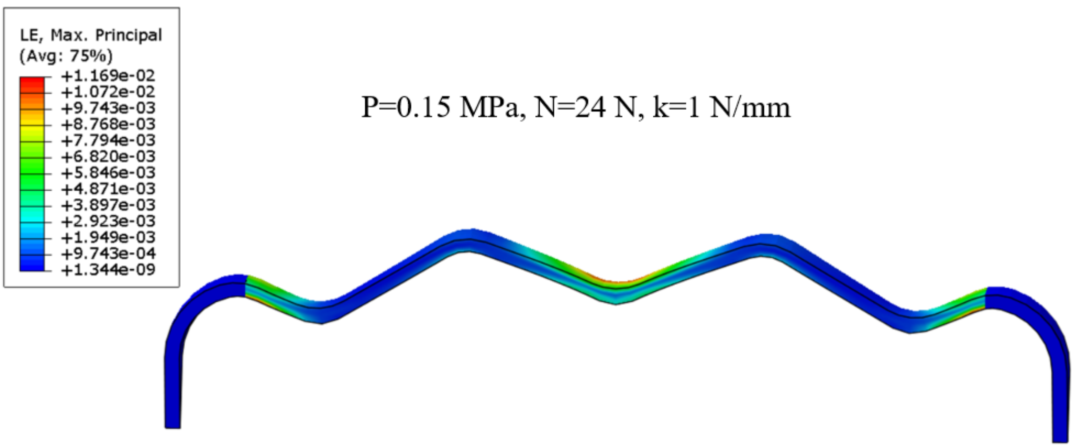

Figure 7.7 : Maximum principal strains at the end of inflation step.

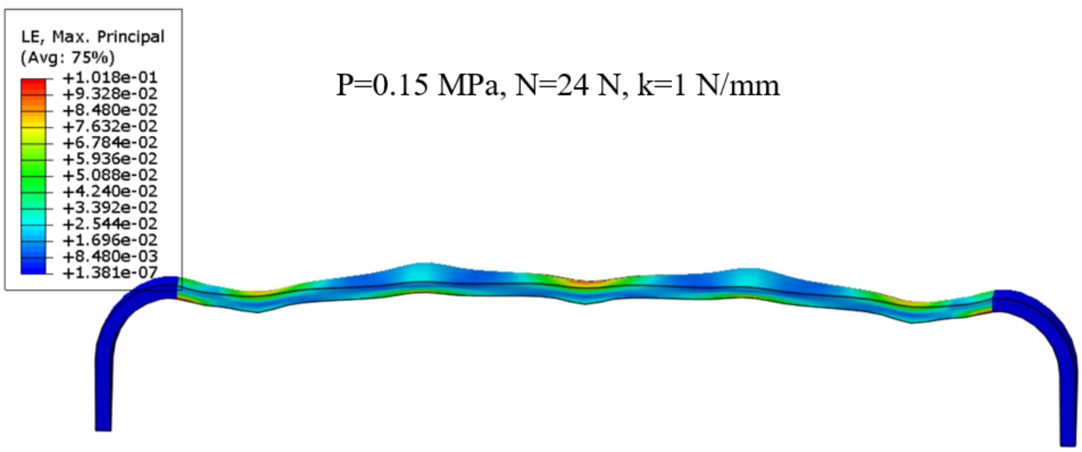

Figure 7.8 : Maximum principal strains at the end of tension step.

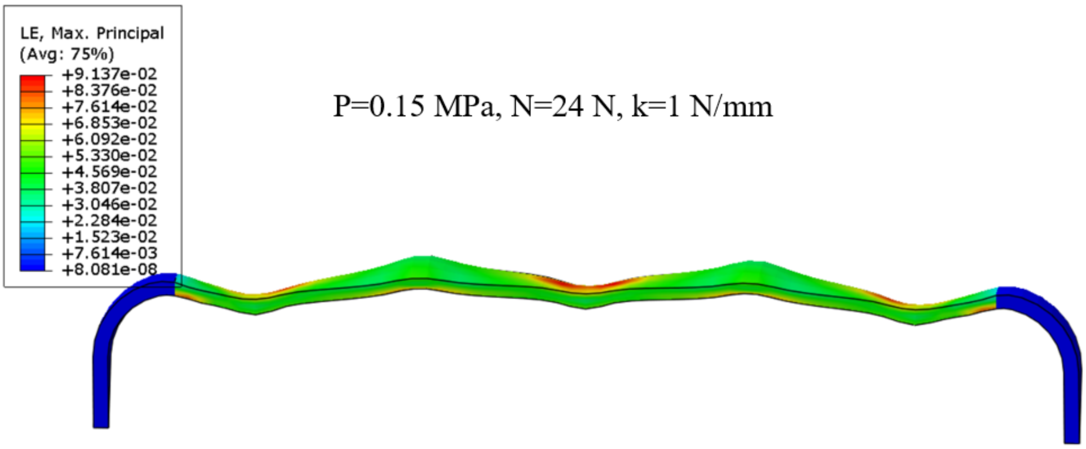

Figure 7.9 : Maximum principal strains at the end of Electric step.

Figure 7.9 shows the displacement of one of the ends throughout the whole procedure for a fibre angle of 20 degrees. As mentioned before, the length change is quite small for inflation step (0.0 mm). With the axial tension the shape returns to cylindrical shape and the force displacement relation is linear reaching 4.77 mm. Actuation by electrical loads results in a further 0.06 mm extention. This value, considering 50 mm length, is quite small and can change with fibre angle therefore it is beneficial to find a relation with fibre angle and actuation outputs.

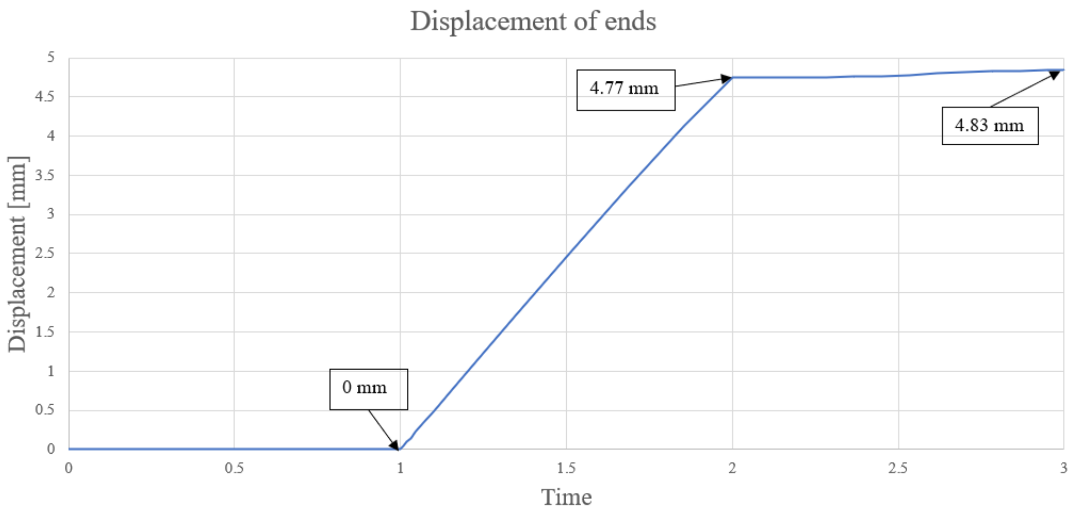

Figure 7.10 : Axial displacement of ends.

Figure 7.10 shows the relation between fibre angles and actuation displacements with 10kPa of inner pressure, 36 N of axial force and 100 kV/mm electric field. As it can be clearly seen again, actuation displacement is a kind of sinusoidal function of fibre angles, which has became a pattern for all the proposed designs in this study, and have a minimum around 25 and 45 degrees and maximum 75 degrees. Curve has also a local maximum around 5 degrees. However, it is suspected that behaviour of curve (i.e. frequency of the wave, amplitude, etc.) is highly related to dimensions, especially the angle between “zigzag” lines of elastomer with its axial direction. Further studies should be conducted to observe the effects of dimensions on the curve represented in the figure.

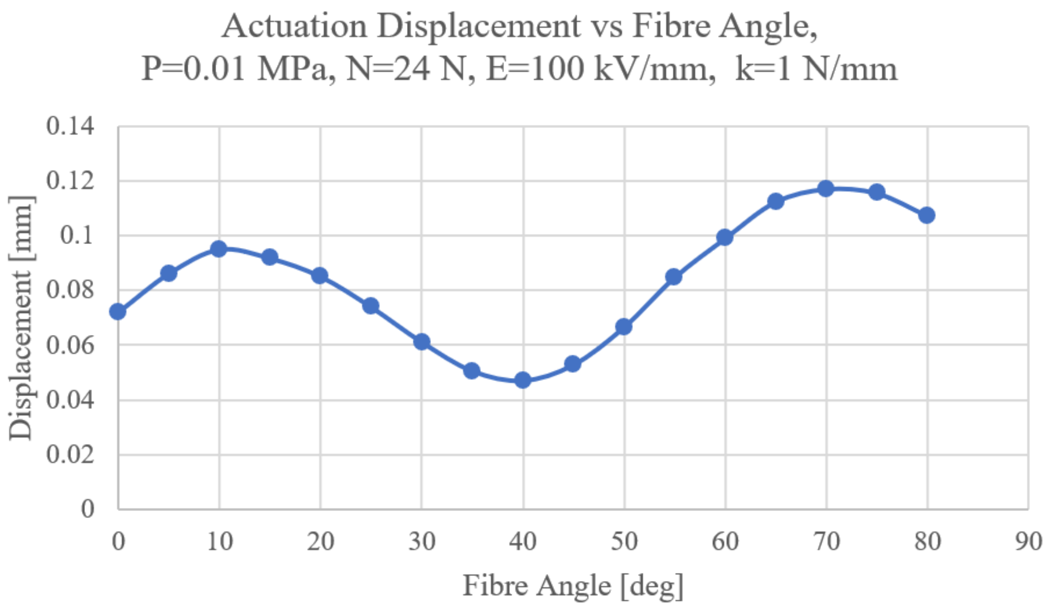

Figure 7.11 : Effects of fibre angle on actuation displacement.

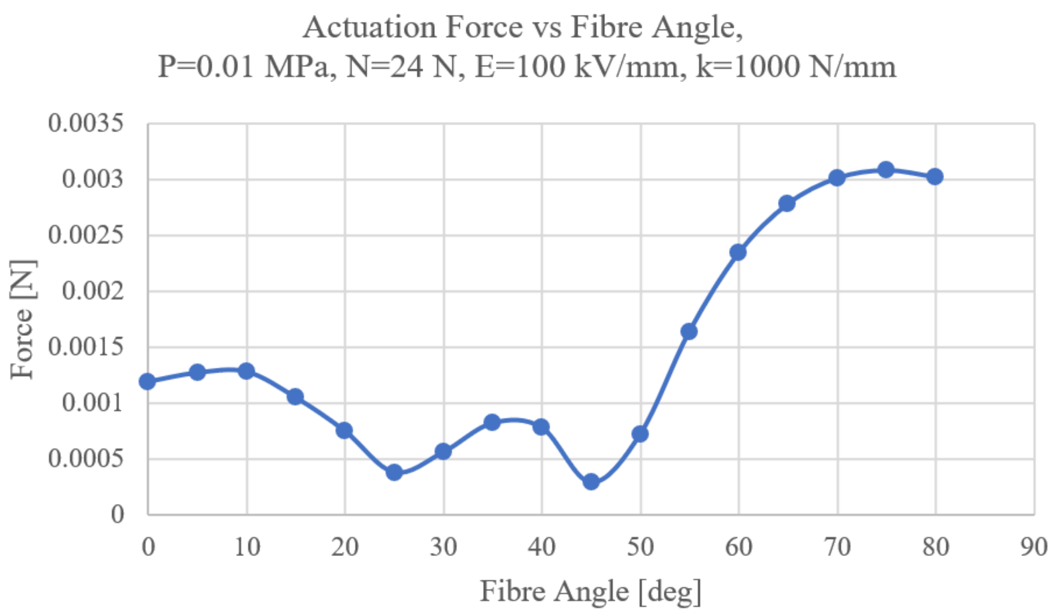

Figure 7.12 : Effects of fibre angle on actuation force.

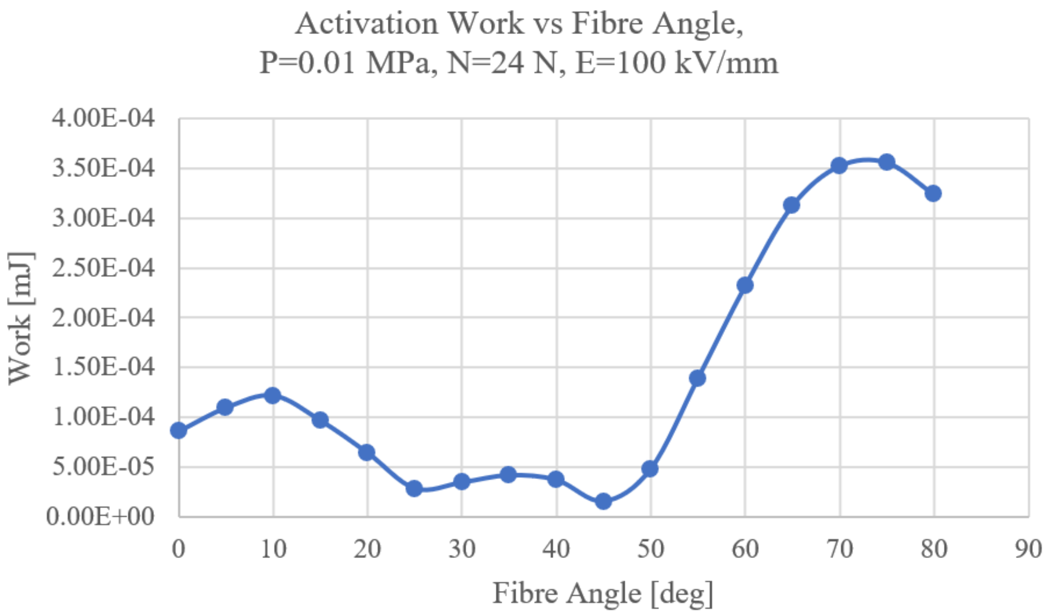

Figure 7.13 : Effects of fibre angle on actuation work.

Displacement outputs obtained in this design are in the same levels as cylindrical DEA design. However, force outputs are quite small because during activation, energy created by electric field is spent on changing the form of the wall (i.e. angles on the zigzag line) when there is a contraint, stiff springs for this case. These values might change dramatically by changing some design parameters such as thickness of elastomer, mid surface radius, accordion profile, etc. Moreover, the unintuitive relation between fibre angles and actuation outputs could be manipulated to enhance force and displacement values.

7.2 Conical Accordion DEA

7.2.1 FE model

7.2.1.1 Geometry and boundary conditions

As said above, conical accordion design is a variation of accordion design having a length of 50 mm, a bottom diameter of 40 mm and 20 mm of top diameter. The radial profile is given in Figure 7.14.

Beside the dimensions given in Figure 7.14, all the modelling parameters and properties are the same as accordion DEA, therefore they will not be repeated in this section.

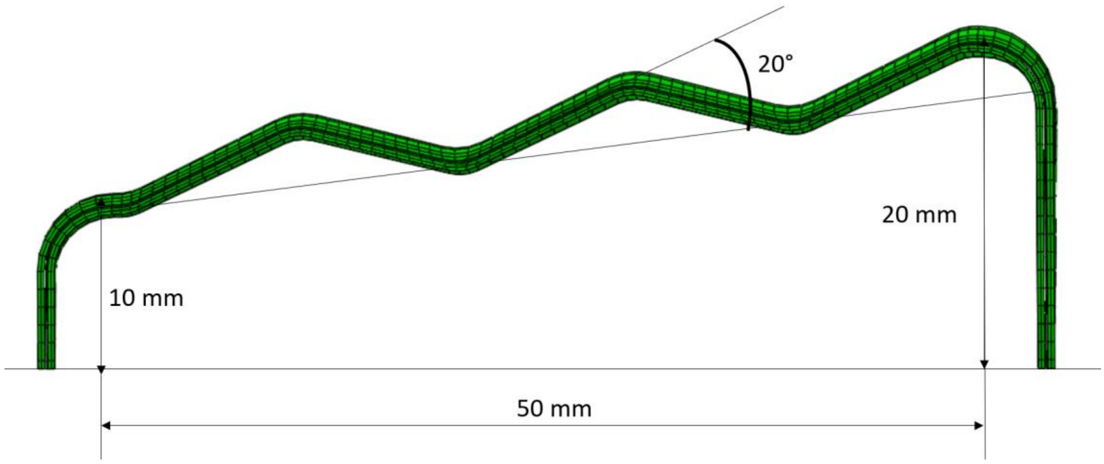

Figure 7.14 : Dimensions of conical accordion DEA.

7.2.2 Results

Figure 6.15 shows the displacements of one end of a generic model with 30 degrees fibre angle. Inflation causes 0.24 mm of decrease in length and with the axial tension 1.26 mm elongation occurs. Electical load causes 0.02 mm actuation.

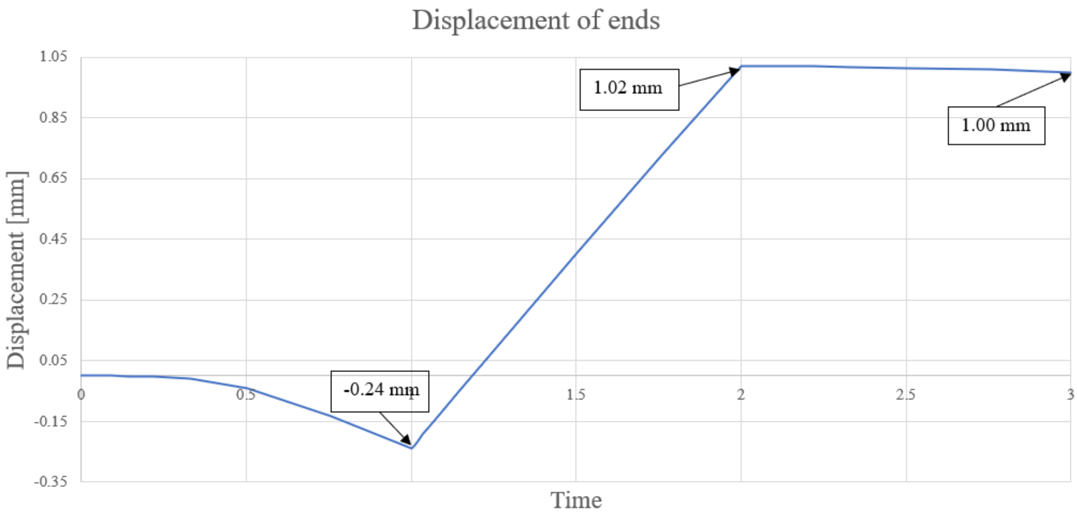

Figure 7.15 : Axial displacement of ends.

Figure 7.15, 7.16 and 7.17 displays the variation of actuation outputs with respect to fibre angle for displacement, force and work respectively for 10 kPa of inner pressure, 36 N of axial tension and 100 kV/mm of electrical load. As can be seen, displacement changes in a different manner from other designs. It is again a sinusodail curve however, it not a simple relation as others. Maximum displacement occurs around 70 degress and minimum is at around 40 degrees. The shape, conical angle and form of the zigzag line might have caused this behaviour.

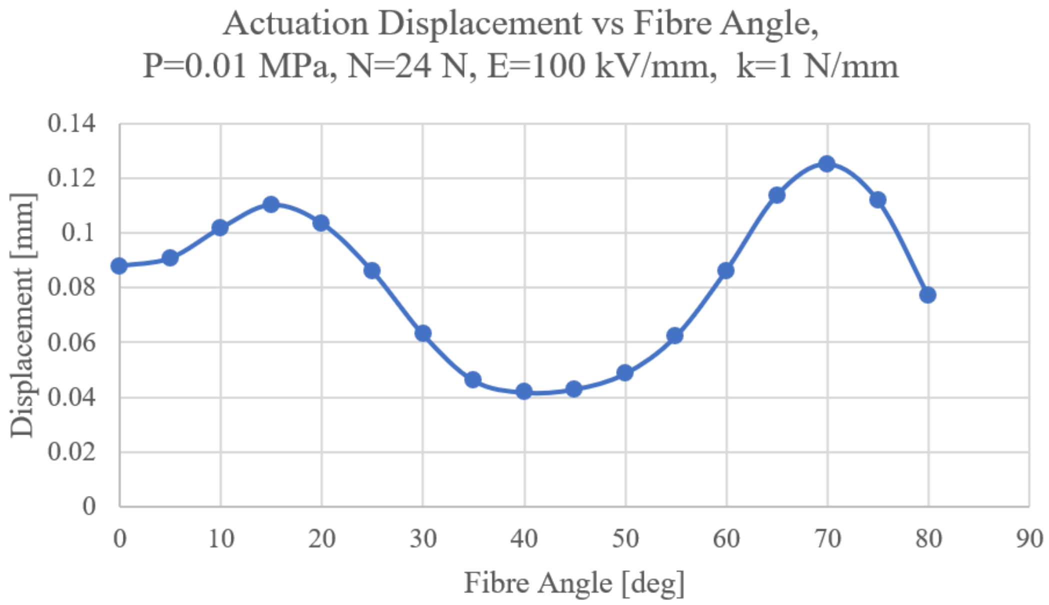

Figure 7.16 : Effects of fibre angle on actuation displacement.

Actuation force (see Figure 7.17) shows a similar behaviour as displacement with respect to fibre angles. DEA creates a maximum force around 65 degrees and a maximum force around 45 degrees.

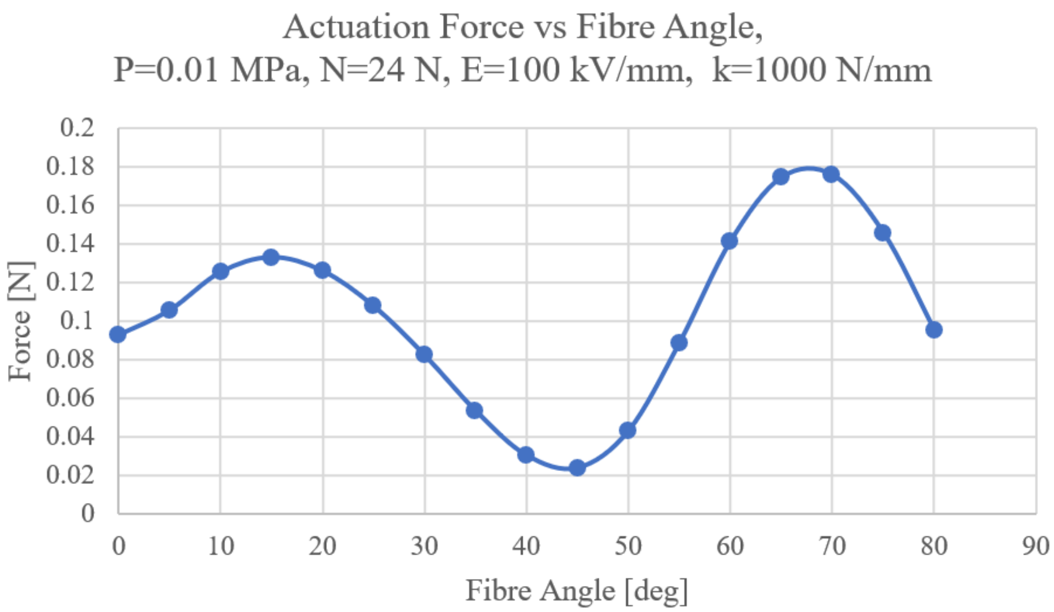

Figure 7.17 : Effects of fibre angle on actuation force.

Figure 7.18 shows the relation between actuation work and fibre angle. Work output is calculated as same as other numerical models. Maximum work occurs around 70 degrees and minimum occurs around 45 degrees. However, around 15 degrees, work-fibre angle curve has a local maximum.

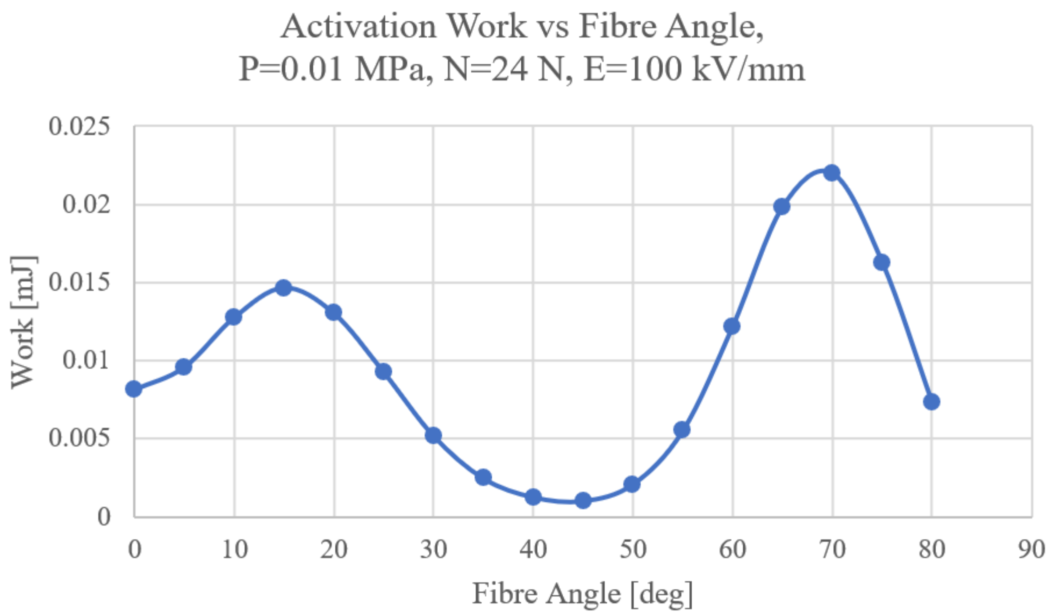

Figure 7.18 : Effects of fibre angle on actuation work.

Force output of conical accordion design is much greater than cylindrical one. Force and displacement values are more or less on the same level thus considerably better work output is obtained.

Unidirectional work created by electric field for accordion DEA design is much smaller than cylindrical DEA design however, additional geometrical parameters grants a possibility to improve outputs, which may surpass the traditional designs by geometric topology optimization.

8. CONCLUSIONS

In this study, to understand the behaviour of fibre reinforced actuators, three different DEA design propositions were investigated using Finite Element Method with different parameters.

Initially, present state of the art available in literature on the subject of DEAs, fibre-matrix relations under electrical load, stability and failure mechanisms reviewed intensively and a summary of current scientific state has been made. Consequently, a brief theoretical background is provided for finite strain theory, dielectric behaviour, transversely isotropic materials and finite element method.

Followed by a mathematical model for an incompressible fibre reinforced tubular DEA under inner pressure, axial tension and electrical load is generated. Expressions for stress components, axial load and inner pressure are obtained using constitutive equations for Neo-Hookean solid with two symmetrical fibre families. Pressure and axial force equations are solved numerically and simultaneously for deformed inner radius a and axial stretch λ. The effect of electrical load on deformed inner radius, axial stretch, 1^{st} and 2^{nd} invariants of Cauchy-Green deformation tensor and stretch of fibres are presented with graphs for different fibre angles.

For cylindrical DEA design proposition, a comprehensive study examining the relation between actuation displacements and forces and pre-stretch parameters as well as fibre orientations is conducted with a design of experiments. For tubular helix and accordion DEA, possible achievements on actuation outputs over cylindrical DEAs are investigated again using Finite Element Method of generic designs for only one parameter that is the fibre orientation.

Dielectric behaviour of DEA is implemented by ABAQUS UMAT subroutine which calculates hyperelastic response as well as dielectric response (i.e. Maxwell Stress), returns a sum of total stress tensor back in ABAQUS for every element at every increment. An ABAQUS ORIENT subroutine is also implemented for tubular helix and accordion DEA design, which calculates correct element orientation following curvature of geometrical shape.

Conclusions of this study can be summarized as follows.

For cylindrical DEAs,

- The most crucial design parameter concerning actuation outputs is fibre orientation. This is caused by the effect of fibre angle on the deformation of the cylinder.
- Fibre orientation also affects the relation between actuation outputs and pre stretch. Actuation outputs are a linear function of inner hydraulic pressure however, fibre angle changes the slope of this linear relation.
- The relation between actuation outputs and electric field applied through the thickness seem to be exponential, which is expected since Maxwell stress is a function of potential difference over thickness squared and thickness decreases exponentially under constant potential difference. Fibre angle affects the actuation response as well. It is found that outputs are higher as the angle approaches 90° degrees for the same electrical load.
- Increase in inner pressure causes an increase in actuation outputs.
- Outputs are higher when expansion occurs in all directions (radial, tangential and axial). Possibility of this situation are a direct result of fibre angle.

For tubular helix DEA design, fibre angle is also a particularly important parameter for design. As in the cylindrical DEA design, actuation outputs are a sinusoidal function of fibre angle. However, it is found that, in contrast to cylindrical DEA, maximum displacement/deformation by activation occurs around 20 degrees of fibre angle and becomes exceedingly small around 50 degrees and changes direction. It is suspected that helix shape is also highly effective on results. Obtained output values are in a comparable level as cylindrical DEA design. Yet, on helix model, element stretch levels are much smaller than cylindrical ones, which means helix design gives unidirectional output more effective than cylindrical shape.

For accordion DEA design, again it is found that fibre angle is a crucial parameter to optimize outputs. Actuation is again a sinusoidal function of fibre angle however with a changing amplitude. For the generic design studied, maximum actuation occurs around 75 degrees and the curve has a minimum around 40 degrees. Displacement levels are changing between 0.12 and 0.24%. However, force outputs are quite small because when constrained, with a stiff spring for this case, activation energy changes the form of zigzag rather than creating elongation or contraction. It is suspected that shape of zigzags forming the wall of the tube is greatly effective on actuation levels. Conical variant of accordion DEA design shows better outputs thanks to better force outputs granting a much greater unidirectional work than cylindrical accordion.

In conclusion, it is found that fibre orientation is the most important design parameter and it is effective on other parameters as well. Cylindrical DEA design shows the most promising results, however, a geometrical parameter optimization of the helix design could bring higher levels of useful work.

For further studies, more comprehensive parameter studies on tubular helix and accordion DEA is suggested to understand working mechanisms, since the possibilities are practically infinite. Obtaining analytical solution for these designs and their deformation would also help immensely to interpret dielectic behaviour and fibre matrix relations, and their effects on actuation outputs for these geometries. Furthermore, trial of alternative designs and comparison with existing design are also suggested to find the optimum candidate in search of substitute for real muscle fibres.

REFERENCES

[1] **Pelrine, R., Sommer-Larsen, P., Kornbluh, R. D., Heydt, R., Kofod, G., Pei, Q., and Gravesen, P.** (2001). Applications of dielectric elastomer actuators. In Proc. SPIE 4329, *Smart Structures and Materials 2001: Electroactive Polymer Actuators and Devices*, https://doi.org/10.1117/12.432665.

[2] **Hollerbach, J., Hunter, I., and Ballantyne, J.**, **(**1992). The Robotics Review, Vol. 2, O. Khatip, J. Craig, T. Lozano-Perez, Eds., MIT Press, Cambridge, 299.

[3] **Bar-Cohen, Y.**, (2004). *Electroactive, Polymer (EAP) Actuators as Artificial Muscle*. 2nd edition, Bellingham, WA: SPIE Press.

[4] **McKay, T. G., Calius, E., and Anderson, I.**, (2007). Modelling a dielectric elastomer actuator based on the McKibben muscle, *Proc. SPIE 6524, Electroactive Polymer Actuators and Devices (EAPAD)* 2007, 65241W (5 April 2007), https://doi.org/10.1117/12.715842.

[5] **Madden, J. D. W. et al.**, (2004). Artificial muscle technology: physical principles and naval prospects, *IEEE Journal of Oceanic Engineering, vol. 29, no. 3,* 706-728, July 2004, doi: 10.1109/JOE.2004.833135.

[6] **Hunter, I. W. and Lafontaine, S.**, (1992). A comparison of muscle with artificial actuators, *Technical Digest IEEE Solid-State Sensor and Actuator Workshop*, Hilton Head Island, SC, USA, 1992, 178-185, doi: 10.1109/SOLSEN.1992.228297.

[7] **Pelrine, R., Kornbluh, R. D., and Joseph, J. P.**, (1998). Eloctrostrciction of polyemer dielectrics with compliant electrodes as a means of actuation, *Sensors and Actuators A 64 (1998)*, 77-85.

[8] **Heydt, R., Kornbluh, R., Pelrine, R., and Mason, V.**, (1998). Design and performance of an electrostrictive-polymer-film acoustic actuator, *Journal of Sound and Vibration 215 (2),* 297-311.

[9] **Pelrine, R., Kornbluh, R., Joseph, J., Heydt, R., Pei, Q., and Chiba, S.**, (2000). High-field deformation of elastomeric dielectrics for actuators, *Materials Science and Engineering C 11*, 89-100.

[10] **Pelrine, R., Kornbluh, R., Pei, Q., and Joseph, J.**, (2000). High-speed electrically actuated elastomers with strain greater than 100%, *Science 287*, 836-839.

[11] **Pei, Q., Pelrine, R., Stanford, S., Kornbluh, R., and Rosenthal, M.**, (2003). Electro-elastomer rolls and their application for biomimetic walking robots, *Synthetic Metals 135-136*, 129-131.

[12] **Carpi, F., Chiarelli, P., Mazzoldi, A., and De Rossi, D.**, (2003). Electromechanical characterisation of dielectric elastomer planar

actuators: comparative evaluation of different electrode materials and different counterloads, *Sensors and Actuators A 107*, 85-95.

[13] **Mulgaonkar, A., Kornbluh, R., and Herr, H.,** (2008). A new frontier for orthotics and prosthetics: application of dielectric elastomer actuators to bionics, *Dielectric Elastomers as Electromechanical Transducers: Fundamentals, Materials, Devices, Models and Applications of an Emerging Electroactive Polymer Technology. Edited by: Carpi F, De Rossi D, Kornbluh R, Pelrine R, Sommer-Larsen P,* Elsevier.

[14] **Roentgen, W. C.,** (1880). About the Changes in Shape and Volume of Dielectrics Caused by Electricity, *Annual Physics and Chemistry Series, Vol. 11, sec III, G. Wiedemann, Eds., J. A. Barth*, Leipzig, Germany 1880, p. 771 German.

[15] **Garcia, L. A. and Trindade, M. A.**, (2019). Finite element modelling and parametric analysis of a dielectric elastomer thin-walled cylindrical actuator. *J Braz. Soc. Mech. Sci. Eng. 41, 18),* https://doi.org/10.1007/s40430-018-1527-4.

[16] **Son, S. and Goulbourne, N. C.,** (2010) Dynamic response of tubular dielectric elastomer transducers, *International Journal of Solids Structure 47,* 2672–2679.

[17] **Liu, W., and Rahn, C. R.,** (2004). Fiber-Reinforced Membrane Models of McKibben Actuators. *ASME. J. Appl. Mech. November 2003; 70(6),* 853–859. https://doi.org/10.1115/1.1630812.

[18] **Nakhiah, C. and Goulbourne, N. C.,** (2006). Cylindrical dielectric elastomer actuators reinforced with inextensible fibers, *Proc. SPIE 6168, Smart Structures and Materials 2006: Electroactive Polymer Actuators and Devices (EAPAD), 61680A*; https://doi.org/10.1117/12.658897.

[19] **Zhao, X. and Suo, Z.,** (2008). Method to analyse programmable deformation of dielectric elastomer layers, *Applied Physics Letters 93:25.*

[20] P**ei, Q., Pelrine, R., Stanford, S., Kornbluh, R., and Rosenthal, M.**, (2003). Multifunctional electroelastomer roll actuators and their application for biomimetic walking robots, *Proc. SPIE 5051, Smart Structures and Materials 2003: Electroactive Polymer Actuators and Devices (EAPAD), (28 July 2003),* https://doi.org/10.1117/12.484392.

[21] **Kovas, G., During, L., Michel, S., and Terrasi, G.,** (2009). Stacked dielectric elastomer actuator for tensile force transmission, *Sensors and Actuators A: Physical, 2009: Vol. 155,* 299-307.

[22] **Wang, H., Cai, S., Carpi, F., and Suo, Z**. (2012). Computational Model of Hydrostatically Coupled Dielectric Elastomer Actuators, *ASME. J. Appl. Mech. May 2012 ;79(3):031008,* https://doi.org/10.1115/1.4005885.

[23] **Plante J. S. and Dubowsky S.,** (2006). Large-scale failure modes of dielectric elastomer actuators, *International Journal of Solids and Structures, Volume 43, Issues 25–26, 2006,* 727-7751, ISSN 0020-7683, https://doi.org/10.1016/j.ijsolstr.2006.03.026.

[24] **Zhao, X. and Suo, Z.**, (2007). Method to analyze electromechanical stability of dielectric elastomers, *Appl. Phys. Lett. 91*, *061921 (2007)*.

[25] **Yang, E., Frecker, M., and Mockensturm, E.,** (2006). Finite element and experimental analyses of non-axisymmetric dielectric elastomer actuators, *Proc. SPIE 6168, Smart Structures and Materials 2006: Electroactive Polymer Actuators and Devices (EAPAD), 61680H (17 March 2006)*, https://doi.org/10.1117/12.658740.

[26] **Zwecker, S., Müller, R., and Klinkel, S.,** (2011). Nonlinear finite element simulation of thin dielectric elastomer structures. CEUR Workshop Proceedings. 750. 33-38.

[27] **Url-1** <https://en.wikipedia.org/wiki/Finite_strain_theory>, data retrieved 01.06.2020.

[28] **Holzaphel**, **G. A.,** (2000). *Nonlinear Solid Mechanics: A Continuum Approach for Engineering* (pp.209-216). John Wiley & Sons.

[29] **Ogden, R. W.,** (1997). *Non-linear elastic deformations*. Courier Corporation.

[30] **Rivlin, R. S.**, (1948). Large elastic deformations of isotropic materials. IV. Further developments of the general theory, *Philosophical Transactions of the Royal Society of London. Series A, Mathematical and Physical Sciences*, *241(835)*, 379–397.

[31] **Bower, A.,** (2009). *Applied Mechanics of Solids.* CRC Press. ISBN 1-4398-0247-5. Retrieved 2018-04-19.

[32] **Holzaphel**, **G. A.,** (2000). *Nonlinear Solid Mechanics: A Continuum Approach for Engineering* (pp.265-276). John Wiley & Sons.

[33] **Griffiths, D. J.,** (2008). *Introduction to Electrodynamics* (pp.351–352). Benjamin Cummings Inc.

[34] **Zienkiewicz, O. C., Taylor, R. L. and Zhu, J. Z**. (2005). *The Finite Element Method: Its Basis and Fundamentals.* Elsevier Butterworth-Heinemann.

[35] **Wriggers, P.,** (2008). *Nonlinear Finite Element Methods* (pp.318-324). Berlin: Springer.

[36] **Abaqus CAE,** (v6.17), Theory Manual.

[37] **Horgan, C. O. and Murphy, J. G**. (2011). Torsion of Incompressible Fiber-Reinforced Nonlinearly Elastic Circular Cylinders. *J Elast 103*, 235–246, https://doi.org/10.1007/s10659-010-9282-5.

[38] **He, L., Lou, J., and Du, J.** (2017). Analytical Solutions for Inextensible Fiber-Reinforced Dielectric Elastomer Torsional Actuators. *ASME. J. Appl. Mech. May 2017; 84(5): 051003*, https://doi.org/10.1115/1.4036193.

[39] **Taber L.A.,** (2004). *Nonlinear theory of elasticity: applications in biomechanics.* Singapore: World Scientific.

APPENDICES

APPENDIX A: DOE results

APPENDIX A

Table A.1 : DOE results for Cylindrical DEA, 1st part.

k [N/mm]	Fiber Angle [°]	Pressure [MPa]	Elec. Load [kV/mm]	Disp. [mm]	Force [N]
1	30	0.01	100	2.04E-02	2.04E-02
1	30	0.02	100	2.53E-02	2.53E-02
1	30	0.03	100	3.91E-02	3.91E-02
1	30	0.04	100	6.43E-02	6.43E-02
1	30	0.05	100	1.05E-01	1.05E-01
1	30	0.06	100	1.70E-01	1.70E-01
1	40	0.01	100	6.57E-02	6.57E-02
1	40	0.02	100	8.46E-02	8.46E-02
1	40	0.03	100	1.08E-01	1.08E-01
1	40	0.04	100	1.35E-01	1.35E-01
1	40	0.05	100	1.68E-01	1.68E-01
1	40	0.06	100	2.10E-01	2.10E-01
1	50	0.01	100	1.51E-01	1.51E-01
1	50	0.02	100	1.68E-01	1.68E-01
1	50	0.03	100	1.87E-01	1.87E-01
1	50	0.04	100	2.08E-01	2.08E-01
1	50	0.05	100	2.32E-01	2.32E-01
1	50	0.06	100	2.61E-01	2.61E-01
1	60	0.01	100	2.36E-01	2.36E-01
1	60	0.02	100	2.49E-01	2.49E-01
1	60	0.03	100	2.63E-01	2.63E-01
1	60	0.04	100	2.80E-01	2.80E-01
1	60	0.05	100	2.99E-01	2.99E-01
1	60	0.06	100	3.22E-01	3.22E-01
1000	30	0.01	100	1.73E-05	1.73E-02
1000	30	0.02	100	3.45E-05	3.45E-02
1000	30	0.03	100	6.46E-05	6.46E-02
1000	30	0.04	100	1.12E-04	1.12E-01
1000	30	0.05	100	1.85E-04	1.85E-01
1000	30	0.06	100	2.97E-04	2.97E-01
1000	40	0.01	100	1.02E-04	1.02E-01
1000	40	0.02	100	1.32E-04	1.32E-01
1000	40	0.03	100	1.68E-04	1.68E-01
1000	40	0.04	100	2.11E-04	2.11E-01
1000	40	0.05	100	2.63E-04	2.63E-01
1000	40	0.06	100	3.28E-04	3.28E-01
1000	50	0.01	100	2.17E-04	2.17E-01
1000	50	0.02	100	2.41E-04	2.41E-01
1000	50	0.03	100	2.69E-04	2.69E-01
1000	50	0.04	100	2.99E-04	2.99E-01
1000	50	0.05	100	3.31E-04	3.31E-01
1000	50	0.06	100	3.73E-04	3.73E-01
1000	60	0.01	100	3.15E-04	3.15E-01
1000	60	0.02	100	3.33E-04	3.33E-01
1000	60	0.03	100	3.52E-04	3.52E-01
1000	60	0.04	100	3.73E-04	3.73E-01
1000	60	0.05	100	3.96E-04	3.96E-01
1000	60	0.06	100	4.22E-04	4.22E-01

Table A.2 : DOE results for Cylindrical DEA, 2nd part.

k [N/mm]	Fiber Angle [°]	Pressure [MPa]	Elec. Load [kV/mm]	Disp. [mm]	Force [N]
1	10	0.01	100	6.14E-02	6.14E-02
1	20	0.01	100	2.92E-02	2.92E-02
1	30	0.01	100	2.04E-02	2.04E-02
1	40	0.01	100	6.57E-02	6.57E-02
1	50	0.01	100	1.51E-01	1.51E-01
1	60	0.01	100	2.36E-01	2.36E-01
1	70	0.01	100	2.94E-01	2.94E-01
1	80	0.01	100	3.25E-01	3.25E-01
1	10	0.01	150	1.17E-01	1.17E-01
1	20	0.01	150	5.24E-02	5.24E-02
1	30	0.01	150	5.78E-02	5.78E-02
1	40	0.01	150	1.75E-01	1.75E-01
1	50	0.01	150	3.65E-01	3.65E-01
1	60	0.01	150	5.55E-01	5.55E-01
1	70	0.01	150	6.90E-01	6.90E-01
1	80	0.01	150	7.65E-01	7.65E-01
1	10	0.01	200	1.73E-01	1.73E-01
1	20	0.01	200	7.71E-02	7.71E-02
1	30	0.01	200	1.56E-01	1.56E-01
1	40	0.01	200	3.88E-01	3.88E-01
1	50	0.01	200	7.07E-01	7.07E-01
1	60	0.01	200	9.87E-01	9.87E-01
1	70	0.01	200	1.19E+00	1.19E+00
1	80	0.01	200	1.31E+00	1.31E+00
1	10	0.01	250	2.46E-01	2.46E-01
1	20	0.01	250	1.30E-01	1.30E-01
1	30	0.01	250	3.04E-01	3.04E-01
1	40	0.01	250	7.36E-01	7.36E-01
1	50	0.01	250	1.19E+00	1.19E+00
1	60	0.01	250	1.50E+00	1.50E+00
1	70	0.01	250	1.73E+00	1.73E+00
1	80	0.01	250	1.86E+00	1.86E+00

Table A.3 : DOE results for Cylindrical DEA, 3rd part.

k [N/mm]	Fiber Angle [°]	Pressure [MPa]	Elec. Load [kV/mm]	Disp. [mm]	Force [N]
1000	10	0.01	100	1.03E-04	1.03E-01
1000	20	0.01	100	2.37E-05	2.37E-02
1000	30	0.01	100	1.73E-05	1.73E-02
1000	40	0.01	100	1.02E-04	1.02E-01
1000	50	0.01	100	2.17E-04	2.17E-01
1000	60	0.01	100	3.15E-04	3.15E-01
1000	70	0.01	100	3.84E-04	3.84E-01
1000	80	0.01	100	4.22E-04	4.22E-01
1000	10	0.01	150	1.16E-04	1.16E-01
1000	20	0.01	150	2.59E-05	2.59E-02
1000	30	0.01	150	5.30E-05	5.30E-02
1000	40	0.01	150	2.63E-04	2.63E-01
1000	50	0.01	150	5.11E-04	5.11E-01
1000	60	0.01	150	7.18E-04	7.18E-01
1000	70	0.01	150	8.53E-04	8.53E-01
1000	80	0.01	150	9.11E-04	9.11E-01
1000	10	0.01	200	1.30E-04	1.30E-01
1000	20	0.01	200	4.07E-05	4.07E-02
1000	30	0.01	200	1.27E-04	1.27E-01
1000	40	0.01	200	4.86E-04	4.86E-01
1000	50	0.01	200	8.54E-04	8.54E-01
1000	60	0.01	200	1.23E-03	1.23E+00
1000	70	0.01	200	1.51E-03	1.51E+00
1000	80	0.01	200	1.65E-03	1.65E+00
1000	10	0.01	250	1.96E-04	1.96E-01
1000	20	0.01	250	6.53E-05	6.53E-02
1000	30	0.01	250	3.06E-04	3.06E-01
1000	40	0.01	250	8.22E-04	8.22E-01
1000	50	0.01	250	1.36E-03	1.36E+00
1000	60	0.01	250	1.87E-03	1.87E+00
1000	70	0.01	250	2.25E-03	2.25E+00
1000	80	0.01	250	2.40E-03	2.40E+00

CURRICULUM VITAE

Name Surname : **Azamet Karoağlan**

Place and Date of Birth : **Sivas 11.02.1993**

E-Mail : **azametkaraoglan@gmail.com**

EDUCATION :

- **B.Sc.** : 2017, Istanbul Technical University, Mechanical Engineering Faculty, Mechanical Engineering
- **M.Sc.** : 2020, Istanbul Technical University, Mechanical Engineering, Solid Mechanics

PROFESSIONAL EXPERIENCE AND REWARDS:

- 2018- A-Ztech LTD. Simulation and CAE Engineer